Title
STRUCTURAL STUDIES OF IRON AND MANGANESE IN PHOTOSYNTHETIC REACTION CENTERS

Author
McDermott, A.E.

Publication Date
1987-11-01

Lawrence Berkeley Laboratory
UNIVERSITY OF CALIFORNIA

CHEMICAL BIODYNAMICS DIVISION

Structural Studies of Iron and Manganese in Photosynthetic Reaction Centers

A.E. McDermott
(Ph.D. Thesis)

November 1987

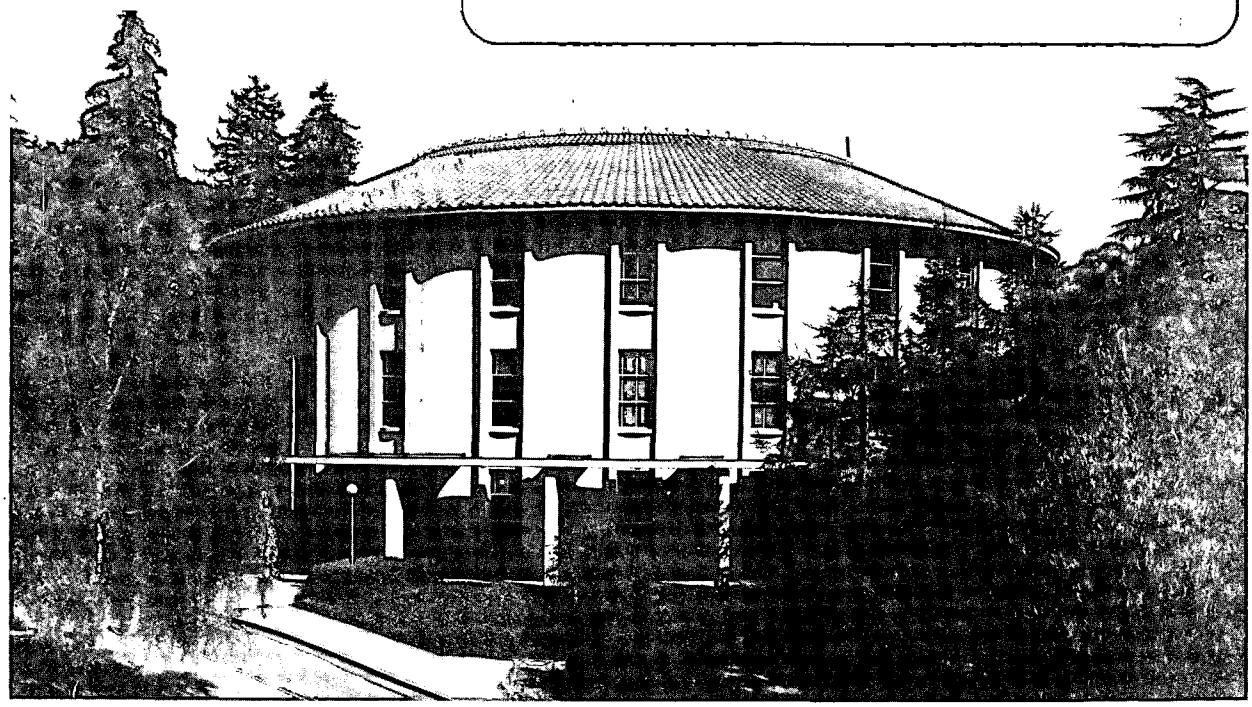

Prepared for the U.S. Department of Energy under Contract DE-AC03-76SF00098

DISCLAIMER

Structural Studies of Iron and Manganese in Photosynthetic Reaction Centers

Ann Elizabeth McDermott
Ph.D. Thesis

November, 1987

Lawrence Berkeley Laboratory
University of California
Berkeley, California 94720

This work was supported by the U.S. Department of Energy
under contract number DE-AC03-76SF00098

Structural Studies of Iron and Manganese in Photosynthetic Reaction Centers

Ann E. McDermott

Abstract

Electron paramagnetic resonance (EPR) and X-ray absorption spectroscopy (XAS) were used to characterize components involved in the light reactions of photosynthetic reaction centers from spinach and a thermophilic cyanobacterium, *Synechococcus* sp.: center X, the low electron potential acceptor in Photosystem I (PS I) and the Mn complex involved in water oxidation and oxygen evolution.

The lineshape of the EPR spectrum of center X is independent of microwave power, indicating a dominant inhomogenous broadening mechanism. The dependence of its EPR amplitude on microwave power and temperature indicate an Orbach spin relaxation mechanism involving an excited state at 40 cm^{-1}. This low energy contributes to its unusually anisotropic g-tensor.

XAS of iron in PS I preparations from spinach and *Synechococcus*, containing ferredoxins A, B and X are consistent with a model with [4Fe-4S] ferredoxins, which are presumably centers A and B and [2Fe-2S] ferredoxins, which would be X.

Illumination of dark-adapted *Synechococcus* PS II samples at 220-240 K results in the formation of the multiline EPR signal previously assigned as a Mn S_2 species, and g=1.8 and 1.9 signals of Fe^{2+} Q_A^-. In contrast to spinach, illumination at 110-160 K produces only a new EPR signal at g=1.6 which we assign to another configuration of Fe^{2+}-Q^-. Following illumination of a S_1 sample at 140 K or 215 K, the Mn X-ray absorption edge inflection energy changes from 6550 eV to 6551 eV, indicating an oxidation of Mn, and average valences greater than Mn(II). Concomitant changes in the shape of the pre-edge spectrum indicate oxidation of Mn(III) to Mn(IV). The

Mn EXAFS spectrum of PS II from *Synechococcus* is similar in the S_1 and S_2 states, indicating O or N ligands at 1.75 ± 0.05 Å, transition metal neighbor(s) at 2.73 ± 0.05 Å, and N and O ligands at 2.2 Å with heterogeneous bond lengths; these data demonstrate the presence of a di-μ-oxo bridged Mn structure. The amplitude of Mn backscattering indicates that a symmetric tetranuclear cluster is unlikely. The striking similarity of the XAS spectra and multiline spectrum to those from spinach PS II indicate a similar Mn complex in prokaryotes and eukaryotes.

Acknowledgments

I am happy to acknowlege the people who have helped me complete this work. Recognizing their contributions is important to me, and it is also nice to have a section of one's thesis which is certain to be read.

I am indebted to my advisors and benefactors, Prof. Kenneth Sauer and Dr. Melvin Klein. Because of their priorities I had the luxury of freely pursuing my education with as much vigor as I pursued tangible work. Ken's impartial yet optimistic overview, and his prompt, vigilant critiques have made us more honest many times. Mel's zeal and insight have provoked me to consider many facets of our problems, and I unvariably was given the license to take the tangents that interested me. Their complementary skills and interests have fostered an environment in which I developed a liking for biophysical chemistry.

I thank Dr. Melvin Klein and Profs. Kenneth Sauer and Richard Malkin for reading this thesis and for their valuable suggestions.

My colleages have created an abundant and challenging intellectual atmosphere, and I recognize their contributions in labor, counsel and morale. Dr. Vittal Yachandra was involved in many aspects of this work: helping to plan many of the experiments, convincing me to complete them, doing the early *Synechococcus* preparations with me, collecting some useful and many useless EPR spectra with me, getting me interested in inorganic chemistry... and so on. Many times he had a more spirited interest in these results than I did! Drs. David Goodin and John McCracken helped me get started in EPR and XAS and shared their insights and suggestions for thesis projects. John's comments provoked me to get interested in Center X ("the trouble with people in PS I is that they learned early on that 4 times 3 is 12"). David's inspiration and suggestions are still significant in the Mn EXAFS projects. Drs. Celic Kayalar, Stephen Worland, Mary Blackwell and particularly Dr. Akihiko Yamigishi taught me biochemistry techniques.

(Dr.) David Britt obliged me many invaluable tutorials in physics and widgetry, and had a never-failing committment to orient me to T.V./techno culture of the 1980's. I particularly thank him for his encouragement. Ron Guiles made many significant suggestions for this work, and was involved in every aspect of the X-ray experimental work. In addition, he was the first person to demonstrate the superior nutritional value of dry ice. I thank Drs. Jim Cole and Jean-Luc Zimmermann for trying to keep me honest with the literature, and Vickie DeRose for taking interest in my writing and for her useful suggestions. Most importantly I acknowledge Sue Dexheimer, Vittal, Dave, Ron, Vicky, Dr. Sun Un, Jim, and Rick Storrs for enduring the SSRL sleep-deprivation/tedium-endurance (SSRL-SDTE) tests without killing me or each other. Their frustration and boredom, their moments of improvisation and inspiration, and their team-spirit made these projects possible.

I thank Prof. John Golbeck for his amicable and flexible approach to collaborating, and for sharing his viewpoint on photosystem I. I also thank Kevin Parret for preparing PS I samples for XAS.

I would like to mention some 'labmates', who were my friends and companions in Chem-Bio: John Casey, Gary Brudvig, Mike Boska, Kerry Karukstis, Mike Saxton, Dave Pearlman, Ti-Sheng Young, Tom Pratum, Sara Hoover, Sarah Tabbutt, Neil Blough, Carolyn Hoener, Trish (and Poindexter) Maxson, Herrmann Keuper, Nathan Hunt, and and especially Paul Selvin and Sun Un who have shared their insights in magnetic resonance, Marc Donsky who found and lent me 100 neccessary lab gismos and Ishita Mukerji who has been known to perform EXAFS rescue missions. By sharing their equipment, advice and company with me, they made my stay more pleasant and more profitable.

Theresa Troxel, Sophia Rex, Dr. Britt Hedmann, and Glenn Kerr at SSRL, and Dr. Joseph Jaklevic at L.B.L. and Phil Eggers and Gary Smith at the Calvin Labs provided excellent experimental and technical assistance, many times on short notice.

Finally, I appreciate the contributions of my family and friends. I thank Heller, Mark, Jeffrey, Scott, Tinku, Carol and Dave Adee, Chris and Lynn, Collette, Steve, Anaya and particularly Lee who helped me keep my life in order at the times when my work came first; Mark Trulson, for his companionship, his confidence in me and for his contagious enthusiasm for science; my siblings Mag, Paul, and Dave for their encouragement, and particularly Heller for everything from distraction to packing my bags and doing my laundry for Stanford, to delivering dinners at lab; and I thank my parents most of all, for their encouragement, sustenance and support in my attempts to pursue my education and test the limits of my abilities.

This work was supported by a grant from the National Science Foundation (PCM 82-16127 and PCM 84-16676) and by the Director, Division of Energy Biosciences, Office of Basic Energy Sciences, Office of Energy Research of the Department of Energy under contract DE-AC03-76SF00098. Synchrotron radiation facilities were provided by the Stanford Synchrotron Radiation Laboratory which is supported by the U. S. Department of Energy, Office of Basic Energy Sciences and the NIH Biotechnology Program, Division of Research Resources.

Table of Contents

Abbreviations

Chl, chlorophyll;

DCMU, 3-(3,4-dichlorophenyl)-1,1-dimethylurea;

DCBQ, 2,6-dichloro-*p*-benzoquinone;

EDTA, ethylenediamine tetraacetic acid;

EPR, electron paramagnetic resonance;

ESE NEM, electron spin echo nuclear magnetic resonance;

EXAFS, extended X-ray absorption fine structure;

Fd, ferredoxin;

HEPES, N-2-Hydroxyethylpiperazine-N'-2-ethanesulfonic acid;

MES, 4-morpholineethanesulfonic acid;

OEC, oxygen-evolving complex;

PMS, phenazine methosulfate or N-methylphenazonium methosulfate;

PMSF, phenylmethylsulfanyl fluoride or α-Toluenesulfanyl fluoride;

PS I, photosystem I;

PS II, photosystem II;

P680, photosystem II reaction center chlorophyll;

P700, photosystem I reaction center chlorophyll;

Q_A and Q_B, quinone electron acceptors in the reaction center of purple nonsulfur bacteria and PS II;

SHE, standard hydrogen electrode;

Tiron, 4,5-dihydroxy-1,3-benzene-disulfonic acid;

Tris, tris(hydroxymethyl)aminomethane.

Chapter I: Introduction

I A. General Introduction to Photosynthesis

Of the 10^{17} watts of electromagnetic radiation incident on the earth, a very small fraction, approximately 10^{13} watts, is converted by biological organisms to chemical potential energy. The conversion of electromagnetic radiation to chemical or electrochemical potential is arguably the most fundamental process of life. This conversion is noteworthy not so much because of its efficiency, but more because of the associated accumulation of considerable order in the form of the entire biosphere. Maintenance of this order is accomplished partly by virtue of the fact that photosynthesis involves chemical rearrangements with considerable kinetic barriers. Naturally, these conversions are catalyzed by some enzyme complex. We are concerned with the detailed molecular structure and mechanisms of this catalyst.

Photosynthesis takes place in a macromolecular complex called a reaction center. The reaction centers of all photosynthetic species are membrane-bound complexes which comprise several polypeptides, lipids and numerous bound cofactors. Almost invariably, photosynthesis is carried out by biological organisms in the following general way. Light is absorbed by a pigment which is found in an array of pigments known as a light harvesting antenna. These pigments have very large optical absorption coefficients, and are coupled in such a fashion that the excited electronic state becomes delocalized among them. The pigments include chlorophyll, bacteriochlorophyll, carotenoids and phycobiliproteins. The exciton (quantum of electronic excitation) is transferred with good efficiency to a specialized chlorophyll or bacteriochlorophyll species. What makes this specialized Chl unique is that the electron can be transferred from the electronic excited state of the specialized Chl to an acceptor species which is located nearby (ca. 10 Å). Acceptor species are generally cofactors with low (0 to -1.0 V) reduction potentials.

Commonly they include chlorophyll, pheophytin, quinones or ferredoxins. The initial acceptor is near additional acceptor species, so that the electron can 'hop' from one side of the membrane to the other along acceptor molecules. This serial electron transfer allows the overall electron transfer reaction to be *irreversible.* Meanwhile a donor species (or series of donor species) can rereduce the specialized Chl. The donor species are characterized by relatively high midpoint potentials (0 to +1 V), and many of these are hemes.

In some reaction centers the electron transfer reactions are cyclic in the sense that a reduced acceptor ultimately does reduce an oxidized donor. However, this occurs by a process which can store energy, such as coupled electron and ion translocation. In this way a proton gradient is formed.

In other reaction centers the electron transfer is linear in the sense that ultimate acceptors and donors are consumed and the reduced acceptors and donors are accumulated. The ultimate donors and acceptors are generally abundant small molecules, and the reduced and oxidized products are characterized by a considerable barrier to spontaneous electrochemical reactions. The most common products are starch and molecular oxygen. Thus energy can be stored as electrochemical potential, and this energy can be later recovered enzymatically. Generally when it is recovered, it is used to form a proton gradient by coupled electron and ion translocation in the membranes of mitochondria or of prokaryotes. The net result, an ion gradient, is similar to the result of photosynthesis with cyclic electron transfer. An important distinction between linear and cyclic electron transfer in photosynthesis is that in linear electron transfer the intermediate stored electrochemical potential may be scavenged by nonphotosynthetic organisms for food or fuel. This storage in starch (or hydrocarbons) and oxygen allows some organisms to consume an amount of power much larger than what they could generate photosynthetically.

In this thesis certain detailed aspects of the structure and function of reaction centers will be explored. Exciting advances in the understanding of membrane proteins have

occurred in the past decade. Of particular significance for photosynthesis is the first three-dimensional X-ray crystal structure of a reaction center (Deisenhofer et al., 1986). The structure these authors obtained is thrilling in at least two respects: first that this structure largely confirms the picture that had been predicted, marking a great achievement for biochemists and spectroscopists, and secondly that this information will allow for much more detailed mechanistic studies in the future.

Of the many types of reaction centers that exist in nature, only one (that from purple nonsulfur bacteria) has been so thoroughly characterized. However, its structure may have general implications for other reaction centers. One of the themes in this thesis is the similarity between a prokaryotic photosynthetic organism, *Synechococcus* sp., and a higher plant, spinach. In addition, analogies with the reaction center from purple nonsulfur bacteria will be used. The comparison of various photosynthetic organisms has been a popular endeavor, motivated partly by the desire to understand what is general about the structure of reaction centers, and partly by the desire to understand the evolutionary contexts of the variations in reaction centers. The next part of this introduction (I B.) will serve to introduce photosynthetic organisms and their reaction centers in a general way. Following that will be a specific description of the two photosystems of plants and cyanobacteria (I C. and I E.), which are the subjects of this thesis. The specific questions which are addressed will also be described (I D. and I F.).

I B. The Classes of Photosynthetic Organisms and Their Reaction Centers

There are three general classes of phototrophic prokaryotes (i.e. single celled organisms without organelle structures capable of living with sunlight as their only energy source). One class is the cyanobacteria, which resemble the chloroplast organelles of eukaryotic photosynthetic organisms in many respects; the other two are green bacteria and purple bacteria (Pfenning, 1978). Cyanobacteria and higher plants carry out oxygenic photosynthesis with two specialized reaction centers, called photosystems I and II. They use water and CO_2 as the ultimate donor and acceptor species and produce

sugars and O_2 as the ultimate products. The involvement of two reaction centers that operate at different potentials and are coupled in series allows these organisms to transfer electrons across a larger electrochemical potential difference than if they used only one reaction center. It is this serial two-quantum design that allowed water to be used as the ultimate donor while NADP is the ultimate acceptor (as in many other CO_2-fixing organisms). These organisms use Chl a and phycobiliproteins or Chl b as the main constituents of their antennae. They probably also use Chl a as the specialized pigment. Oxygen-evolving photosynthetic organisms of this type probably appeared between 2.5 and 3 billion years ago (Shopf, 1978).

Work in this thesis and in other recent publications supports the idea that the reaction centers of plants and cyanobacteria are structurally quite similar and involve similar redox components. The electron transfer participants that have been identified in chloroplasts and cyanobacteria are usually summarized indicated in a 'Z-scheme' such as Figure I-1. PS II obtains electrons from water, thus producing molecular oxygen and protons, and transfers the electrons to low potential quinone acceptors. The acceptors of PS II donate electrons to the donor of PS I *via* the plastoquinone 'pool', which are quite mobile within the chloroplast membrane, and *via* the Rieske/ cytochrome b_6-f complex, which is a multi-subunit, membrane bound metalloprotein. Electrons are shuttled from this complex to PS I by either plastocyanin or, in some cyanobacteria, a c-type cytochrome (Ho & Krogmann, 1982). PS I produces reducing equivalents of potential approximately -.5 V. In both cyanobacteria and eukaryotes PS I donates electrons to a soluble ferredoxin which then donates electrons to $NADP^+$ to form NADPH, the biochemical currency of reducing equivalents. These reducing equivalents are generally used in carbon fixation. Although the architecture of reaction centers is highly preserved from prokaryotes to eukaryotes, the precise biochemical pathways in which they participate are quite varied. For example, in cyanobacteria PS I donates electrons directly to other enzymes such as the nitrate and nitrite reductases to form ammonia (Ho & Krogmann, 1982). The cyanobacteria are also capable of anaerobic photosynthetic

growth using H_2S as a donor to PS I (Padan & Cohen, 1982). This ability to grow aerobically or anaerobically has not been observed for any eukaryotic organisms.

The homology between the cyanobacterial genome and the genome of the chloroplasts in plants or algae is much greater than that between cyanobacteria and other prokaryotes. Based on this gene homology it has been proposed that eukaryotic photosynthetic organisms occurred when symbiosis between a cyanobacterium and another nonphotosynthetic organism, analogous to the symbiosis in lichens, resulted in the nonphotosynthetic organism engulfing the cyanobacteria to form a chloroplast (reviewed in Schwartz & Dayhoff, 1981).

In contrast, the phototrophic green and purple bacteria carry out anoxygenic photosynthesis using only one type of reaction center. They employ electron donors of lower reduction potential than that of water, such as reduced sulfur compounds, H_2, or simple organic molecules to fix CO_2 photosynthetically. The purple non-sulfur bacteria achieve this by cyclic electron transfer, while the green bacteria use linear electron transfer. These organisms use BChl in place of Chl; the principal red absorption of the BChl compounds occurs between 710 and 1035 nm while that of Chl is around 670. These organisms are thus adapted to a very different set of ecological conditions than the green plants or the cyanobacteria. Although the Chl-containing organisms have two reaction centers and are thus more complex than the BChl containing organisms, the biosynthesis of BChl and Chl suggest that the BChl organisms evolved from Chl organisms (Mauzerall, 1978).

PS I is remarkably similar to the reaction centers of green bacteria, and PS II to the reaction centers of purple nonsulfur bacteria, except that PS II has an associate Mn-containing oxygen evolution complex (Mn-OEC). These pairs (PS II and purple nonsulfur bacteria, PS I and green bacteria) are particularly similar in the chemical nature of the acceptor species. In PS I and green bacteria the acceptors include several low potential ferredoxins and two intermediate acceptor species with g=2 EPR signals (Nitschke et.al, 1987). In PS II and purple nonsulfur bacteria the acceptors include

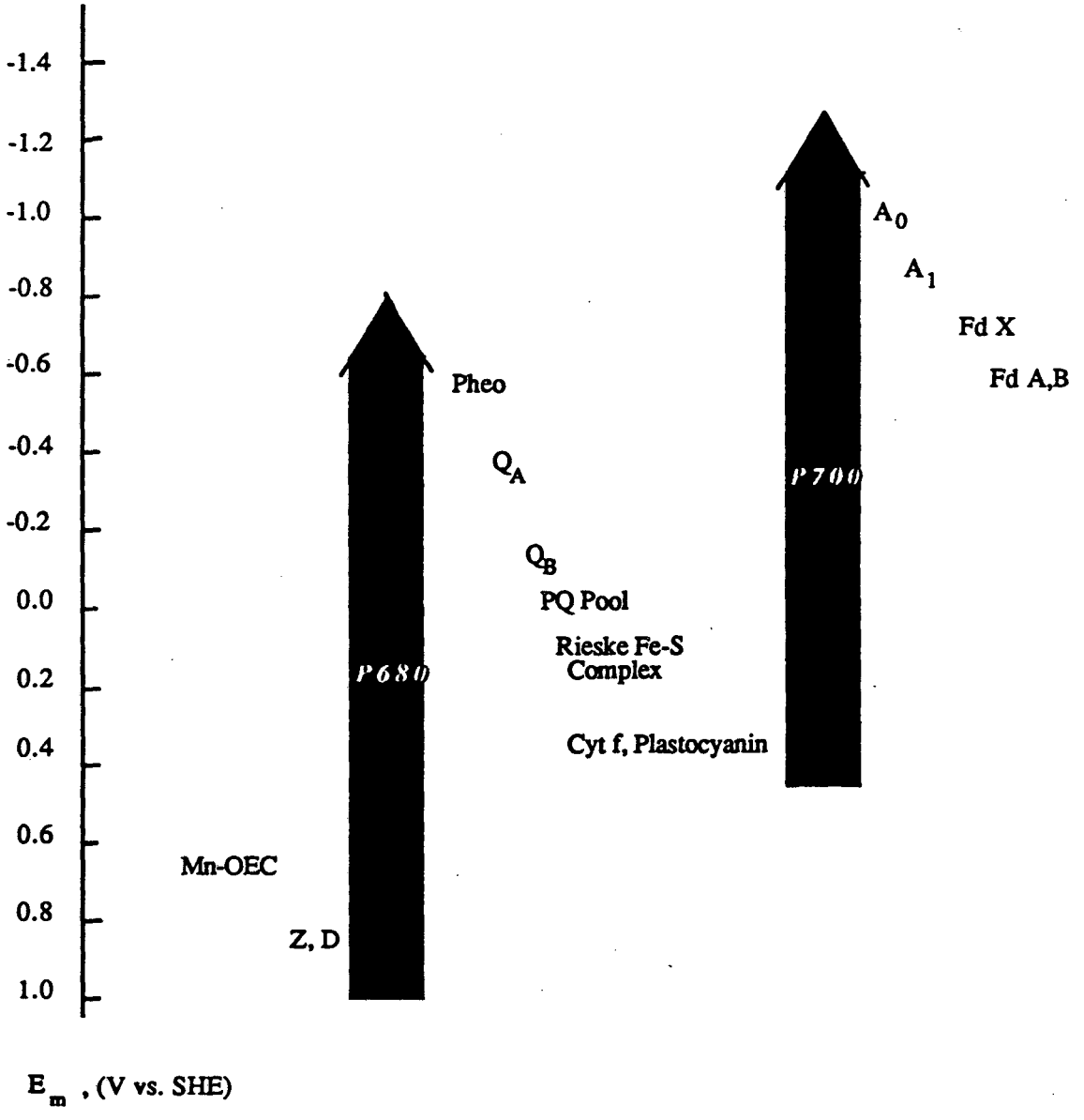

Figure I-1. Z-scheme. The ordinate indicates the reduction potential of the electron transfer components. The lengths of the arrows for P680 and P700 indicate the corresponding photon energy (in eV).

an iron quinone complex with two quinone acceptors, and an intermediate pheophytin species. The protein sequences for the reaction center polypeptides in purple nonsulfur bacteria and PS II are known (Youvan et al., 1984, Williams & Chisholm, 1987, Curtis & Haselkorn, 1984). While much of the sequences is not homologous, the three dimensional folding patterns probably are similar (Trebst, A., 1986), and a few amino acids which are involved in binding donors and acceptors are conserved. (With relatively few amino acids retained, the functioning of the reaction center was preserved. This indicates that the essential features of the reaction centers are relatively simple, which is encouraging for the synthesis of biomimetic solar energy catalysts.) The portions of D1 and D2 that are either altered relative to L and M or are not found in L and M have been discussed in terms of a role in the Mn-OEC (Sauer et al., 1987). The gene sequence homology between PS II and purple bacteria is thought to be sufficient to support the notion that purple nonsulfur bacteria and plants have a common ancestor which made use of the same set of electron transfer cofactors for its reaction center (Hearst, 1986). A similar evolutionary relationship is likely to exist for PS I and green bacteria.

I C. The PS I Reaction Center

Photosystem I (PS I), found in green plants, algae and cyanobacteria, catalyzes light-driven electron transfer reactions from weak oxidants to strong reductants. An excited electronic state of a Chl species bound in PS I (called P700) produces strong reducing equivalents which are ultimately used to reduce CO_2 and form carbohydrates. These electron transfer reactions are mediated by a number of PS I electron acceptors. These include A_0, which is thought to be a chlorophyll species, A_1, which may be a phylloquinone, two ferredoxins in close proximity to each other, called centers A and B and and another species called X of uncertain structure, but which is probably also a ferredoxin (for recent reviews, see Evans, 1982, Rutherford, & Heathcote, 1985). The path of electron transfer among these acceptors is not well understood. Subsequently several soluble mediators are involved, including the soluble [2Fe-2S] ferredoxin and $NADP^+$. Compared with other biological redox components, the midpoint potentials

(E_m, pH 10, vs. SHE) of the acceptors are very low: -530 mV for center A, -590 mV for center B, -705 mV for X (Ke et al., 1973a, Evans et al., 1974, Chamorovsky & Cammack, 1982) and presumably lower for A_0 and A_1. In the hydrophobic protein environment these electron mediators can accumulate strong reducing equivalents without reducing water or oxygen.

P700, A_0 and A_1 are bound on two highly homologous peptides called PSI-A1 and PSI-A2; reaction center preparations containing only these peptides and electron transfer components are generally referred to as CP1 preparations (Thurnauer & Gast, 1985). The sequence of these peptides is known (Fish et al., 1985). Recent evidence suggests that these peptides also bind X (Golbeck & Cornelius, 1986, Warden & Golbeck, 1986). It is likely one copy of each peptide is present per P700, but is it not known which amino acids participate in binding the electron cofactors.

Some specialized Chl species that are associated with PS I have red-shifted absorption maxima, and thus are candidates for P700 or A_0. One is a chloro-chlorophyll called chlorophyll RC1 (Dörnemann & Senger, 1986); others are a Chl a enol (Wasielewski et al., 1981) or a pair of Chl a C10 epimers, called Chl a'. (Watanabe et al., 1985, Hiyama et al., 1987).

Two phylloquinones per P700 are found in PS I reaction centers and seem to be bound on CP1 (Katoh et al.,1985, Malkin, 1986, Schoeder & Lockau, 1986). Several experiments indicate that these are associated with A_1 (Thurnauer et al., 1987, Brettel et al., 1986, Mansfield & Evans, 1986). However, this assignment has recently been disputed (Palace et al., 1987, Ziegler et al., 1987).

The EPR spectra of centers A and B strongly resemble those of the [2Fe-2S], [4Fe-4S] and [8Fe-8S] ferredoxins, having anisotropic signals with $g_{ave} < 2$. Mössbauer spectra indicate that both center A and center B are [4Fe-4S] ferredoxins (Evans et al., 1979). Magnetic interactions between A and B suggested that they are located in close proximity (Evans, 1982). Recently, an 8 kDa protein in PS I has been identified which

has a significant homology to the [8Fe-8S] bacterial ferredoxins (Oh-oka et al., 1987). This protein is presumably the binding site of centers A and B.

The structure of X is unclear. Since X is the subject of much of this thesis, I will review the known spectral and biochemical aspects of X in some detail in I D. The existence of 10-14 irons and 10-13 acid labile sulfides in PS I (far in excess of the amount associated with centers A and B) indicates an Fe-S assignment for X (Golbeck, 1980). At present, the spectroscopic evidence supports such an assignment. To discuss what type of Fe-S center X might be, it is useful to review the classes of ferredoxins and their biochemical and biophysical properties.

I D. A Comparison of Centers A, B and X with Ferredoxins

The ferredoxins are ubiquitous in biology and were probably involved in energy transducing and electron transfer enzymes in the earliest life forms. A variety of cluster types have been discovered, and more examples continue to appear in the literature. For this discussion, we will limit ourselves to clusters that contain Fe and no other metals, as these are most relevant as models for X. Currently the Fe-S clusters fit in the following general categories: [1Fe], [2Fe-2S], [3Fe-xS], [4Fe-4S], [8Fe-8S], HiPIP, and Rieske-type Fe-S centers (Orme-Johnson & Orme-Johnson, 1982, Stout, 1982). The structures of the Fe-S clusters are illustrated in Fig I-2. The clusters are generally ligated by the cysteine residues in the polypeptide to complete a set of four S ligands for each Fe.

EPR spectra and redox potential measurements are useful for describing and catagorizing the ferredoxins. The [1Fe] ferredoxins, or rubredoxins may be thought of as the building block for the other ferredoxins. The iron has an almost tetrahedral symmetry with four sulfur ligands. The midpoint potential for the Fe^{+2} to Fe^{+3} redox transition can be between 0 and -.4 V. In the oxidized form, the S=5/2 ground state gives rise to an EPR signal at g=4.3 (typical for rhombic S=5/2 systems), while the reduced state is also high spin (S=2). Because the reduced form it is an integral spin system, it lacks strong EPR transitions.

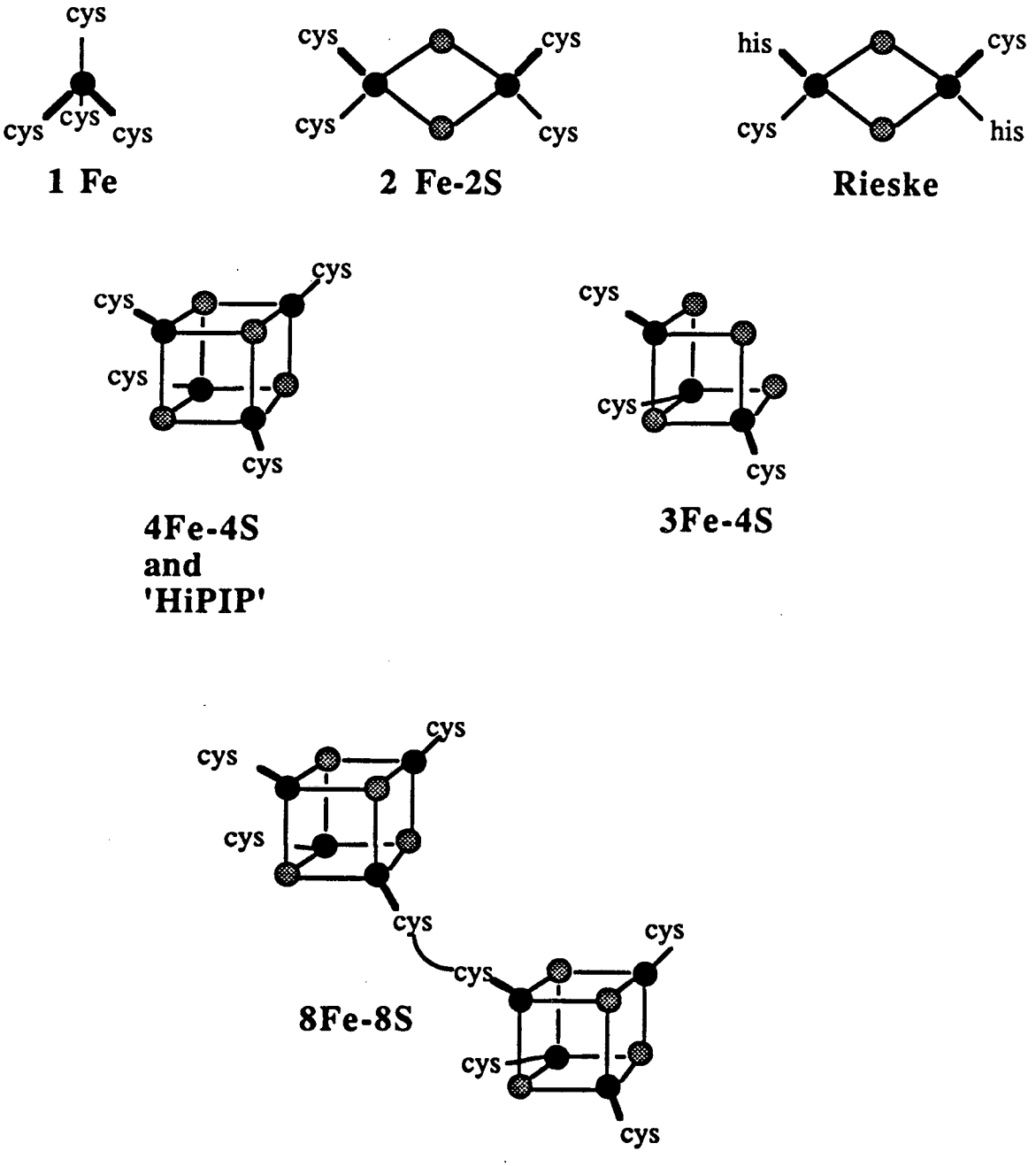

Figure I-2. Core structure for the various classes of ferredoxins. Terminal S ligands are cysteines in the case of proteins or other thiolates in the case of synthetic clusters. All structures except the Rieske and the [3Fe-xS] are known from crystallography. The linear trimeric and distorted tetranuclear clusters (next page) exist as synthetic complexes and have not yet been observed in proteins. They are included here because of possible relevance as models for center X.

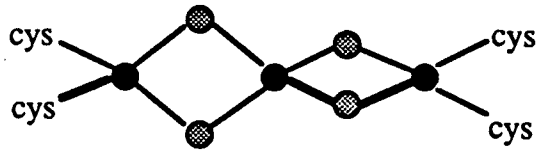

'Linear Trimer'

3Fe-4S

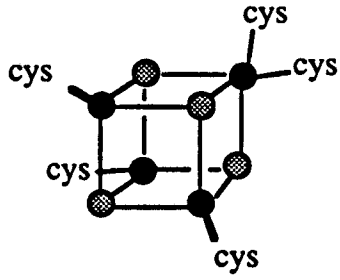

'Distorted Tetranuclear Cluster'

4Fe-4S

Figure I-2., cont. See Figure I-2., pp 11.

The $[2Fe\text{-}2S]^{1+,2+}$ and $[4Fe\text{-}4S]^{1+,2+}$ ferredoxins have many physical characteristics in common. The [8Fe-8S] ferredoxins consist of two [4Fe-4S] clusters in one peptide, and share properties with [4Fe-4S] clusters. The midpoint potentials of [2Fe-2S] and [4Fe-4S] ferredoxins are generally -.25 to -.45 V. All three classes are paramagnetic in their reduced state (1+) and diamagnetic in their oxidized states (2+), due to antiferromagnetic coupling among S=5/2 ferric and S=2 ferrous ions. The reduced ferredoxins generally have S=1/2 ground states with the exception of a few [4Fe-4S] centers that have ground states with higher spin. All of these ferredoxins have anisotropic EPR spectra with $g_{ave} < 2$. This general type of EPR spectrum can be predicted from coupling of two high spin Fe ions; in fact, the EPR spectrum of plant ferredoxins provided the basis for the first correct structural assignment (Gibson et al., 1966). For most [2Fe-2S] ferredoxins the spectra are rhombic with typical g-values being 2.01-2.04, 1.94-1.96 and 1.88-1.94 (Bertrand & Gayda, 1979). For a few [2Fe-2S] ferredoxins the spectra are axial with g-values of 2.02 and 1.94. [4Fe-4S] ferredoxins have rhombic spectra very similar to those of the [2Fe-2S] ferredoxins, with typical g-values of 2.02-2.07, 1.93-1.95, and 1.88-1.92 (Gayda et al., 1981).

In the bacterial [8Fe-8S] ferredoxins, interactions between two [4Fe-4S] clusters (which are 12 Å apart) give rise to a zero field splitting in the EPR spectrum. A detailed analysis of this splitting resulted in the conclusion that the interaction is due principally to an exchange coupling with J=350 MHz (0.012 cm^{-1}) (Schepler, 1975). The dipole-dipole interaction is considerably smaller (ca. 50 MHz). These interactions are thought to be the cause of the changes in the EPR lineshape as the clusters are progressively reduced.

The Rieske-type centers have a [2Fe-2S] cluster, but at least one of the terminal ligands of the cluster is a histidine residue rather than a cysteine (Fee et al., 1984). These clusters are also characterized by rhombic EPR spectra with g-values of 2.01-2.03, 1.87-1.91 and 1.73-1.87 (summarized in Bertrand et al., 1985); these g-values are significantly lower than the other types of ferredoxins. The midpoint potentials of the

Rieske-type Fe-S centers are approximately 0.28 V. The substitution of a less electron donating ligand (N) for S would explain the higher midpoint potential of the Rieske centers. An explanation of the difference in the g-tensor in terms of the existence of a N ligand has also been discussed (Bertrand et al., 1985).

The HiPIP ferredoxins could also be termed $[4Fe\text{-}4S]^{2+,3+}$ ferredoxins; they have the same cluster structure as [4Fe-4S] ferredoxins but attain a different set of redox states in a reversible fashion. The midpoint potential for the 2+ to 3+ transition is approximately 0.35 V. These ferredoxins are also diamagnetic in the 2+ (here reduced) state. The oxidized state (3+) is characterized by an EPR signal near g=2 with a small g-anisotropy; typical g-values are between 2.15 and 2.05 for all three tensor elements.

Finally, the [3Fe-xS] ferredoxins have properties similar to those of the HiPIP ferredoxins; they are EPR active in the oxidized state, and their EPR spectra have a small g anisotropy, with g values between 2.0 and 2.05 (Beinert & Thomson, 1983). For the [3Fe-xS] and the [4Fe-4S] ferredoxins, there is a great degree of delocalization among the iron and sulfur atoms in the valence orbitals (Noodleman & Baerends, 1984). This makes a theoretical treatment of their redox potentials and EPR spectra exceedingly complex.

The EPR spectrum of X is similar to those of [2Fe-2S] or [4Fe-4S] ferredoxins, in that it is rhombic with $g_{ave} < 2$. Like the [2Fe-2S] ferredoxins it has a low mid-point potential. However, its EPR spectrum is broader than those of other characterized ferredoxins, with g-values of 2.11, 1.85 and 1.76. Bolton (1977) has suggested that X may be an iron quinone species by analogy with acceptor species in purple nonsulfur bacteria, which are characterized by very broad EPR spectra. This suggestion was also made on the basis of EPR power saturation studies (Rupp et al., 1979). Power saturation studies probe the homogeneous and inhomogeneous components of signal linewidths. The homogeneous linewidth is often dominant for organic radicals, while for metalloproteins the linewidths are often dominated by inhomogeneous broadening

owing to a large number of unresolved hyperfine couplings or to g-strain. Many ferredoxins are intermediate between these two cases, having a Gaussian broadened linewidth whose underlying Lorentzian components can be retrieved by simulations (Gayda et al., 1976). In their studies of X, Rupp et al. (1979) concluded that X has an appreciable homogeneous contribution to the overall linewidth. They suggested an organic radical assignment for X. In Chapter III I present a re-evaluation of the EPR power saturation and g values of X; in that study I conclude that the EPR properties are consistent with ferredoxin assignment for X.

Mössbauer spectra of PS I preparations (Evans et al., 1981) were interpreted to indicate that X is a [4Fe-4S] ferredoxin. Concomitant with the reduction of X, 17% of the iron in the Mössbauer spectrum of PS I changed in a way that is similar to the behaviour of [4Fe-4S] ferredoxins and dissimilar to that of [2Fe-2S] ferredoxins. Mössbauer spectroscopy is a powerful method for studying ferredoxins; however the studies of X were compromised by a poor signal-to-noise ratio and an apparently incomplete reduction of X. Some of the iron (35%) did not change on reduction of A, B and X. This portion of the iron has been interpreted as X centers which were not reduced (Evans et al, 1981, Bonnerjea & Evans, 1984), and a heterogeneity of X species and a stoichiometry of two X per P700 has been suggested (Bonnerjea & Evans, 1984). However, the proposal of four [4Fe-4S] centers per P700 is inconsistent with the stoichiometry of 10-14 iron atoms and 10-13 acid labile sulfide per P700 (Golbeck, 1980, Lundell et al., 1985). It is known that centers A and B are [4Fe-4S] ferredoxins and are found in a 1:1 stoichiometry with respect to P700 (Bearden & Malkin, 1972, Williams-Smith et al., 1978, Heathcote et al., 1978), and that there are 10-14 irons, 10-13 acid-labile sulfides and 2 phylloquinones per P 700. One can therefore conclude that X involves *at most* two phylloquinones, six irons and five acid-labile sulfides, and probably involves at least two S and two Fe.

Recent core extrusion studies of PS I indicate the presence of [2Fe-2S] clusters in PS I which are likely to be associated with X (Golbeck et al., 1987). Evidence from

EXAFS spectra for the existence of [2Fe-2S] clusters in PS I is discussed in Chapter IV.

Protein sequences are also characteristic of ferredoxin type. In the peptide sequences of [1Fe], [2Fe-2S], [3Fe-4S], [4Fe-4S] and [8Fe-8S] ferredoxins, cysteines are found in a cys-x-x-cys pattern. Within each class of ferredoxin there are additional characteristic or invariant amino acid sequences (reviewed in Stout, 1982). Exceptions to the cys-x-x-cys pattern occur in the the Rieske Fe-S centers, all of which seem to contain a cys-pro-cys-his and a cys-thr-his-leu-gly-cys-val pattern; these unique patterns may be related to the fact that the Fe in the Rieske ferredoxins have one or more histidine ligands rather than all cysteine ligands (Pfefferkorn & Meyer, 1986, Beckmann et al., 1987, Gabellini & Sebald, 1985, Harnisch et al., 1985). There is no obvious homology between CP1-A1 or A2 and the classes of ferredoxins described above; this would tend to support an unusual structural assignment for X.

The ligands for X are likely to be entirely cysteines. N or O ligands are less electron donating than S, and would raise the midpoint potential of X. Since the midpoint potential of X is the lowest known among ferredoxins, the existence of such ligands is unlikely. One copy of each peptide (two peptides total) would provide a total of six cysteines for binding X (Fish et al., 1985), which is sufficient to bind one cluster. It is unclear whether all of these cysteines are in close proximity when the protein is assembled. However, other peptides or additional copies of PSI-A1 and A2 could be involved.

In summary, centers A and B are sufficiently similar to [4Fe-4S] or [8Fe-8S] ferredoxins to allow a definite assignment. Their midpoint potentials (-.55 to -.6 V) are lower than those of other [4Fe-4S] ferredoxins (-.25 to -.45 V). Center X, on the other hand, does not have an obvious assignment. Its EPR and redox properties are more similar to the [2Fe-2S] and [4Fe-4S] ferredoxins than to any other class, but the midpoint potential is quite unusual (-.72 V). Both the cys-x-x-cys and the characteristic Rieske sequence elements are missing in the protein sequence of PSI-A1 and PSI-A2 published by Fish

et al. (1985). Part of the work in this thesis concerns the structure of center X (Chapters III and IV).

Another issue of interest in this thesis is the cause of the low midpoint potential of X. The ferredoxins have a variety of midpoint potentials which are, of course, relevant to their roles as electron transfer cofactors. There has been considerable interest in understanding what controls the midpoint potential of the ferredoxins. There are several hypotheses concerning this question. (i) One parameter which is probably relevant for A, B and X is the hydrophobicity or polarity of the surrounding matrix. All other things being equal, Fe-S clusters (and organometallic species in general) have lower midpoint potentials in nonpolar solvents than in water or other polar solvents. This solvent effect is the most quantitatively studied determinant of midpoint potential in ferredoxins (Hill et al., 1977). (ii) X-ray crystal structures of inorganic [4Fe-4S] complexes indicate the appearance of structural distortions in the clusters upon reduction (Laskowski et al., 1979). This observation has led to the notion that midpoint potentials may be controlled by strains imposed by the proteins which act against these distortions. However, EXAFS measurements of Fe-Fe distances in a variety of Fe-S clusters do not indicate a variation in Fe-Fe distances with redox potential or redox state (Teo et al., 1979). (iii) A specific extension of this idea concerns a variation in cluster distortions which give rise to a variation in antiferromagnetic coupling (Bertrand & Gayda, 1982). A different antiferromagnetic coupling in the reduced and oxidized state can contribute substantially to a shift in the midpoint potential. Separating the electronic energies into an exchange contribution and the coulombic contribution is useful because the exchange coupling can be independently measured. We will return to this idea in Chapter III, as it may be relevant to X. (iv) A variation in the number and strength of S-amine or S-amide hydrogen bonding, and variation in the charge distribution in the protein near the cluster, are thought to affect the midpoint potentials of the ferredoxins. Evidence for this hypothesis is found in the X-ray crystal structures of HiPIP and [4Fe-4S] ferredoxins (Stout, 1982). (v) Substitution or addition of ligands has a profound effect on the midpoint potential.

Addition or substitution of O or N ligands shifts the potential to more positive values (Johnson et al., 1983), while addition of S ligands (to form five-coordinate iron) shifts it to more negative values (Kanatzidis et al., 1983). For X, A and B the hydrophobic environment of a membrane protein is likely to contribute to their low midpoint potentials. Our EXAFS and EPR data can partially address hypotheses (ii), (iii) and (v). Unfortunately, currently we have little data concerning the local protein structure and so cannot address hypothesis (iv).

I E. The Structure of PS II and the Mn-OEC

Photosystem II consists of a reaction center quite similar to the well characterized reaction center of purple nonsulfur bacteria (Deisenhofer et al., 1985), together with a donor complex which extracts electrons from water. The bacterial reaction center and the reaction center of PS II catalyze the light-dependent electron transfer from a specialized chlorophyll pigment to a quinone. The PS II reaction center includes two proteins called D1 and D2 which are homologous to the bacterial reaction center proteins L and M (Hearst, 1986). Like L and M, the D1 and D2 proteins bind the primary electron donor chlorophyll species, a pheophytin transient acceptor (Nanba & Satoh, 1987) and two quinone electron acceptors, Q_B (Pfister et al., 1981) and Q_A (Hearst, 1986). Both the bacterial reaction center and PS II reaction center have associated hemes as well; in the bacterial reaction center the hemes are c-type cytochromes which act as electron donors to the specialized BChl, and in PS II a b-type cytochrome is associated with the donor complex in an enigmatic way.

The donor complex couples the four-electron chemistry of O_2 production from water to the one-electron reactions of the reaction center by serial accumulation of oxidizing equivalents such that oxygen is released on every fourth charge separation step (Joliot et al., 1969, Kok et al., 1970). The coupling of the reaction center to the water-oxidizing complex involves an additional electron transfer species, designated 'Z', which has recently been identified as a tyrosine residue (Barry & Babcock, 1987). The partially oxidized intermediates of the donor complex are called S states; S_1 is the principal S

state of a long-term dark adapted sample, and the S state advances by one on each charge separation of the reaction center until S_4 is produced, which decays to form S_0 and oxygen. This model, the Kok scheme, is often summarized in an 'S-state clock', such as in Figure I-3. In contrast to the products of serial, uncatalyzed, one-electron oxidation of water to O_2, S_1 is very stable, and S_2 and S_3 are stable on the timescale a few minutes (Renger, 1977, Sauer, 1980). A protein bound Mn complex is thought to be the catalyst for water oxidation. A point mutation in D1 interferes with the binding of Mn, suggesting that D1 may provide ligands for the Mn (Metz et al., 1986). In the carboxy terminal region of D1 and D2 there is a region not present in L or M containing many amino acids with carboxylic acid side groups. These amino acids are good candidates for Mn ligands (Sauer, 1987).

A picture has emerged from EPR and X-ray absorption studies of PS II from spinach in which the manganese catalyst is a cluster containing two to four manganese atoms which are primarily Mn(III) and/or Mn(IV). The first spectroscopic signature of the Mn involved in water oxidation arose from the S_2 state and was an EPR signal centered at g=2 with a large number of hyperfine lines, called the multiline signal (Dismukes & Siderer, 1980). This signal is similar to the EPR spectra of a variety of Mn(III,IV) binuclear species with ground S=1/2 states (Cooper et al., 1978, Plaksin et al., 1978, Sheats et al., 1987). Around this time EXAFS difference spectra demonstrated the existence of a μ-oxo bridged Mn cluster in chloroplast membranes (Kirby et al., 1981a), and X-ray absorption K-edge studies demonstrated that the active Mn site has an average oxidation state greater than Mn(II) (Kirby et al., 1981b). A second EPR signal at g=4.1 was subsequently discovered (Casey & Sauer, 1984) and assigned as a Mn species in the S_2 state (Zimmermann & Rutherford, 1986, Cole, et al., 1987a). This signal resembles EPR spectra from the S=3/2 state of axially distorted Mn(IV) monomeric inorganic complexes (Lynch et al., 1984, Magers et al., 1980, Richens et al., 1979). ESE NEM studies of the multiline signal indicated little modulation by nitrogen ligands, suggesting mostly oxygen ligands for the manganese (Britt et al., 1987). Yachandra et al. (1986b)

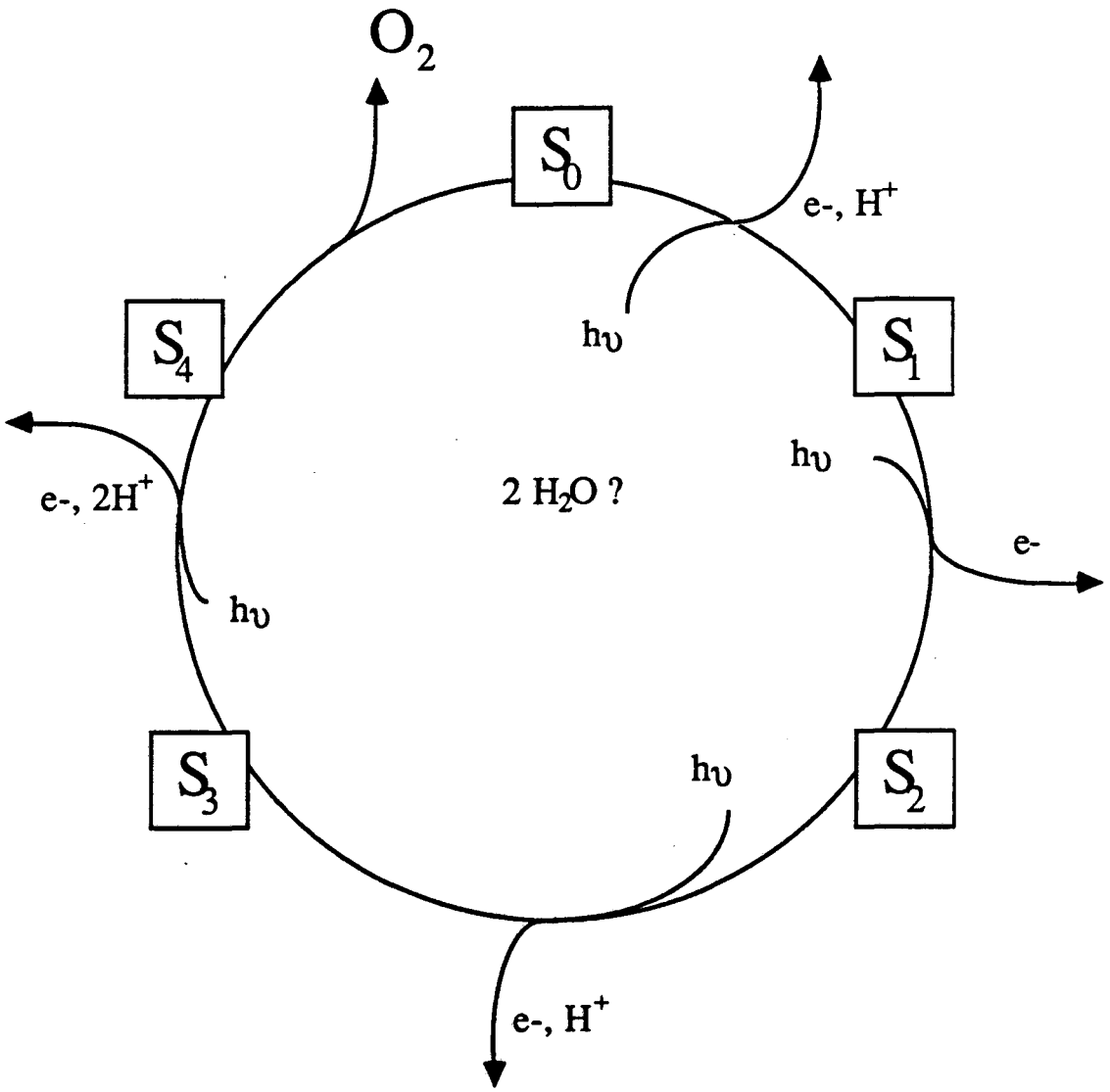

Figure I-3. The S-state clock, describing catalysis of water oxidation by the Mn-OEC. S_1 is the dark-stable state of the OEC. Four S state conversions, 0-1, 1-2, 2-3 and 3-4, are driven by electron abstraction by the PS II reaction center. This electron abstraction is, in turn, driven by a light-induced charge separation in the PS II reaction center that generates powerful oxidants on 'Z'. The spontaneous decay of S_4 to produce S_0 is accompanied by release of O_2. The S-states at which water binds remains controversial.

concluded that there are no exchangeable halides directly ligated to the multiline Mn species. Recent EXAFS and X-ray absorption edge studies have addressed the issues of nuclearity, ligand identity and valence in PS II particles. Yachandra et al. (1986a, 1987) report 1) the presence of a μ-oxo bridged Mn complex 2) an average valence between Mn(III) and Mn(IV) for the S_1 state 3) an oxidation of Mn by one to two equivalents per reaction center in the S_1 to S_2 transition, without an apparent change in structure and 4) ligands for the Mn complex which are mostly O and N.

I F. Motivation for a Comparison of PS II from Prokaryotes and Eukaryotes

Although most of the spectroscopic characterization of the Mn in PS II has focussed on the more easily prepared spinach PS II, in some respects it is more useful to work with prokaryotic sources of PS II. For example, isotopic labeling and site specific genetic modifications provide useful techniques for studies of ligand identity and are most conveniently done with a prokaryote. These techniques are most pertinent to addressing the nature of the terminal ligands of the cluster, which are poorly defined in the spectroscopic studies to date. The EXAFS spectra are dominated by features due to the the μ-oxo ligands and Mn neighbors, and features due to the terminal ligands are washed out because of disorder.

A detailed comparison of the spectral properties of the Mn complex in PS II between cyanobacteria and plants is lacking. Therefore, before beginning to do spectroscopic work on prokaryotic PS II, it is useful to conduct a systematic comparison of the EPR signals in the cyanobacteria and spinach. This is the focus of Chapter V.

Chapter II: Methods

II A. X-ray Absorption Spectroscopy

II A. 1. General Introduction to X-ray Absorption Spectroscopy

X-ray absorption spectroscopy has been used to study a variety of metalloproteins (reviewed in Powers, 1982, & Teo, 1986). X-ray absorption spectroscopy includes the measurement of bound state transitions from core electronic states of the metal to excited electronic states or continuum states, which is X-ray edge spectroscopy, as well as the study of the fine structure in the absorption cross section at energies greater than the threshold for electron release, which is Extended X-ray Absorption Fine Structure (EXAFS). These two measurements give complementary information, the edge spectra reporting oxidation state and symmetry and the EXAFS reporting numbers, types and distances to ligands and neighboring atoms. The great strength of these techniques is that the approximate transition energies are characteristic of the absorbing atom, so that one may probe a given element specifically. In addition, the transitions can always be measured; the intensities of the transitions are not sensitive to relaxation rates.

The X-ray K-edge inflection energy is an indicator of the coordination charge of a metal. The K-edge inflection energy of a first-row transition metal principally reflects the 1s to 4p transition energy convolved with the 1s ionization energy (Kutzler et al., 1980; Schulman et al., 1976). The sense of this shift with coordination charge can be derived from a simple electrostatic model involving orbitals with spherical charge distribution in which one imagines promoting charge from the inner shell to an outer orbital. The total energy difference for promotion decreases with increasing electron density in outer and intermediate orbitals. These edge shifts have been extensively studied, and in general a more reduced metal or a metal with more electron donating ligands is characterized by a lower edge inflection energy and a lower energy for bound

state transitions (Cramer et al., 1976; Kirby et al., 1981; Nigam & Srivastava, 1971). This correlation allows an approximate oxidation state assignment for the metal when the nature of the ligands is known.

The structure of the absorption spectrum near the X-ray absorption edge yields symmetry information. Spectra of a variety of complexes have been studied (Srivastava & Nigam, 1972). The probabilities for the bound state transitions depend on ligand field symmetry and ligand types *via* the mixing of the hydrogenic one electron orbitals. For example, the 1s to 3d transition, which is formally unallowed, becomes prominent in complexes with non-centrosymmetric geometries because of p-d mixing and is systematically larger in tetrahedral complexes than in octahedral complexes (Roe et al., 1984). A quantitative treatment of near-edge structure based on spectroscopic tables or based on X-alpha calculations has been attempted; for systems that are largely ionic the predictions have been more successful (Shulman et al., 1976; Kutzler et al., 1980; Natoli et al., 1980).

X-ray absorption fine structure (EXAFS) refers to the broad oscillations in absorption cross-section past the X-ray absorption edge of an element. The oscillations occur when photoelectrons that are emitted in the direction of a neighboring atom are scattered by the neighbor back to the emitting atom. As the wavelength of the photoelectron is tuned by scanning the incident X-ray energy there are maxima in the X-ray absorption cross section when the interference of the outgoing and the backscattered photoelectron waves is constructive, and minima when the interference is destructive. For each type of neighboring atom one observes an almost sinusoidal oscillation in the absorption cross-section as a function of photoelectron wave vector, k, and the frequency of this oscillation can be used to measure interatomic distances very accurately. The exact envelope of the oscillation pattern, the phase of the oscillation, α, and the detailed dependence of the phase on k, are functions of the nuclear charge of the neighboring atom. These parameters can be used to determine the chemical identity of the scattering atoms. This description pertains to single scattering processes, i.e. processes that

involve interactions with only the (X-ray) absorbing and (photoelectron) backscattering atoms. Multiple scattering processes, which involve interactions with an intervening atom before the electron backscatters off a third atom, have also been described (Teo, 1986).

The theory of EXAFS resulting from single scattering is well understood. The dependence of the EXAFS oscillations on the neighbor type and bond distance is expressed in eqn. 1 (Teo, 1986). The oscillations from all of the backscattering atoms are summed.

eqn. 1 $$\chi(k) = \frac{(\mu(k)-\mu_s(k))}{\mu_0} = S_f \sum_j N_j |f_j(\pi,k)| \frac{\sin[2kR_j+\alpha_j(k)]}{kR_j^2} e^{-\sigma_j^2 k^2} e^{-2R_j/\lambda(k)}$$

In this equation, χ is the normalized EXAFS spectrum as a function of k, the photoelectron wavevector; μ is the measured X-ray absorption; μ_s is the smooth background in the absorption; μ_0 is the absorption of the free atom; S_f is a chemically independent scaling factor for the scattering amplitudes which is empirically derived; N_j is the number of atoms in the j^{th} scattering atom group; $f_j(\pi,k)$ is the calculated back-scattering amplitude for the j^{th} scattering neighbors; R_j is the distance from the absorbing atom to the j^{th} scattering atom(s); α_j is the photoelectron wave phase shift due to interactions with the absorbing and scattering atoms; σ_j, the Debye-Waller factor, is the mean square deviation in the absorber/scatterer bond distance, and λ is the photoelectron mean free path.

Eqn 1 can be used to simulate EXAFS spectra. The amplitude, $f_j(\pi,k)$, and phase, $\alpha_j(k)$, functions have been calculated by Teo and Lee (1979) for most elements and agree well with experimental results, apart from the overall scaling factor, S_f. Curve fitting analysis of EXAFS spectra, using calculated or experimentally derived functions for these parameters, has been used with great success in the study of metalloproteins to obtain accurate metal-to-ligand distances and information about types of neighboring atoms (Powers, 1982). A review of the EXAFS technique is available (Teo, 1986).

II A. 2. X-ray Absorption Data Collection

The X-ray absorption measurements are somewhat analogous to optical absorption and fluorescence excitation measurements. The spectrometer consists of a source (Synchrotron radiation), a monochromator (a Bragg diffraction device), a measurement of incoming flux (an ion chamber, or a photomultiplier tube measuring scattering), a sample, and measurements of transmitted flux and fluorescence at 90°. In addition, a reference compound may be measured using the 'leftover' radiation in-line and downstream from the sample. In this case two additional detectors (also ion chambers) are included downstream from the sample. Figure II-1 is a diagram of the experiment. Here we will briefly discuss the qualities of the radiation source, the characteristics of the monochromator and the details of fluorescence detection. We have recently studied the relative merits of energy resolved and unresolved X-ray absorption measurements for dilute Mn samples. This discussion of fluorescence detection will document some of our conclusions.

The synchrotron radiation is the Bremstrallung radiation produced by the acceleration of relativistic electrons by magnetic fields. This radiation spans frequencies from sub-optical to hard X-rays. The X-ray intensities generated by this means are significantly higher than those from any other X-ray source; this technology makes X-ray absorption measurements of dilute metals feasible. The characteristics of the electron beam and of the magnets used are significant in determining the quality of the radiation for spectroscopy. The use of many magnets in succession, a wiggler source, increases the intensity of the X-rays dramatically. The intensity and spectrum of the radiation are approximately determined as follows. The synchrotron radiation rapidly decreases in intensity near the cutoff energy, E_c. This cutoff energy is proportional to the magnetic field of the bending or wiggler magnet and the cube of the electron energy. Below the cutoff, the intensity at any energy is roughly proportional to the current in the storage ring, the magnetic field and the number of poles in the wiggler. For relatively high magnetic fields the spectrum below the cutoff energy is relatively flat, and the lower cutoff is

Figure II-1. Schematic of the instrumental apparatus for X-ray absorption measurements. Synchrotron radiation is focussed by a mirror and rendered mono- chromatic by Bragg reflection from a pair of channel-cut crystals. Beam intensity is measured at I_0, I_1 and I_2, and sample fluorescence is monitored at right angles to the measuring beam. The monochromator is controlled from the computer (PDP-11) and the data, after voltage-to-frequency conversion and digitization, are stored by the computer.

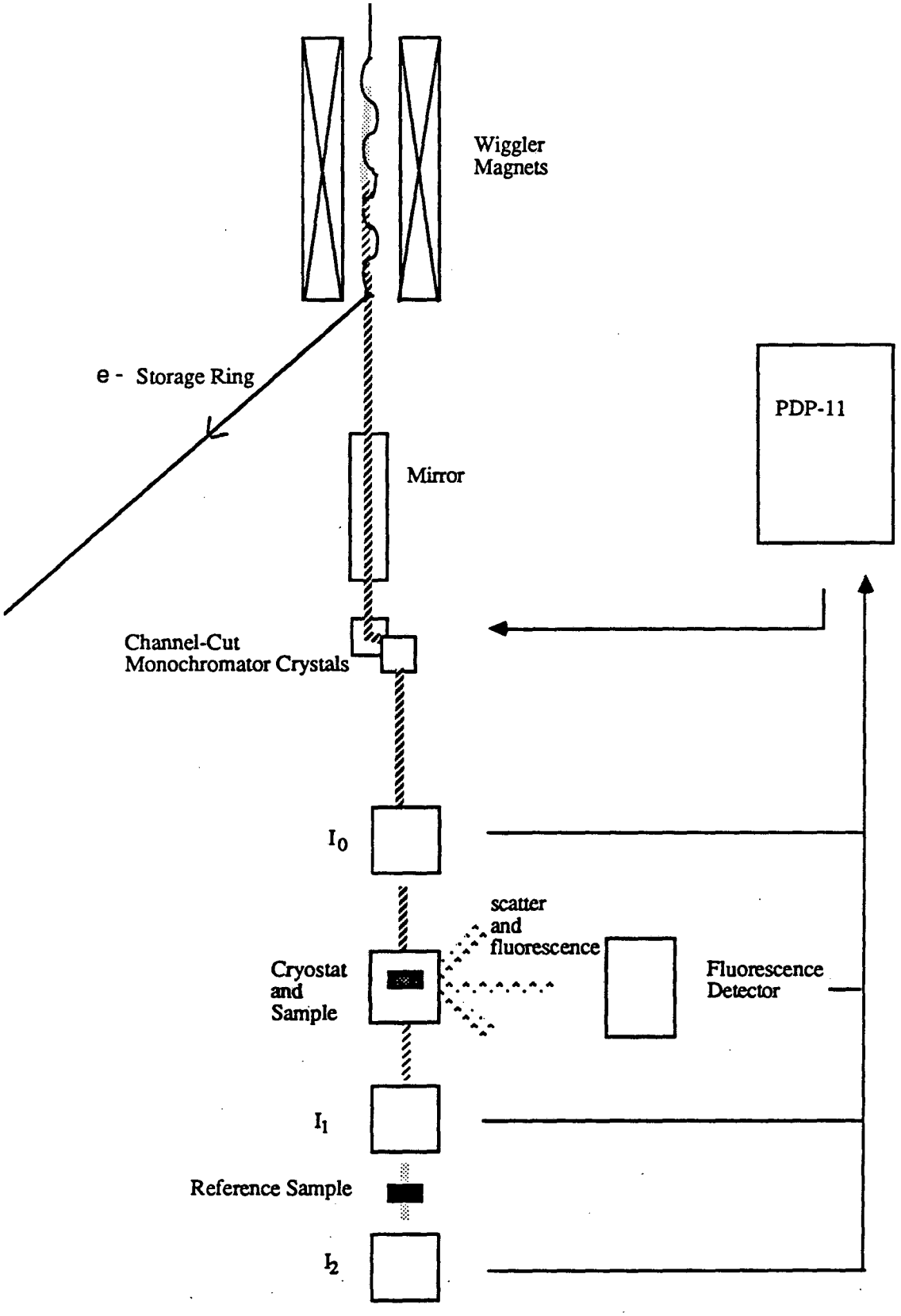
Wiggler
Magnets
e - Storage Ring
PDP-11
Mirror
Channel-Cut
Monochromator Crystals
I_0
scatter
and
fluorescence
Cryostat
and
Sample
Fluorescence
Detector
I_1
Reference Sample
I_2

determined by the attenuation of the beam path (windows, gas etc.). For lower magnetic fields, peaks are apparent in the radiation spectrum; these occur for wavelengths such that in the relativistic frame of the electron the magnet pole spacing matches a multiple of the wavelength of the emitted X-ray. The width of these features is sensitive to a number of experimental parameters including the wiggler field, and when the magnetic field is in the normal operating range these features are too broad to be observed. Of all experimental the experimental parameters mentioned above, only the wiggler field is under the user's control, and that only by an involved procedure. Nonetheless, these parameters are all worth noting.

The monochromator consists of a matched pair of parallel crystals that disperse the X-rays by Bragg diffraction. They can be rotated together, and the angle of the total assembly then determines what X-ray energy is passed in-line with respect to the incident white radiation. Many different types of crystals are available, and it is important to make a careful choice of crystal type. The relevant variables are whether they 'pass' beam harmonics, what their spectral resolution is, and whether they possess 'glitches'. The energy resolution of the monochromator (or the Darwin reflection width) is best for crystals with a small separation between the diffraction planes. The presence of harmonics is undesirable because they degrade the linearity of the detectors, especially if a different type of detector is used for the initial flux measurement and the fluorescence measurement. If the crystals do pass harmonics, the relative proportion of fundamental to harmonic in the beam may be adjusted by rotating the crystals relative to one another in the azimuthal plane. This adjustment is called 'detuning'. For very small rotation angle, detuning generally causes a more dramatic loss of the harmonic radiation than of fundamental radiation. 'Glitches' refers to orientations during normal operation in which additional Bragg planes come into alignment and diffract away a considerable portion of the beam. They are apparent as sharp dips in the intensity of the beam as the energy is scanned. Because no set of detectors is perfectly linear, these dips in intensity give rise to discontinuities in the data; thus the term crystal glitches. The only

currently available set of crystals that lack large glitches in the Mn EXAFS region is the Si < 400 > crystals.

A reflecting mirror may be present in the beam, generally upstream from the monochromator. This mirror can focus a larger portion of the synchrotron radiation onto the monochromator crystals and thus increase the flux, generally by a factor of approximately 5. Because the radiation is then focussed and not parallel, the mirror may degrade the energy resolution of the monochromator. The mirror may also selectively absorb higher energy X-rays, depending on the reflection angle and the energy of the harmonics. This property is useful for removing beam harmonics.

For dilute samples, fluorescence detection has an enormous advantage over absorption measurements (Jaklevic et al., 1977). If one looks at the radiation emitted from the sample at right angles to the excitation, there are many components arriving at the detector. These are illustrated in Fig II-2 for the example of dilute Mn measurements. In addition to Mn 2p-1s fluorescence (Mn $K\alpha$ and $K\beta$ fluorescence), there is scattering from the carbon matrix and scattering or fluorescence associated with beam harmonics (the harmonics are not included in Fig II-2).

These other beam components contribute to noise and to artifacts and it is obviously desirable to select for fluorescence for the metal of interest, which in our case is Mn or Fe. When measuring an element of atomic number Z, a foil made of the element of atomic number Z-1, when placed between the sample and detector, can markedly reduce the scattered radiation (Stern & Heald, 1979). Such a foil has the property of absorbing the scattered radiation and passing the fluorescence. For example, for a 1 mM Mn sample, a 0.0013 cm (0.5 mil) Cr foil can reduce scattering from the matrix from 20-50 times the Mn fluorescence to 3-6 time the Mn fluorescence (depending on exact geometry of the apparatus). However, the foil will also fluoresce, so the characteristic fluorescence of the Cr foil is shown on Fig II-2. Despite the fluorescence of the foil, there is a tremendous improvement in signal-to-noise ratio.

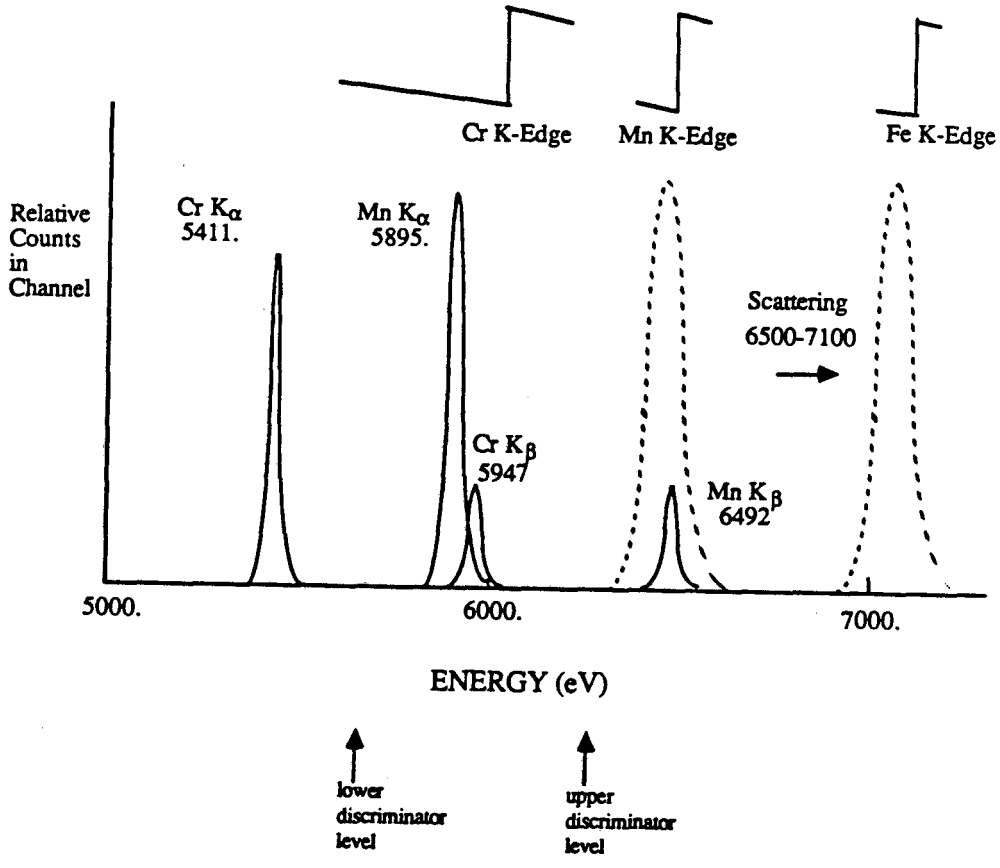

Figure II-2. Cartoon of the components of the radiation arriving at the fluorescence detector from a dilute Mn sample, with the energies of K-edge features. The Cr fluorescence features result from absorption of scattered X-rays by a thin Cr filter, followed by fluorescence of the Cr. During data collection with the Si:Li detector, all pulses between the indicated discriminator levels are counted. Actual peak widths when measured with the Si:Li are 330 eV fwhm, significantly wider than those shown.

The choice of the detector depends on three main features, which are the maximum count rate the detector can process linearly, the energy resolution of the detector and the active area of the detector element. In general there is a trade-off between these three variables. For example, good energy resolution generally implies slower count rates (as will be discussed later). Which variable is most important depends on the nature of the experiment. Dilute samples (*ca.* 2 mM in metal or less) result in a large scattering background as compared with the fluorescence counts. The fluorescence-to-scatter ratio (F/S) is particularly low for elements with lower atomic number. This is because the fluorescence quantum yield increases with increasing Z. EXAFS measurements of dilute, low-Z elements are subject to artifacts associated with the scattering. These artifacts are not always removable by computer fitting techniques or subtraction techniques. In this case it is useful to use an energy discriminating detector to remove the scattering background. On the other hand, measurements of concentrated samples and measurements of heavier elements generally have much more fluorescence than scatter and can give rise to relatively high fluorescence count rates. In this case it is not so important to discriminate between scatter and fluorescence, and it is desirable to have a fast detector. Here 'fast' counting means *ca.* 10^5 to 10^7 cps and 'slow' would be *ca.* 10^2 to 10^4 cps. In Appendix I, I estimate the counting rates we expect for a Mn X-ray experiment to illustrate what factors determine the counting rate of our experiment. These calculations, which agree approximately with our measurements, indicate that we are generally in the slow regime, and that we have considerably more scatter than fluorescence.

The choice of the detector active area presents its own trade-off: a larger active area (or solid angle subtended) receives a greater the fluorescence rate, but with a worse scatter-to-fluorescence ratio. The latter is true because, due to the polarization of the X-ray beam, elastic scattering of the sample does not have a spherically symmetric spatial distribution and is smallest at right angles to the incoming beam. In contrast, the fluorescence is approximately spherically symmetric. An attractive solution to the

question of detector size is to have an array of small detectors, so that the channels may be individually inspected. In addition, the inherent count rate limitations of the detector may apply to each element separately if the associated electronics is appropriately designed. Thus, if the count rate is limited by the detector and not the sample and beam intensity, the use of may elements may substantially improve the signal-to-noise ratio by improving the total count rate. Of course it will also similarly 'improve' the cost of the device...

Since much of our work concerns dilute Mn samples, we are interested in energy resolving detectors. Therefore, the advantages of energy resolution will be examined in some detail here. Figure II-2 illustrates that the Mn Kα fluorescence may be separated from the Cr Kα fluorescence and the scattering with relative ease, but that the Mn Kα fluorescence and the Cr Kβ fluorescence are quite close and that the Mn Kβ fluorescence is quite close to the scattering at the beginning of the scan. Realistic energy resolution will separate the peaks which are *ca* 500 eV apart, but not those that are 50 eV apart. Thus our energy resolved measurements will include Mn Kα and Cr Kβ fluorescence, but not Mn Kβ fluorescence.

The detector and associated electronics which were used in these measurements are shown in Fig II-3. The detector element consists of Si with a Li diffused layer (Si:Li detector) to which a large voltage (1 KV) is applied. This detector has been described (Goulding et al., 1983). The Si:Li output is a current pulse whose total charge is proportional to the energy of the incoming X-ray. The purpose of the amplifier is to output narrow, shaped pulses whose voltage is proportional to the charge output of the Si:Li (Goulding et al., 1983). Such pulses may be used to develop a histogram of beam components (such as the cartoon in Fig II-2). Alternatively, the pulses in a selected voltage range may be selected by a discriminator and counted, which is the process by which energy resolved data are collected.

The Si:Li and associated amplifier have a characteristic trade-off between energy resolution and count rate. The count rate limitation depends on amplifier output pulse

Figure II-3. Experimental arrangement used for fluorescence detection. The core of the electronics is the amplifier which outputs a shaped pulse with a voltage proportional to the total charge in the detector output pulse. These pulses then can be counted in selected windows by the discriminator. Rateme-ters may be used to check the linearity of the amplifier, using the 'fast out' as a measure of the input rate. A pulse height analyzer may be used to monitor the histogram of pulses yielding a profile roughly like the cartoon in Fig II-2. The usual settings are also indicated.

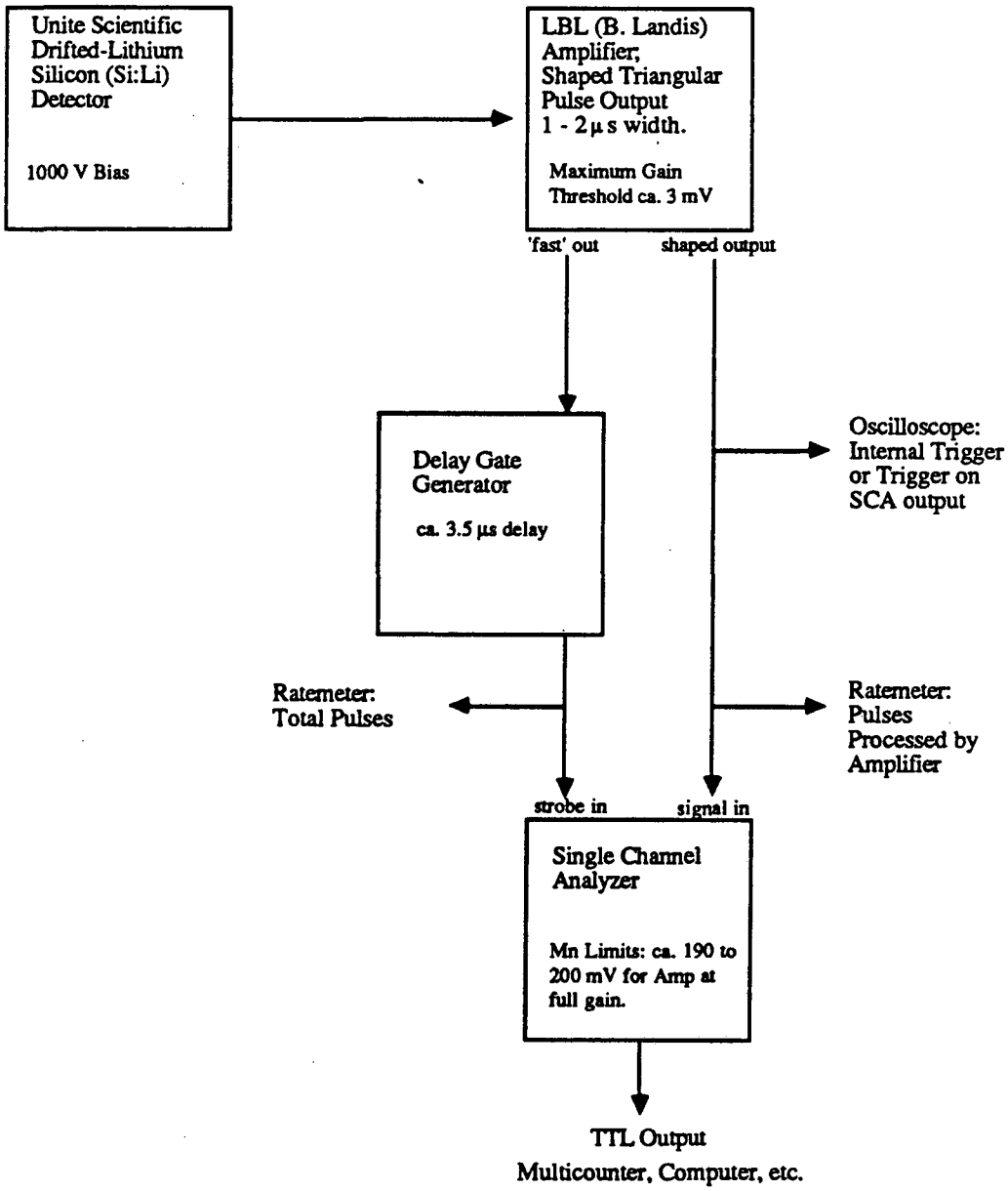
Unite Scientific
Drifted-Lithium
Silicon (Si:Li)
Detector
1000 V Bias
LBL (B. Landis)
Amplifier;
Shaped Triangular
Pulse Output
1 - 2 μs width.
Maximum Gain
Threshold ca. 3 mV
'fast' out
shaped output
Delay Gate
Generator
ca. 3.5 μs delay
Oscilloscope:
Internal Trigger
or Trigger on
SCA output
Ratemeter:
Total Pulses
Ratemeter:
Pulses
Processed by
Amplifier
strobe in
signal in
Single Channel
Analyzer
Mn Limits: ca. 190 to
200 mV for Amp at
full gain.
TTL Output
Multicounter, Computer, etc.

width. It is desirable that the amplifier output count rate be proportional to the incoming X-ray count rate. However this is not necessarily so if pulses are sufficiently broad and frequent that they begin to overlap. To avoid count rate nonlinearities that result from overlapping pulses, it is necessary to limit the incoming flux to approximately $1/10\tau$ cpm, where τ is the baseline-to-baseline pulse width (within experimental error, which is ca. 95% of signal amplitude recovery). It is also possible to use the detector under nonlinear conditions and empirically correct for the detection nonlinearities. In this case, one would choose a count rate which would result in the maximum signal-to-noise ratio. (As pointed out by Dr. Jaklevic, LBL, the S/N is likely to be best at a counting rate at which $[\delta O/\delta I]\sqrt{O}$ is maximized, where I is amplifier input count rate and O is the amplifier output count rate.) This approach would allow one to count considerably faster, but was not initially adopted. Whichever approach is taken, shorter pulses are necessary for faster counting rates.

However, as the pulse width is narrowed, the noise associated with measuring the pulse voltage increases. This is because some of the components of the amplifier have high frequency noise output which is convolved with the pulses (Goulding et al., 1983). The noise in the pulse height measurement gives rise to an approximately gaussian shaped distribution of voltage pulses for a narrow incoming X-ray pulse; this gaussian width determines our ability to resolve X-rays of various energies. The peak widths for the detector will be characterized here by the full width at half maximum (fwhm) expressed in terms of the energies of the corresponding X-rays in eV. This width is conveniently measured on a pulse height analyzer, as indicated in Fig II-3. To decide what combination of energy resolution and count rate is ideal for our experiment, it is necessary to first evaluate our energy resolution needs, and our count rate needs, and decide whether they can be simultaneously accommodated.

How does the S/N depend on the energy resolution for realistic energy resolutions? To illustrate this dependence, I made some simplifying assumptions. I assumed that the discriminator levels used in the experiments were fixed at values midway between

the Mn Kα peak and the Cr Kα peak, on the low side and midway between the Mn Kα peak and 6500. eV on the high side, as illustrated in Fig II-2. In addition, I assumed that the Cr fluorescence rate and the scattering rate were both twice the Mn fluorescence rate. This is typical for the experimental conditions for photosynthetic preparations. I assumed that the solid angle subtended by the detector was constant for all measurements and the the incoming flux was constant (i.e. no 'detuning'). I assumed that the peak widths are gaussian, and that the S/N is given by $F/\sqrt{T}$ where F is the Mn fluorescence count rate in the discriminator window, and T is the total count rate in the discriminator window (i.e. scatter plus Cr and Mn fluorescence). These rates were evaluated using tabulated values for integrals of gaussian functions for various assumed peak widths. With all these assumptions, the S/N was calculated as a function of peak width, and was expressed relative to the S/N that would be obtained without energy resolution. The results are plotted in Fig II-4.

While the exact functional form depends on making an accurate model of the experiment, the general shape of the function in Fig II-4 illustrates several points. One observation is that if the energy resolution is very bad (fwhm approximately equal to or greater than the peak separation) the use of energy discrimination actually reduces the S/N because the discriminator reduces the total count rate. Another observation is that increasing the energy resolution beyond a point has a diminishing improvement on the S/N; this occurs when the fwhm is less than approximately one-third of the peak separation. In the intermediate range the S/N depends on the energy resolution in a relatively significant way. Thus it is apparent that we desire an energy resolution with fwhm significantly smaller than the relevant peak separations, but not necessarily smaller than one-third the peak separation (i.e. we want 200-300 eV for Mn fluorescence). The third observation is that even with ideal energy resolution, the S/N improves only by slightly more than a factor of two. In reality, the energy resolving detector may have a smaller active area than a non-resolving detector and will have serious count rate limitations; thus it is not realistic to expect a great improvement in S/N by the use of an

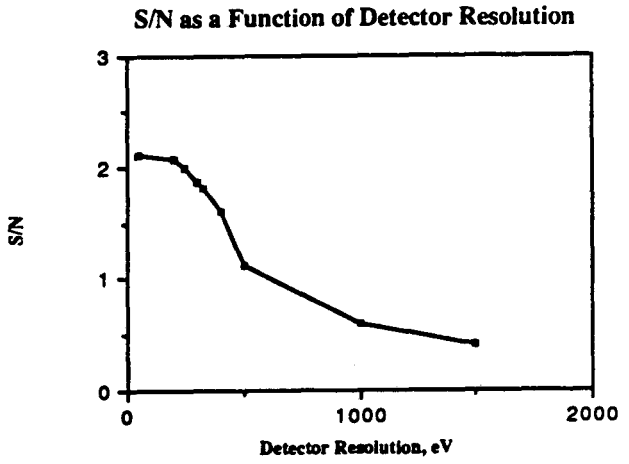

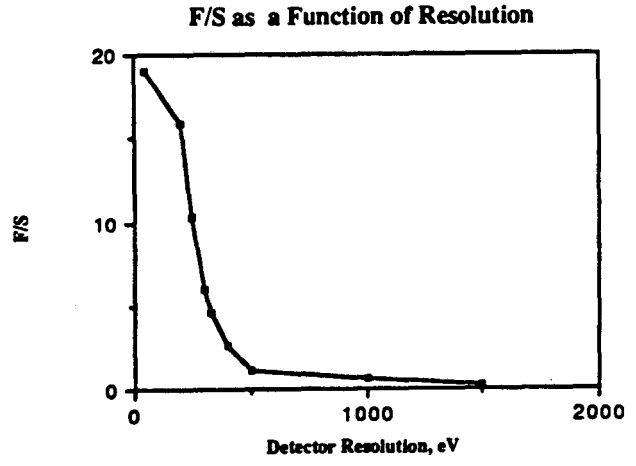

Figure II-4. Dependence of signal-to-noise ratio and the fluorescence-to-scatter ratio on the fwhm peak widths of the detector and amplifier assembly. The S/N ratio is relative to a predicted value for data collected without energy resolution. These values were estimated assuming a gaussian shape for the peak histograms and a square function for the discriminators.

energy resolving detector. However, there is another very important reason for using an energy resolving detector, which is that in some cases it will alleviate the problem of artifacts in EXAFS data because the scattering, the fluorescence of the Cr filter and the associated Cr EXAFS are removed. Figure II-4 illustrates the ratio of Fluorescence to Scatter (F/S) as a function of detector resolution, which was estimated with a similar set of assumptions as was the S/N. The F/S ratio is probably indicative of the ratio of EXAFS features to troublesome artifacts. This ratio is essentially equivalent to the figure-of-merit defined by J. Stöhr (1987), which he used to compare X-ray detectors. It is apparent that the F/S ratio is a very strong function of resolution. Almost any extent of energy resolution may help to remove artifacts, especially if they arise more from the harmonics than the fundamental.

The other consideration in the choice of energy resolution is the count rate needed. This is also determined by the requirements for a good signal-to-noise ratio, and the requirement that we be able to collect the data in less than six years. EXAFS oscillations as small as 1% of the total edge height may be important for analysis. Therefore one would like to collect a S/N of at least 200 in the final summed spectrum. If we would like to collect less than 100 scans, each scan should have a S/N of at least 30. This implies that a fluorescence count rate of approximately 1000 cps is needed in order to collect analyzable or ideal EXAFS within a finite amount of time. So, if the samples and the beam intensity can generate a fluorescence rate of 1000 to 5000 cps at the detector, it is very desirable that the detector accommodate the full count rate in its linear range.

In fact, with the current typical range of Wiggler intensities on BL VI-2 and IV-2, and with our typical experimental geometry, the active area of the Si:Li receives approximately 2000 to 6000 cps of Mn fluorescence at the top of the Mn K-edge from photosynthetic membrane samples containing 0.5 to 0.8 mM Mn. Typically there is three to ten times as much scatter at the detector as there is fluorescence in our experiments. Appendix I contains some calculations that illustrate the factors determining these count

rates. These rates imply that it is desirable to have a detector which can accommodate up to approximately 10,000 - 50,000 cps total in its linear range.

Using an amplifier such as that described previously (Goulding et al., 1983) and an appropriate shaping time, (peak width baseline-to-baseline of 5 μ-sec), the Si:Li detector can accommodate a count rate of 40,000 linearly (within 5%) and at the same time provide energy resolution with a fwhm of approximately 330 eV. This combination of qualities is ideal for our experiment, because we can reduce the background scattering from approximately 4 times the fluorescence to one fifth of the fluorescence and still collect an acceptable S/N ratio. Indeed, data collected with such a small scattering background have been simulated with much more success than data containing a lot of scattering. Background removal at the detector has many advantages over background removal at the computer terminal!

For fast X-ray photon counting without energy resolution we used a NE104 plastic scintillation array similar to that described previously (Powers et al., 1981). This detector uses a scintillating plastic to convert X-ray photons to bursts of photons of energy approximately 3 eV (ca. 400 nm). These photons are then detected with a high-gain photomultiplier tube. The pulses from the photomultiplier are quite narrow, approximately 50 ns baseline-to-baseline. Therefore, counting rates up to 2 MHz are possible. (This rate is close to inherent rate limitations related to the bunched structure of the electrons in the storage ring.) The number of photons that result from an X-ray photon depends on the energy of the X-ray. One might then expect that the current output of the photomultiplier could be used as a basis for energy discrimination. In addition to the presence of high frequency noise associated with amplifiers and pre-amplifiers (as described in reference to the Si:Li detector), this detector has another source of peak broadening related to counting statistics. If one assumes that a 6 KeV photon is converted to 3 eV photons with a 20% yield at the photomultiplier, then each X-ray would result in approximately 400 U.V. photons. Counting statistics then would predict that we would not receive exactly 400 photons, but a distribution with a fwhm of 46

photons. (The fwhm is 2.3 times the root of the number of photons). Therefore we would have a distribution in pulse heights corresponding to apparent energies of 6000 eVx46/400, or 700 eV. This resolution is useless for discriminating between scatter and Mn fluorescence. However, it might be used to discriminate between visible light or dark counts and X-rays, and it may be used to discriminate between fundamental and harmonic. The photomultiplier pulses due to 6.5 KeV X-rays are approximately 50 to 100 mV in amplitude. Since most discriminators only accommodate threshold values of 50 mV and greater, it is convenient to use an amplifier between the photomultiplier and the discriminator.

The specific details of data collection for the spectra included in this thesis are described below. The Fe EXAFS and X-ray edge spectra reported here were collected at the Stanford Synchrotron Radiation Laboratory on beam lines VII-3 and IV-1 (unfocused Wiggler lines with energy resolution of about 1 eV) using a set of Si(111) monochromator crystals provided by SSRL. Electron energies were 3.0 GeV with ring current between 20 and 90 ma. The EXAFS and edge data are fluorescence excitation spectra (Jaklevic et al., 1977), collected using the NE104 plastic scintillator array. Between the sample and the detector, a Mn filter and Soller slits were used to select for fluorescent photons from Fe. The signal from each photomultiplier was input into a constant fraction discriminator. The photomultiplier count rates were roughly 10^4 to 5 x 10^4 sec^{-1}, a range where the response is linear. An absorption spectrum of $K_3Fe(CN)_6$ was simultaneously monitored, and the sharp feature at 7130.1 eV was used as an energy calibration marker.

X-Ray absorption edge spectra of Mn were measured on beamline IV-1, and Mn EXAFS spectra were measured on beamlines VI-2 and IV-2 during dedicated operation of the SPEAR storage ring at the Stanford Synchrotron Radiation Laboratory (SSRL). For X-ray absorption edge studies Si-(111) monochromator crystals were used, and for EXAFS spectra Si-(400) crystals were used. The integrated photomultiplier current due to scattering of X-rays off a thin mylar film was used as a measure of the initial flux.

The sample fluorescence was monitored (Jaklevic et al., 1977) using a NE104 plastic scintillation array for photon counting as described previously (Powers et al., 1981) or a United Scientific Corporation silicon-lithium detector. The scattered X-rays were selectively absorbed by placing a Cr filter between the sample and detector. Energy calibration was maintained by simultaneously measuring the absorption spectrum of $KMnO_4$ with two additional detectors (Goodin et al., 1979).

The total data collection time was about 2 to 3 h for ferredoxin samples and five to twenty hours for Mn-OEC samples. The samples were routinely cooled to -85 to -100°C, and sometimes to -140°C using a liquid nitrogen boil-off jet. At these temperatures X-ray damage is minimized. The samples were contained in a lucite sample holder in which illumination, EPR and X-ray absorption measurements could be made. The EPR spectra of the samples were measured both before and after X-ray beam exposure to ensure sample integrity.

II A. 3. X-ray Absorption Data Analysis

For each spectrum the X-ray fluorescence was normalized point-by-point to the incoming beam intensity. The data were weighted by the incoming intensity and the data collection time, and individual spectra were added to improve the signal-to-noise ratio. After addition, the pre-edge background was fit to a linear function and subtracted from the data, the scan was normalized with the edge height defined as unity and the oscillations were divided by the free atom contribution (Teo & Lee, 1979). The scattering contribution, the effects of the Cr or Mn filters and various other background components (μ_o in eqn. 1) were subtracted. Because these generally cannot be calculated analytically, we subtracted a second- or third-order polynomial function that approximates the data curvature, and then subtracted a running average of the data, averaged over a broad range (greater than 50 eV or 2.5 $Å^{-1}$) so that background features were removed, but EXAFS oscillations were not. The validity of the separation of background from data was checked by comparing the removed background with spectra of iron-free buffers and by analysis of reference compounds.

The data were then converted from a function of incoming X-ray energy, E, to a function of outgoing photoelectron wave vector, k, using a threshold energy for electron release, E_0, of 7130 eV. This value for E_0 was chosen by varying E_0 in a fit of the data to eqn (1), and monitoring the quality of fit. The data were then truncated to include only the region between 3.5 and approximately 11.0 $Å^{-1}$. Below this region there are contributions from physical processes other than EXAFS, and equation (1) is not valid. Above this region the signal-to-noise deteriorates. The data were then weighted by k^3 to emphasize the backscattering of the iron shell, which peaks at higher k values than the sulfur backscattering. The data are then Fourier transformed to evaluate the noise level, the background removal, the number of resolved peaks in the typical EXAFS range (*ca.* 1.2 to 3.5 Å), and the k-weighting 'behaviour' of these features. This inspection often yields insight for improving background removal or for indicating what types of simulations might be successful. Finally, we Fourier filtered the data before fitting, using a window that is wide compared to the obvious Fourier components. This has the effect of removing high frequency noise in the spectrum. This filtering, like the background removal, can greatly improve the convergence of the fitting procedure.

The Fourier-filtered, k^3- weighted data were then fit using parameters determined by Teo & Lee (1979). The fits had two or three types of ligands, with four adjustable parameters per ligand: the bond distance R; the number of atoms N; the Debye-Waller factor, σ; and a parameter, ΔE_0, which shifts E_0. In addition, the chemical identity of the ligand is specified. The Debye-Waller factor was chosen by comparison with models and by the quality of fit, as described in the Discussion, and ΔE_0 was varied within the range +10 to -10 eV. EXAFS spectra of reference compounds containing [2Fe-2S] and [4Fe-4S] clusters and soluble spinach [2Fe-2S] ferredoxin were also analyzed to check the validity of the fits and to determine the scaling factor, S_f, for the EXAFS amplitudes.

Other details of the data analysis methods and programs are described elsewhere (Goodin, 1983, Kirby, 1981, Robertson, 1979).

II B. Biochemical Methods

Specific protocols were developed for preparing PS I and PS II for X-ray absorption analysis. For these samples, our primary concerns are to obtain a good yield in a very large scale preparation, and to ensure that the metal of interest is as homogeneous as possible. In addition, it is important to avoid degradation of the metal center of interest (i.e. the oxygen evolution enzyme or center X). On the other hand, it is not particularly important to remove all peptide impurities of fluorescent impurities. Thus these protocols are good for the preparation of samples for XAS or EPR, but are probably not ideal for biochemical or optical studies.

II B. 1. Preparation of O_2-Evolving PS II from *Synechococcus*

This Photosystem II preparation is similar to one recently reported from *Synechococcus* (Satoh et al., 1985). Thermophilic *Synechococcus* sp., a generous gift of Prof. S. Katoh, University of Tokyo, was grown at 50 - 55° C using 50 - 100 *L* of a medium similar to that described previously (Dyer & Gafford, 1961) with increased copper and iron concentrations of 75 μM each (as $CuSO_4$ and $FeCl_3$). Whole cells were collected using a continuous flow Sharples centrifuge. The cells were washed in 50 mM HEPES, pH 7.5, 10 mM NaCl and 1 mM PMSF and centrifuged at 16000 g for 12 min. The cells were then incubated with 100 mg lysozyme at 37° C for 1 h in the dark in 100 m*L* of a medium containing 0.4 M mannitol, 5 mM EDTA, 50 mM HEPES, pH 7.5 and 1mM PMSF. The cells were then centrifuged as above and resuspended in a medium containing 50 mM MES, pH 6.2, 10 mM NaCl and 1 mM PMSF. This suspension was passed twice through a French pressure cell operating at 3.4 x10^7 Pascal to obtain thylakoid fragments. The DNA in the resulting suspension was degraded by addition of approximately 1 μg DNAase (Sigma) and 5 mM $MgCl_2$. This mixture was stirred at 0°C for 1 h in the dark. The DNAase reaction was stopped by addition of 10 mM EDTA. Unbroken cells were removed by centrifugation at 12000 g for 15 min, and thylakoid fragments were collected by centrifuging at 300000 g for 1 h. The thylakoid

fragments were resuspended in a medium containing 0.5 M sucrose, 50 mM MES, pH 6.2, 5 mM $MgCl_2$ and 0.5 mM PMSF (medium A). The suspension was then spun at 12000 g for 10 min and the thylakoid fragments were collected by centrifugation as described above.

The thylakoid fragments were resuspended in medium A to a concentration of 1 mg Chl mL^{-1}, and the PS II was extracted at 21 - 22°C under dim light using the detergent β-octyl glucoside. During each preparation a range of detergent concentrations from 0.4% to 0.8% was tested in small aliquots of sample. The samples, which had a clearing distance of 0.8 cm, were then spun at 300000 g for 30 min. The supernatants of this spin were analyzed for Chl, P700 and O_2 evolution activity (as described below). The optimum detergent concentration to extract over 85% of the O_2 evolution activity with less than 2% of the P700 of the unfractionated thylakoid fragments was approximately 0.63 %. This extract also contained approximately 10-15% of the total chlorophyll. The bulk of the thylakoids were then extracted using the optimum detergent concentration. The thylakoid detergent mixture was then centrifuged in a Ti50.2 rotor (Beckman) at 300000 g for 2.5 h. The supernatant of this spin was collected and diluted with an equal volume of water, and the PS II were concentrated by centrifugation at 300000 g for 3 h. Before freezing the resulting PS II pellet at 77 K, an equal volume of glycerol was added to the sample.

We caution that the extraction of PS I occurred at a detergent concentration of approximately 0.8%, only 0.15% higher than the extraction of PS II. To avoid contamination by PS I, it is critical that the survey aliquots are extracted under the same conditions (especially temperature) as the bulk of the preparation. Figure II-5 shows the extraction curves for O_2-evolving PS II and PS I.

The thylakoid fragments typically had a specific O_2 evolution activity of 300 μmol O_2 (mg Chl)$^{-1}$ h^{-1}. PMSF was found to be important for preserving the O_2 evolution activity. Assays of O_2 evolution activity (as described below) directly following cell disruption indicated that the total O_2 activity was stable. The activity was also quite

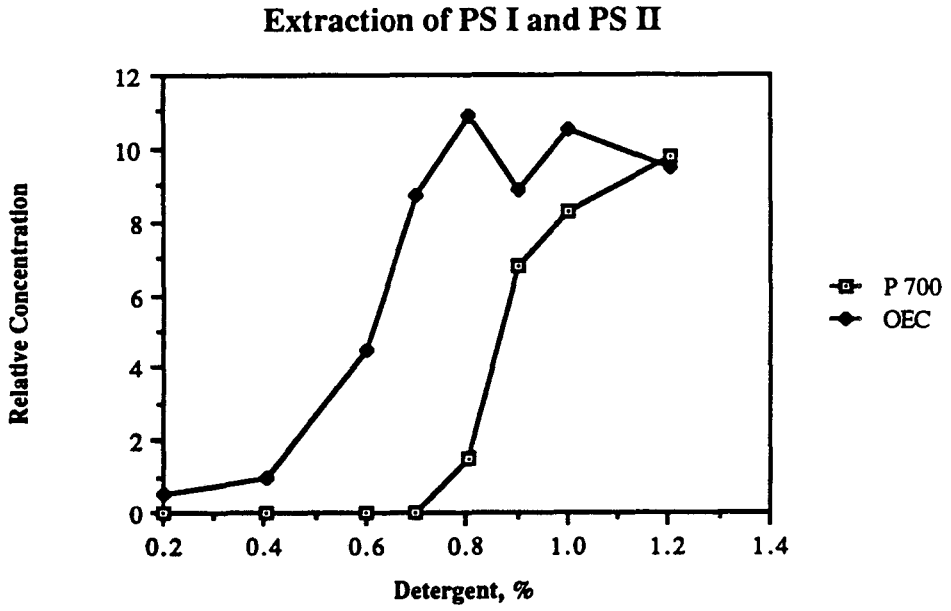

Figure II-5. P700 concentration and O_2-evolving activity in supernatants of 300,000 g spins (30 min) following treatment with various concentrations of β-octyl glucoside. The extraction of PS II occurs at 0.6 to 0.7% detergent while the extraction of PS I occurs at 0.8 to 0.85%.

stable in the EDTA treatment step, although we have observed that repeated washes with EDTA may lead to inactivation. To characterize the stability of the oxygen evolution activity during purification of PS II, we use the 'total O_2 evolution activity', a quantity defined as the specific activity multiplied by the total Chl. In contrast to activities which are normalized to the amount of Chl, the total O_2 evolution activity does not depend on the amount of Chl associated with the preparation. The total O_2-evolution activity was quite stable during the extraction of PS II, and any activity that was missing from the PS II supernatant was found in the pellet. However, we have found that the use of β-octyl glucoside in the presence of higher concentrations of NaCl or other salts causes a slow decay of total activity and release of Mn. Specific activities of the resulting PS II were approximately 2000 μ-mol O_2 (mg Chl)$^{-1}$ h^{-1} when measured at 21 to 23°C.

The PS II preparation can be purified by a column procedure involving diethyl aminoethyl (DEAE) column materials (cellulose or acrylic beads). PS II is suspended in medium A containing .05% β-octyl glucoside at .1 to .2 mg Chl (mL^{-1}), and loaded onto a DEAE CL-6B sepharose column that was pre-equilibrated with medium A. A 30 mL column was used per 0.3 mg Chl. The column was washed with five column volumes of medium A. Phycobiliproteins were observed to bind in the top 1 to 3 mL of the column, while PS II bound to approximately 15 mL of the column. The bili-proteins were eluted with medium A with .5 M NaCl. The column was washed with two column volumes of medium A, then with two column volumes of medium A with 1% lauryl maltoside and 70 mM NaCl. In this wash carotenoids were removed. Then PS II was eluted with two column volumes of medium A with 0.5% lauryl maltoside and 150 mM NaCl. The PS II was diluted into 5 volumes of medium A immediately after elution. The use of lauryl maltoside to elute the PS II, rather than β-octyl glucoside, was essential for preserving oxygen evolution activity. The exposure of PS II to the detergent-salt medium should be less than fifteen minutes; an exposure of two to four hours causes significant Mn release and approximately half of the oxygen evolution activity to decay. An alternate procedure for removing the phycobiliproteins is to pass the PS II over a

DEAE CL-6B sepharose column of a much smaller volume, approximately 1 mL per .3 mg Chl. In this procedure, 80% of the PS II and 10% of the phycobiliproteins pass through the column and are retained. This procedure has the advantage that the PS II is not exposed to a detergent-salt medium.

II B. 2. Preparation of PS I from Spinach

This preparation is similar to the PS I preparation of Ke *et al.* (1973b). All procedures were carried out near 4°C. Chloroplasts were prepared by grinding deveined market spinach leaves in a buffer containing 0.4 M sucrose, 50 mM Tris, pH 7.5, 20 mM NaCl, 5 mM EDTA and 5 μM PMSF, filtering through 8 layers of cheesecloth and 2-4 layers of Miracloth and then centrifuging the chloroplasts at 5000 x g for 6 min. The chloroplasts were resuspended in the same buffer, filtered again through Miracloth and again centrifuged. The chloroplasts were washed free of ribulose bisphosphate carboxylase by suspending at 0.1 mg Chl mL^{-1} in 10 mM sodium pyrophosphate, pH 7.5, with 1 mM EDTA and 5 μM PMSF, and pelleting at 10000 g for 10 min. This wash was performed twice. The membranes were then washed to remove coupling factor by suspending at 0.2 mg Chl mL^{-1} in 2 M NaBr, 20 mM Tris, pH 7.5, 1 mM EDTA and 5 μM PMSF, incubating for 20-30 min, then diluting to twice the volume with water and pelleting at 11000 g for 15 min. The thylakoids were resuspended in a buffer containing 5 mM $MgCl_2$, 20 mM Tris, pH 7.5 and 5 μM PMSF, at roughly 1 mg Chl mL^{-1}, and incubated for 30-60 min to ensure stacking. The thylakoids were pelleted (10000 g, 10 min) and resuspended in the same buffer to remove bromide. Triton X-100 (Sigma) was added to a concentration of 5 mg Triton (mg Chl)$^{-1}$. PS II and most of the PS I were then pelleted by centrifugation at 40000 g for 30 min. The supernatant was discarded. It contained most of the cytochrome b_6 /f complex, and roughly 10% of the PS I. The pellet was resuspended in the same buffer again at about 1 mg chl mL^{-1}, and Triton X-100 was added to 20 mg Triton (mg Chl)$^{-1}$. This mixture was again centrifuged at

40000 g for 45 min to separate PS I and PS II. The supernatant of this spin contained a crude preparation of PS I.

PS I was then refined using sucrose density gradients. Roughly 5 mg Triton X-100 (mg Chl)$^{-1}$ was added to the supernatant, and the suspension was centrifuged at 160000 g for 8 h to concentrate PS I. The pellet typically contained 100-130 Chl per P700. This pellet was resuspended to a concentration of approximately 1 mg Chl mL^{-1}. Digitonin and lauryl maltoside (1% w/v each) were added. Any remaining clumps were removed by centrifugation at 30000 g for 15 min. The suspension (1.5 to 3 mL) was layered over a 30 mL 6 - 22% sucrose gradient. The gradients were made in a buffer containing 0.2% lauryl maltoside and 10 mM Tris, pH 7.5. The gradients were centrifuged at 27000 rpm in an SW28 rotor for 18 to 30 h. After centrifuging, two major green bands could be seen which contained PS I (the lower band) and the dissociated PS I Chl-binding proteins with trace amounts of PS II nearby (the higher band). The upper band was highly fluorescent, but the lower band was not fluorescent to the eye. The lower band was siphoned in 1 to 2 mL fractions. Those tubes with Chl to P700 ratios less than about fifty and those lacking cytochromes and antenna proteins (as determined by peptide analysis) were pooled and saved. The preparation contained four obvious bands by SDS-PAGE: a peptide of MW 60 kDa which binds P700 and other electron transfer components, and three peptides of MW between 16 and 22 kDa.

II B. 3. Preparation of PS I from Thermophilic *Synechococcus*

Thylakoids were prepared from *Synechococcus* exactly as described in II B. 1. PS II was extracted with approximately 0.7% β-octyl glucoside at 1 mg Chl mL^{-1} as described above. The extracted thylakoids were then centrifuged at 300000 g for 1 h. The thylakoid pellet was resuspended to 2.5 mg Chl mL^{-1} in 50 mM Tris, pH 7.5, 10 mM NaCl (medium B) with 1% Triton X-100, and the washed thylakoids were collected in a pellet by centrifugation as in the previous step. The PS I was then extracted by resuspending the pellet to 1 to 2.5 mg Chl mL^{-1} in medium B, adding 20 mg Triton

X-100 (mL Chl)$^{-1}$, then centrifuging the insoluble material from solution using 40000 g for 30 min. The supernatant was then purified on sucrose gradients by the same procedure as for spinach PS I (II. C. 2.).

II B. 4. Chemical and Biochemical Analysis

Chl concentrations were determined by extracting into 80% acetone, centrifuging to remove protein and measuring the optical absorbance as described by Arnon (1949).

The analysis for P700 was done by monitoring reversible photobleaching. The sample was diluted to 5 to 30 μM Chl in a medium containing 20 mM Tris, pH 7.5, 0.1% Triton X-100, 10 μM PMS, 10 μM methyl viologen and 0.1 mM sodium ascorbate. The sample was illuminated in a Cary 14 or DW-2 Aminco spectrophotometer at right angles to the measuring beam using a tungsten filament lamp, the light from which was filtered through a water (IR) filter and a 400 to 560 nm bandpass filter and focused on the sample. A 700 nm interference filter was placed in front of the photomultiplier to prevent the exciting beam from reaching the photomultiplier. The bleaching at 700 nm (approximately the wavelength of maximum bleaching) was measured under saturating illumination. The extinction coefficient determined by Hiyama & Ke (1973), 64 mM^{-1} cm^{-1} at 700 nm, was then used to calculate the concentration of P700. The sensitivity of this assay is such that 1% of the P700 in an unfractionated thylakoid sample may be detected reliably.

The preparations were analyzed for iron content by atomic absorption. The sample was mixed with twice its volume of 70% nitric acid, and digested by boiling until it became clear (approximately 10 min). The samples were diluted in distilled water and analyzed with a Perkin Elmer model 303 flameless graphite tube atomic absorption spectrometer. Typical final concentrations ranged from 0.5 to 5 μM. The samples were compared with commercially available iron standards diluted in a similar medium.

Analysis for acid-labile sulfide was carried out by a modification of the method of Fogo and Popowski (1949) similar to that described by Golbeck and San Pietro (1976).

The sample was taken into cold 80% acetone under nitrogen in a sealed microfuge tube. The tubes were then centrifuged at about 20000 g for 10 min to separate the denatured protein pellet from the Chl extract. The pellet was then rinsed under nitrogen with cold 80% acetone. The pellet was analyzed by the method of Fogo and Popowski (1949); the methylene blue product was partitioned quantitatively into hexanol, and its concentration was monitored at 660 nm.

Oxygen evolution assays were measured at 2- 20 μM Chl in a suspension medium containing 50 mM MES, pH 6.2, 0.5 M sucrose, 10 mM NaCl, 5 mM $MgCl_2$, 0.5 mM DCBQ, 1 mM $K_3Fe(CN)_6$ and 1 mM $K_4Fe(CN)_6$ using a Clark-type oxygen electrode biased at -0.6 V vs. Ag/AgCl during saturating actinic illumination of the sample. Estimation of the PS II reaction center concentration was made by integrating the EPR signals resulting from D^+ and Z^+ (Babcock et al., 1983). The Mn content was determined (for the same samples) by atomic absorption analysis of nitric acid-digested samples.

Peptide analysis by SDS PAGE was done according to Laemmli (1970), except that slab gels were used and the separating gels were 15% acrylamide. When analyzing the PS I preparation from *Synechococcus*, 6M urea was included in the gels and samples.

A particular concern in the X-ray absorption experiments is the possibility of X-ray damage to the samples. We have found that maintaining the samples at temperatures below -70° C minimizes damage. All samples were analyzed for X-ray damage by measuring the EPR spectrum before and after beam exposure. In addition, Chl to P700 ratios were used to characterize PS I, and oxygen evolution assays were used to characterize PS II. By these criteria the preparations were not degraded by beam exposure more than 10%. Iron assays together with UV/ VIS spectra and EPR spectra were used to characterize the soluble spinach [2Fe-2S] ferredoxin and soluble *Clostridium pasteurianum* [4Fe-4S] ferredoxin. The ratio of total iron to intact ferredoxin indicated that in the soluble spinach [2Fe-2S] ferredoxin, greater than 94% of the iron and, in the

soluble *Clostridium pasteurianum* [4Fe-4S] ferredoxin, approximately 83% of the iron was in intact cores before and after beam exposure.

PS I samples were reduced in a degassed 0.1 to 0.2 M glycine buffer at pH 10 using 10 mM dithionite with 10 μM phenazine methosulfate and methyl viologen. The potential under these conditions was -0.62 V vs SHE when measured with a Pt electrode and a Ag/AgCl reference. The sample was then frozen in liquid nitrogen while being illuminated by a focussed 400 W tungsten filament lamp. A water filter was used to minimize IR heating from the lamp.

PS II samples prepared as described above were dark adapted for 1 to 2 h and frozen in liquid nitrogen. Illuminations were done for 2 min with continuous light from a 400 W tungsten lamp passing through a heat filter consisting of a 3 cm path of 5% aqueous $CuSO_4$. During illumination the sample was cooled in a N_2 gas flow while monitoring the temperature with a copper-constantan thermocouple.

Low temperature EPR spectra were obtained using a Varian E-109 spectrometer operating at X-band using a model E102 microwave bridge and a TE-102 cavity with 100 kHz field modulation. An Air-Products Helitran cryostat was used to cool the sample to between 6 and 11 K.

Chapter III: EPR Studies of Center X in PS I

III A. Introduction

The suggestion that X is an iron-quinone species was based on CW EPR power saturation studies (Rupp et al., 1979). Since the balance of evidence at this point indicates an Fe-S structure for X, it is interesting to re-evaluate the EPR power saturation, relaxation and lineshape of X.

Power saturation studies may measure the homogeneous and inhomogenous components of signal line-widths. If the homogeneous linewidth is dominant, which is often the case for organic radicals, the relaxation processes may be studied by measuring the signal linewidth as a function of temperature and microwave power. For metalloproteins the linewidths are often dominated by inhomogeneous broadening due to a large number of unresolved hyperfine couplings or due to 'g strain'. In this case a common method for characterizing the relaxation mechanism involves measuring the power saturation of the signal as a function of temperature (Rupp et al., 1978; Salerno et al., 1977). Many ferredoxins are intermediate between these two cases, having a Gaussian broadened linewidth whose underlying Lorentzian components can be retrieved by simulations (Gayda et al., 1976). In their studies of X, Rupp et al. (1979) concluded that X has an appreciable homogeneous contribution to the overall linewidth, and therefore they suggested an organic radical assignment for X.

The two common mechanisms for spin-lattice relaxation in metalloproteins are called the Raman-Van Vleck and the Orbach processes. The theories of these processes predict distinct temperature dependences which have been experimentally confirmed not only in inorganic solids but also in metalloproteins (Blum et al., 1977; Allen et al., 1982). Both relaxation processes can be significant for ferredoxins and iron-sulfur complexes (Gayda et al., 1979; Beardwood et al., 1983).

In this study we re-examine the power saturation behaviour of X and find that it is consistent with behaviour expected for a ferredoxin. We present evidence that X has one or more unusually low-lying excited spin states as compared with other ferredoxins.

III B. Methods

The preparation and characterization of PS I, and the EPR spectroscopy, was done as described in Chapter II.

The amplitude of the g_x feature was recorded at a variety of microwave powers at each of 7 temperatures. A power saturation curve was then plotted; the abscissa is the logarithm of the square root of the power in milliwatts, and the ordinate is the logarithm of the first derivative intensity of the signal (in arbitrary units) normalized by the square root of the microwave power. To obtain a value for $P_{1/2}$ from these data, $I/\sqrt{P}$ as a function of P was fit using the expression derived by Castner (1959) as described by Rupp et al. (1978): $\chi''=C/(1+P/P_{1/2})^{b/2}$ where χ'' is the imaginary (absorptive) component of the magnetic susceptibility and is proportional to the ratio of the intensity to the square root of microwave power, C is a parameter describing the equilibrium spin populations, $P_{1/2}$ is the half-saturation point which is proportional to $1/T_1T_2$, (T_1 and T_2 are the spin-lattice and spin-spin relaxation rates), and b is a 'homogeneity' parameter which varies from 1 for inhomogeneously broadened lines to 4 for homogeneously broadened lines. In these simulations $P_{1/2}$, C and b were adjustable parameters. For all of the simulations shown, b=1 and the $P_{1/2}$ value that gave rise to the smallest sum of residual errors is given in Table III-1. The simulations had well defined minima in residuals with respect to changes in $P_{1/2}$. For each power saturation curve, the range in which the error was less than double that for the best fit is is indicated as an error estimate for the $P_{1/2}$ value (Table III-1).

III C. Results

Figure III-1 shows the X-band EPR spectrum of PS I particles with X, A and reduced.

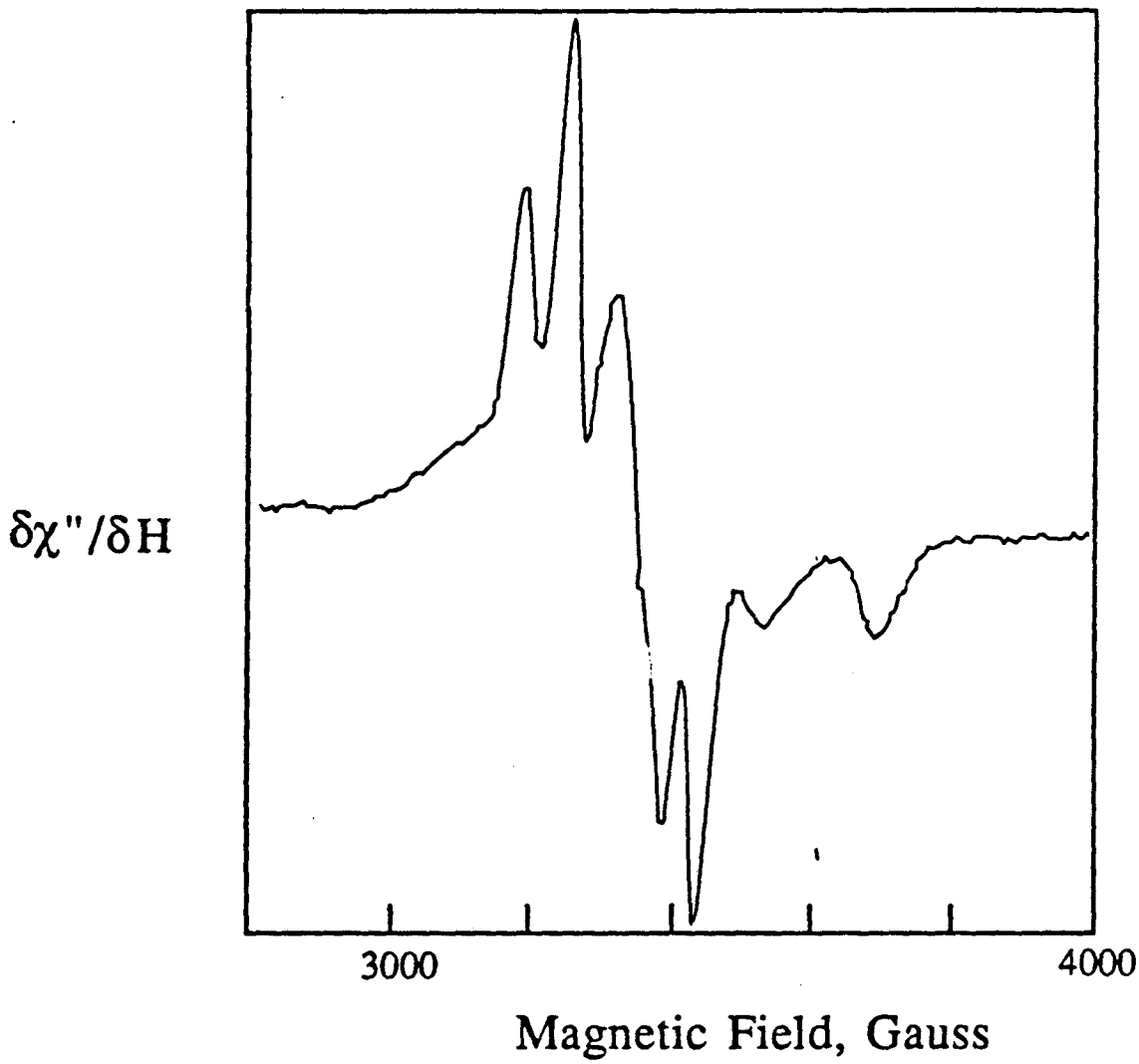

Figure III-1. X-band EPR spectrum of PS I particles reduced using dithionite at pH 10 and frozen during illumination. The spectrum was collected at 6 K with 30 mW microwave power, field modulation 25 G, microwave frequency 9.21 GHz, gain 1250. The g_x feature of X at 3690 G has a fwhm $\Delta H=80\pm5$ G in the first derivative. The other g-values of X are partly obscured by interference from centers A and B.

Figure III-2 shows an illuminated-minus-dark EPR spectrum of dithionite-reduced PS I particles, which exhibits the EPR spectrum of X without interference from the signals due to centers A and B. This subtraction indicates g-values of 2.11, 1.85 and 1.76 (± 0.01), in agreement with previously reported values (Evans, 1982).

The linewidth of the high-field feature of X was independent of power and temperature (within 5%) from 4 K to 11 K and from 1 μ-W to 0.2 W. Since these include measurements far below saturation ($P/P_{1/2} \approx .003$) and measurements above saturation ($P/P_{1/2} \approx 100$), we conclude that the linewidth of X is dominated by inhomogeneous broadening. All power saturation curves were measured using this high field feature. Because this feature is well separated from any features due to centers A and B, the amplitude was measured in the illuminated spectrum and no dark subtraction was necessary.

Figure III-3 shows the power saturation curves of the high field feature of X. The slopes of the curves in the saturated regime indicate that the linewidth is dominated by inhomogeneously broadening. At non-saturating powers the intensity of the signal as a function of temperature is consistent with the assignment of X as a ground state species; our previous observation that the signal disappears at temperatures below 7 K resulted from power saturation at lower temperatures (McDermott et al., 1987). The curves were simulated using the expression derived by Castner (1959) describing inhomogeneously broadened EPR signals. The best fit curves are plotted through the data points. The resulting values for $P_{1/2}$ are entered in Table III-1.

The half-power points show a dramatic dependence on temperature. We have attempted to fit these data to both the Orbach and the Raman-Van Vleck mechanisms. At low temperatures, for Kramers doublets relaxing by the Raman process, T_1 varies as $T^{(3+2d)}$ where d is the fractal dimension of the protein (Allen et al., 1982). This result is due to the dependence of the density of phonon modes on the fractal dimension of the lattice, as previously described (Allen et al., 1982). The values of d for molecular species are always less than or equal to 3. For many simple salts d is equal to 3 and for

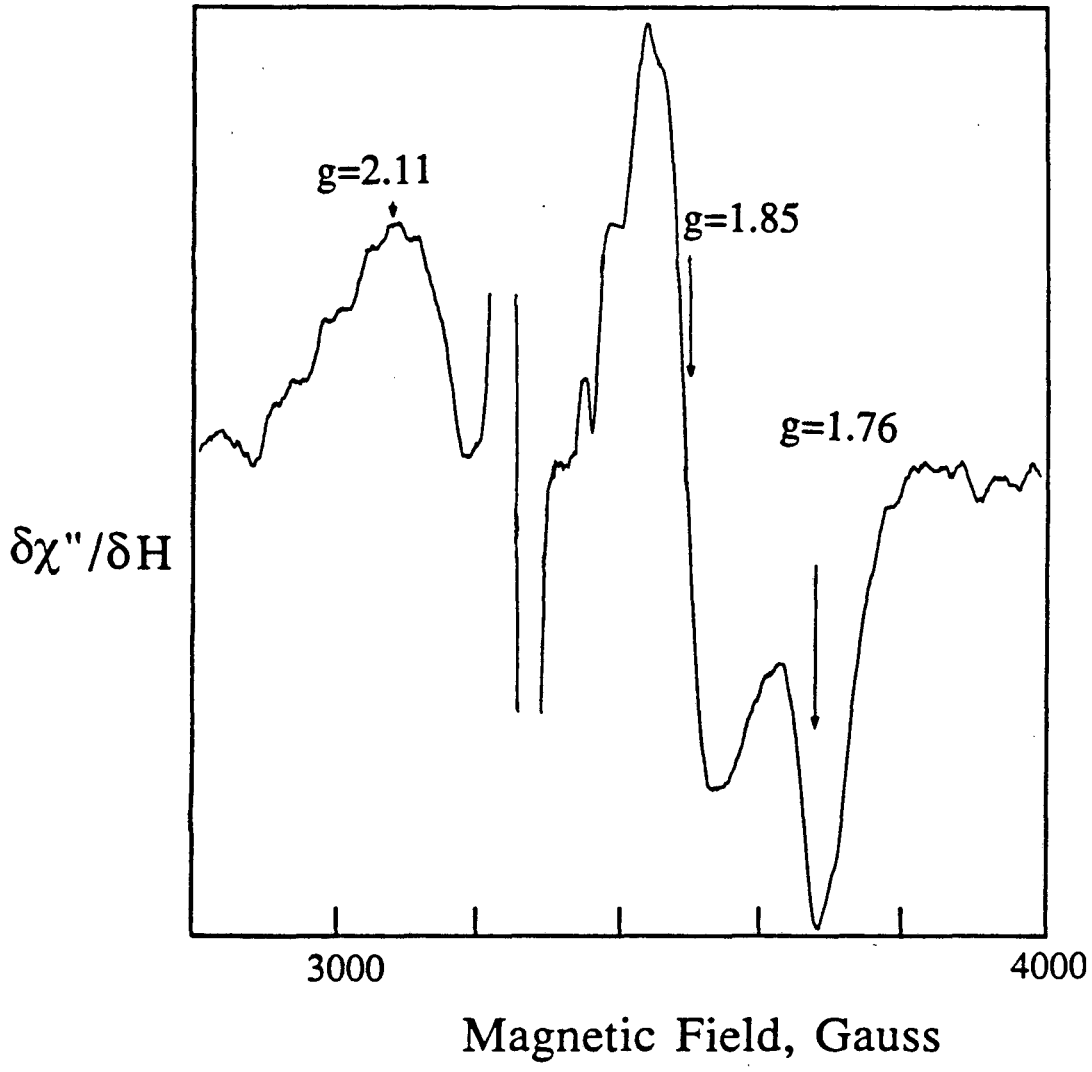

Figure III-2. Illuminated-minus-dark spectrum at 6 K of PS I reduced using dithionite at pH 10, showing reduced center X. Conditions as in Fig III-1.

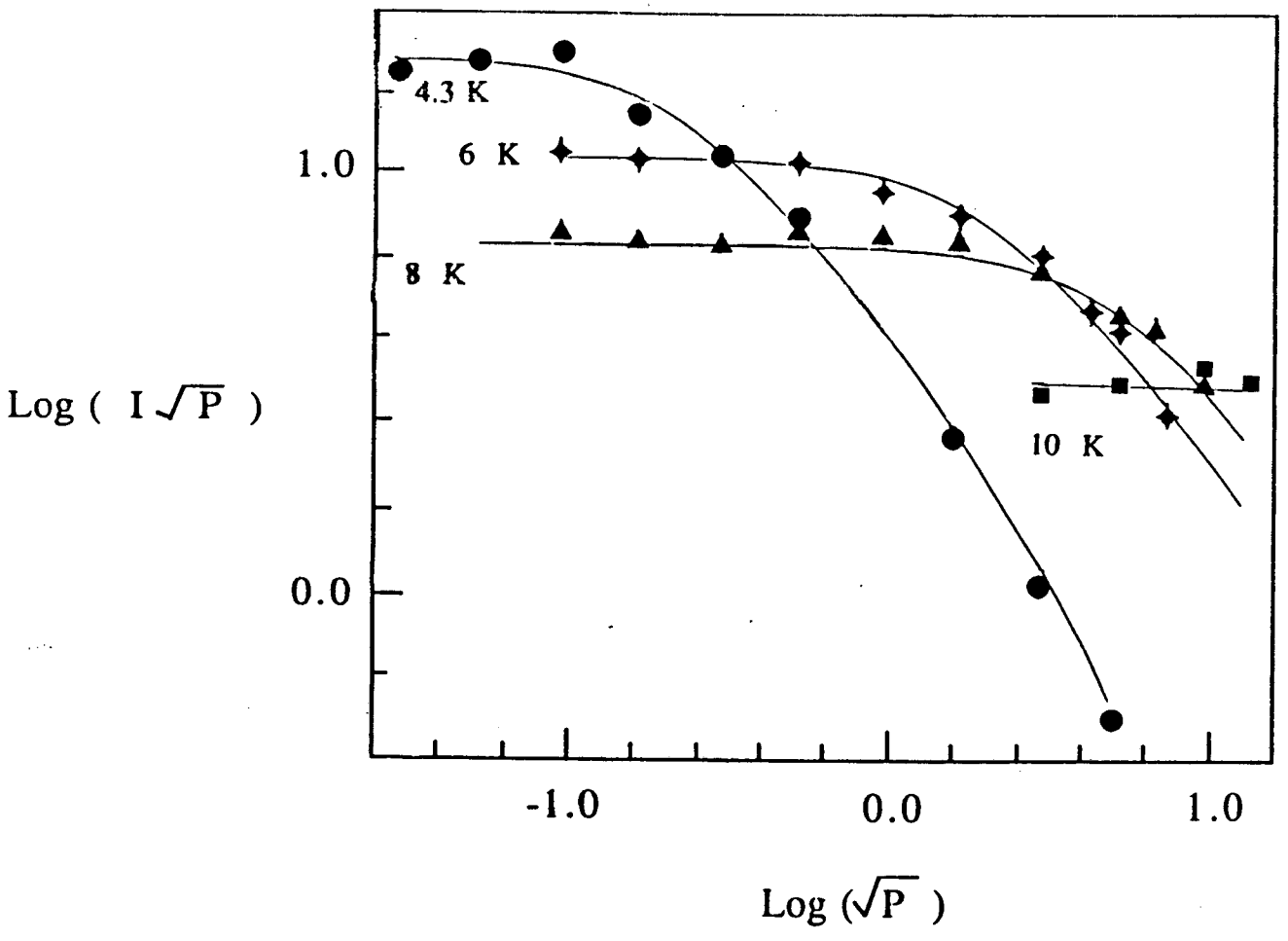

Figure III-3. Typical power saturation curves for center X. The first derivative amplitude of the g_x feature was measured at the indicated temperatures. The measurements are indicated by points; estimated errors are ± 5%. The curves are computer-simulated best fits calculated using the expression for inhomogeneously broadened signals $\chi''=C/\sqrt{1+P/P_{1/2}}$ (Castner, 1959). The data are divided into two panels, III-3A and -3B for clarity. The resulting values for $P_{1/2}$ are indicated in Table III-1. Note that the amplitude at nonsaturating powers increases with decreasing temperature in the range from 4 to 12 K.

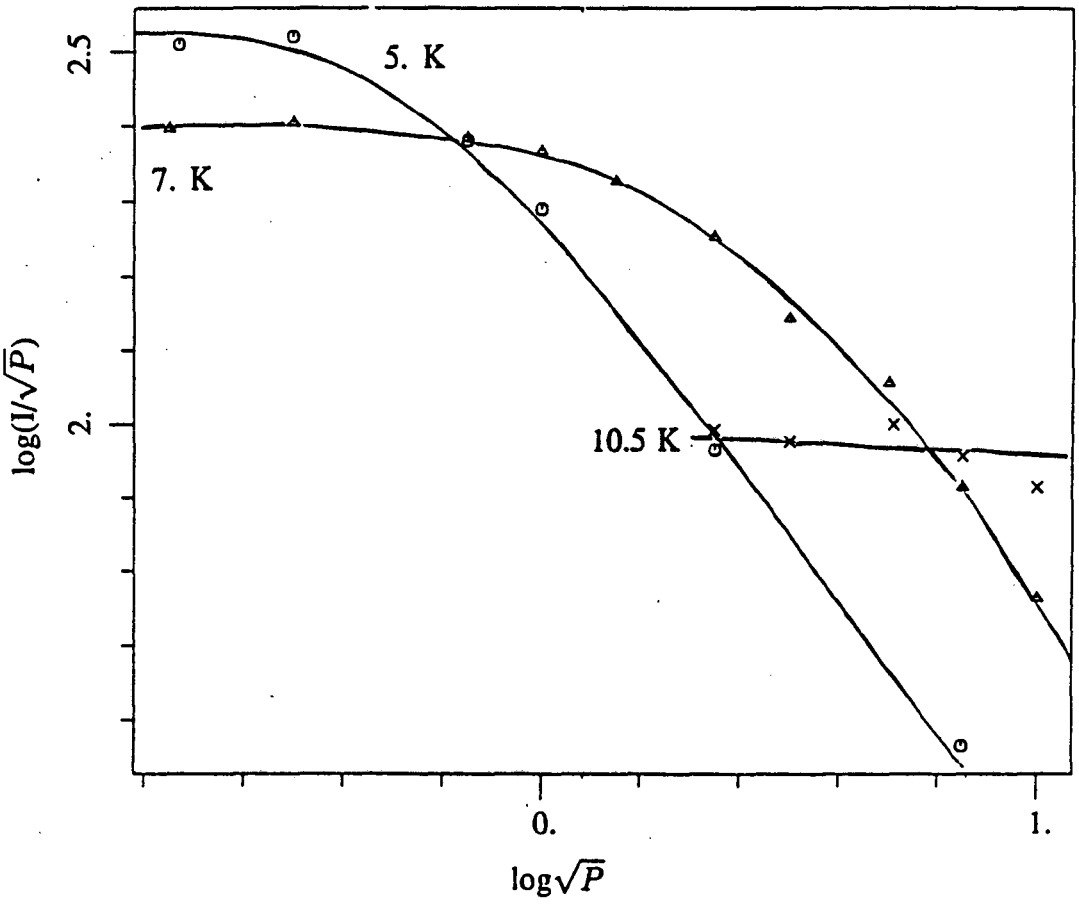

Figure III-3B. See III-3A for caption.

TABLE III-1

Power Saturation of X[1]

T(K)	$P_{1/2}$(mW)	Estimated Error Range(mW)
4.3	.1	.01-.3
5	.35	.2 -.4
6	3.9	2.-12.
7	5.4	3.- 7.
8	23.5	10.-50.
10	>500.	300.-1000.

[1]Values obtained by fitting the CW-EPR power saturation data to the expression derived by Castner (1959).

proteins d is between 1 and 2. Under the assumption that $P_{1/2}$ is proportional to $1/T_1$, a plot of ln(T) vs. $\ln(P_{1/2})$ yields a line with slope m. When fit to the Raman-Van Vleck process, as shown in Figure III-4, these data yield a slope, m, greater than 9, which is not physically reasonable (Allen et al., 1982). For the Orbach process, T_1 varies as $e^{-\Delta/kT}$ where Δ is the splitting between the observed (ground) state and the first excited state. In this case, if $P_{1/2}$ is proportional to $1/T_1$, a plot of 1/T vs. $\ln(P_{1/2})$ yields a line with slope of Δ/k. Our data can be fit to an Orbach process with $\Delta = 40 \pm 10$ cm^{-1}, as shown in Figure III-5.

III D. Discussion

At all temperatures and powers used, the first derivative linewidth is independent of power, indicating that the linewidth of X is dominated by inhomogeneous broadening, in contrast to the results of Rupp et al. (1979). The power saturation data are not suggestive of an organic radical assignment for X, but are consistent with a metalloprotein assignment such as a ferredoxin.

At non-saturating powers the intensity of the signal as a function of temperature is consistent with the assignment of X as a ground state species. We have searched for EPR signals that might be associated with other spin states of X and have not observed any.

The half-power points indicated by simulation of the power saturation data are a dramatic function of temperature (Table III-1). We have attempted to fit these data to both the Orbach and the Raman-Van Vleck mechanisms, assuming that the dependence is entirely due to variation of spin-lattice relaxation time, T_1. When we fit our data to this mechanism we obtain a value for d which is greater than three (Figure III-4). This would correspond to a dimensionality greater than three, which is unphysical. Thus, the strength of the temperature dependence of $P_{1/2}$ rules out the Raman process as the main relaxation pathway. A very likely alternative is the Orbach process. If the Orbach process is the dominant process, an excited spin state or states near 40 cm^{-1} are predicted (Figure III-5).

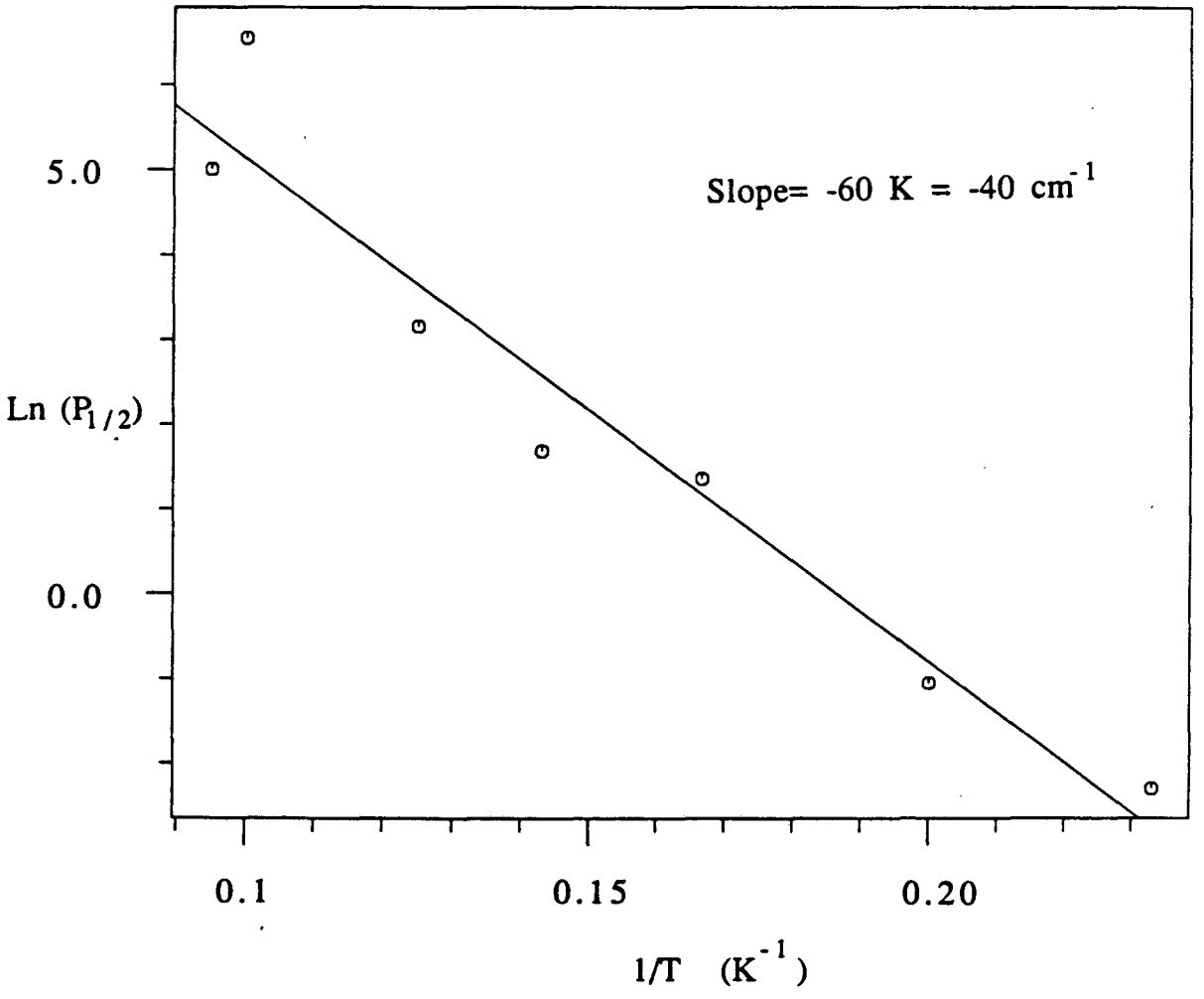

Figure III-4. The power saturation points (Table III-1) are fit to a Raman-Van Vleck mechanism, assuming that the temperature dependence of $P_{1/2}$ is entirely due to the temperature dependence of T_1. The slope yields an exponent of 10 ± 1, which is not physically reasonable.

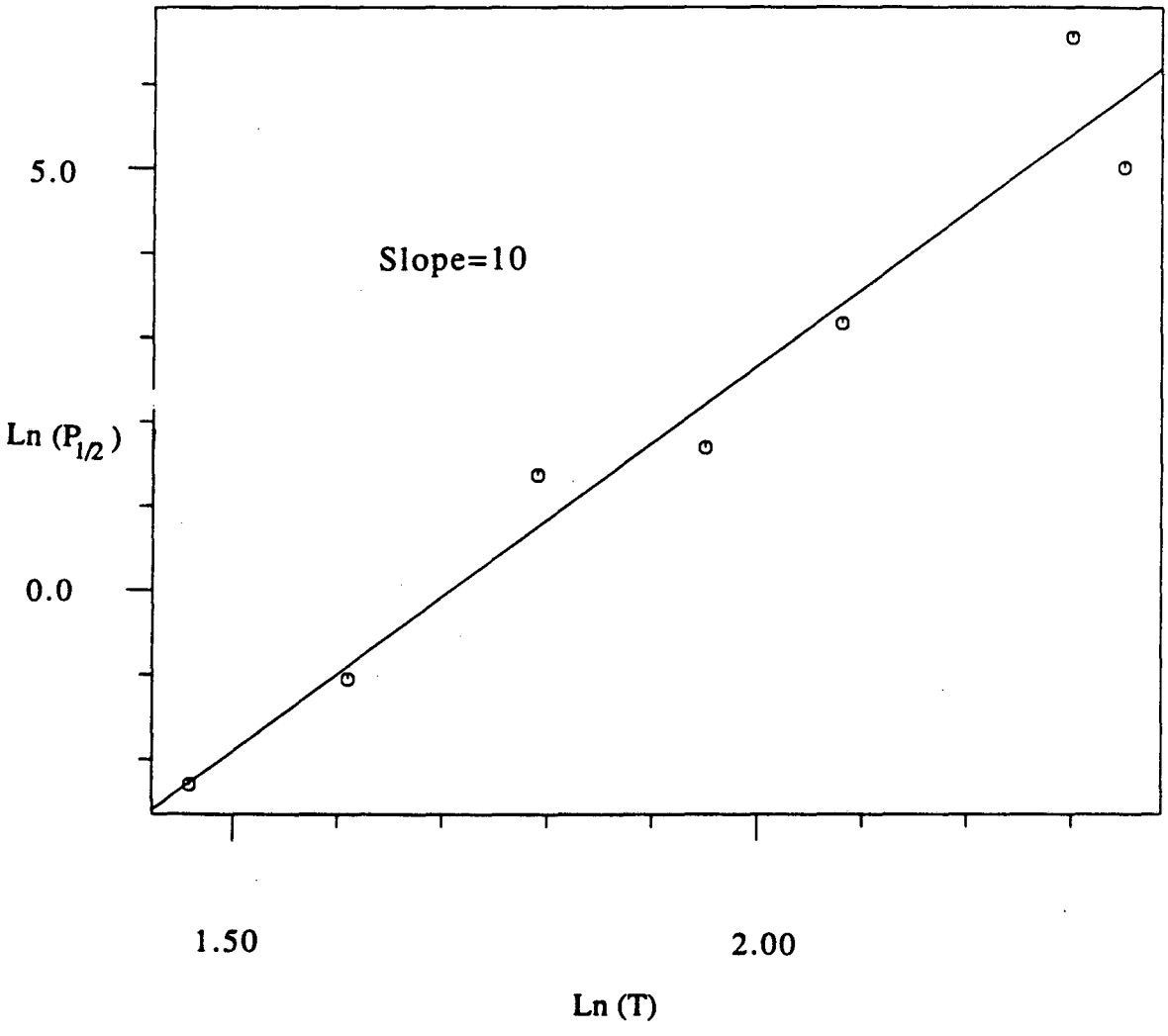

Figure III-5. The power saturation points (Table III-1) are fit to an Orbach spin-lattice mechanism, assuming that the temperature dependence of $P_{1/2}$ is entirely due to the temperature dependence of T_1. The slope yields an excited state energy of 60 K, which is equivalent to 40 cm^{-1}.

The balance of chemical and spectroscopic data are consistent with the assignment that X is some kind of ferredoxin. Proposed structural assignments for X have included [4Fe-4S] cluster(s) (Evans et al., 1981), highly distorted [4Fe-4S] clusters (McDermott et al., 1987), [2Fe-2S] cluster(s) (Golbeck et al., 1987) or some unprecedented type of iron-sulfur cluster (McDermott et al., 1987). The energies of the first excited spin states have been determined for a number of ferredoxins. No clear-cut differentiation between [2Fe-2S] and [4Fe-4S] ferredoxins is possible on the basis of the relaxation properties. Reduced [2Fe-2S] ferredoxins with rhombic EPR signals have a first excited state at approximately 200 to 300 cm^{-1} (Salerno et al., 1977), while reduced [4Fe-4S] ferredoxins have states at 100 to 300 cm^{-1} (Gayda et al., 1981). Thus, the [4Fe-4S] ferredoxins can have somewhat lower first excited states and faster spin relaxation than [2Fe-2S] ferredoxins, but there is considerable overlap in the properties of these two classes. In addition, the value we obtain for X, 40 cm^{-1}, is lower than a typical value for either class of ferredoxins.

For [2Fe-2S] and [4Fe-4S] ferredoxins the g anisotropy is correlated with the energy of the first excited spin state (Salerno et al., 1977; Gayda et al., 1981). Orbital angular momentum contribution to the g-value results from spin-orbit coupling, and the extent of this contribution is partially determined by the separation between the ground spin state and excited states which mix with the ground state. A treatment of spin-orbit coupling and Zeeman coupling for simple ions results in the expression $g'=g_e(1\pm\lambda/\Delta)$, where g_e and g' are the g-values of a free electron and an electron in a bound state characterized by a spin-orbit coupling constant λ and an energy gap, Δ, to the first excited state (Pake & Estle, 1973). This expression does not apply for covalent systems and therefore is far from exact for ferredoxins. However, all other things being equal, a smaller energy gap should result in a greater deviation of the g-value from 2.0. X behaves consistently with this pattern in that it has an unusually low first excited spin state and an unusually anisotropic g-tensor. The EPR properties of X are consistent with an assignment as a

[2Fe-2S] or a [4Fe-4S] ferredoxin with low excited states, but these properties do not prove which structure is more likely.

The differences in first excited spin state energies among [2Fe-2S] ferredoxins reflects differences in exchange or J coupling. The strength of the J coupling in turn reflects a number of structural parameters, including the internal bond angles of the cluster and the metal-metal distance. A correlation between the rhombic distortion of a [2Fe-2S] center and the exchange interaction has been proposed; larger rhombic distortions result in greater mixing of d orbitals, poorer overlap of the iron and sulfur orbitals and smaller exchange couplings (Bertrand & Gayda, 1979). If X is a [2Fe-2S] ferredoxin, as many experiments would indicate (McDermott et al., 1987, Golbeck et al., 1987), its seemingly unusual EPR properties may result from distortions similar to those described for other [2Fe-2S] ferredoxins, but larger in magnitude. For [4Fe-4S] ferredoxins, effects of covalency and delocalization in the cluster are important in determining both the g tensor and the energy of excited spin states (Noodleman & Baerends, 1984). Thus, the causes for differences in J-coupling and g anisotropy are more difficult to identify than for [2FE-2S] ferredoxins.

The above discussion assumes that the antiferromagnetic cluster reflected in the excited state at 40 cm^{-1} is 'intra-cluster' coupling. Another possibility is that this coupling is between two discrete clusters. The antiferromagnetic coupling between the clusters in [8Fe-8S] ferredoxins is of the order of 350 MHz, or 0.012 cm^{-1} (Schepler, 1975). These clusters are approximately 12 Å apart. This coupling is three orders of magnitude weaker than the coupling measured for X. This indicates that that the state at 40 cm^{-1} arises from a ladder of states localized on a cluster.

The exchange integral is one of two contributions to the electronic energy (the other being called coulombic) (reviewed in Ginsberg, 1971); these two integrals in turn reflect the overall geometry of the molecule. The exchange integral determines the spacing of the ladder of spin states, and these higher spin states are partially occupied at room temperature. Thus J is one factor determining the total energy of both the reduced

and oxidized protein, and it is conveniently measured. Calculations of the effect of a difference in exchange integral in the reduced an oxidized states of a ferredoxin indicate that such differences can substantially contribute to reduction potential differences (Bertrand & Gayda, 1982). Therefore the midpoint potentials of [2Fe-2S] ferredoxins might largely reflect differences in the exchange coupling terms in the reduced and oxidized states (Bertrand & Gayda, 1982). A weak coupling in the reduced state and a stronger coupling in the oxidized state, as seen in some [2Fe-2S] ferredoxins (Petersson et al., 1980, Palmer et al., 1971), favors a lower midpoint potential. It is interesting to consider the relatively small exchange coupling for X in light of its very low reduction potential. Currently there is no evidence concerning the exchange interaction for X in the oxidized state. However, if the exchange interaction for X in the oxidized state is a typical value, then the weak exchange interaction in the reduced state would be related to the low midpoint potential of X.

Chapter IV: XAS Studies of the Ferredoxins in PS I

IV. A. Introduction

This chapter concerns the use of XAS to address the structure of center X in PS I. Extended X-ray absorption fine structure, EXAFS, is capable of discriminating between [4Fe-4S] clusters, [2Fe-2S] clusters and six coordinate Fe with oxygen and nitrogen ligands such as is found in the Fe-Q acceptor complex of bacterial reaction centers. A variety of Fe-S inorganic complexes and proteins have been studied by EXAFS spectroscopy (Teo et al., 1979). In [2Fe-2S] and [4Fe-4S] ferredoxins, the Fe has four sulfur neighbors at about 2.25 Å. The EXAFS spectra of these compounds have a frequency component corresponding to the four sulfurs, and this component is very similar in [2Fe-2S] ferredoxins and [4Fe-4S] ferredoxins. In both [2Fe-2S] ferredoxins and [4Fe-4S] ferredoxins every Fe atom also has Fe neighbor(s) at about 2.74 Å; in the [2Fe-2S] ferredoxins each Fe has only one Fe neighbor, whereas in the [4Fe-4S] ferredoxins each Fe has three. The difference in the number of Fe neighbors for the two clusters gives rise to a difference in the amplitude of the Fe backscattering that has a pronounced effect on the oscillation patterns. No scattering atoms other than Fe and sulfur contribute significantly to the Fe EXAFS spectrum of Fe-S centers. EXAFS studies of the the Fe-Q acceptor complex in bacterial reaction centers demonstrated that the Fe is coordinated by six ligands at 2.1 Å which are a mixture of oxygen and nitrogen (Bunker et al., 1982, Eisenberger et al., 1982). These conclusions were confirmed by the X-ray crystal structure of the bacterial reaction center which indicated that the Fe has two oxygen ligands from a glutamate and four nitrogen ligands from histidines (Deisenhofer et al., 1986). This structure is readily distinguished from an Fe sulfur center by EXAFS.

The structure of the absorption spectrum near the X-ray absorption edge is also different for a hexacoordinate iron complex, such as that found in the Fe-Q complex,

and an Fe-S cluster. The 1s to 3d transition, which is formally unallowed in octahedral complexes, is prominent in tetrahedral complexes because of p-d mixing (Roe et al., 1984). While the K-edge spectra of [2Fe-2S] and [4Fe-4S] complexes are quite similar, the K-edge spectrum may be used to discriminate between Fe-S complexes, an Fe-Q complex or a mixture of the two.

In this chapter I present the X-ray absorption spectra of PS I preparations containing A, B and X. These spectra are used to address whether X may be an Fe-Q, a symmetric [4Fe-4S] cluster or one or more [2Fe-2S] clusters.

One of the challenges to the EXAFS analysis of Fe in PS I is that three Fe-S clusters are present. Our main interest is in X, but the data reflect centers X, A and B. Recently, Golbeck and coworkers have been successful in developing preparations in which centers A and B have been removed (Golbeck & Cornelius, 1986, Warden & Golbeck, 1986). According to room temperature optical measurements of the backreactions of $P700^+$ with acceptors, X is present in these preparations. The procedure for these preparations involves a brief treatment of a control PS I preparation with LDS, followed by crude fractionation through an Amicon ultrafiltration cell. The destruction of clusters is selective, but approximately 20 to 30 % of centers A and B remain present and 10 to 20% of X may be lost in the procedure. Analysis of these preparations for Fe and acid-labile S shows approximately six sulfides, and 12 ± 2 irons per P700. Treatment with a chelating agent, Tiron, resulted in partial removal of Fe leaving 5± 2 Fe per P700. (The partial removal of iron by chelation occurred without loss in the amplitude of the kinetic phase of P700 backreaction that was assigned to X.)

EPR spectra of the LDS-treated PS I preparations at 5 K show a very broad ferredoxin-like spectrum that is altered relative to the spectrum of X in control PS I preparations (Warden & Golbeck, 1986). Estimation of the midpoint potential by chemical reduction while monitoring the P700-X backreaction optically indicated that the midpoint potential is lower than -600 mV. These data indicated that X is still func-

tioning in these preparations as a low-potential acceptor. However, it is unclear whether X is structurally altered relative to control PS I preparations.

These preparations were used to study the structure of X by EXAFS without interference from centers A and B.

IV B. Results

The PS I preparations from spinach and *Synechococcus* are very similar in terms of chemical and spectroscopic properties. Both have 35-60 Chl molecules, 11-14 Fe atoms and 9-12 acid-labile sulfur atoms per P700, in agreement with other determinations (Golbeck, 1980, Lundell et al., 1985). They have the following predominant polypeptides, as shown in Figure IV-1 : 60 kDa subunits which are known to bind P700 and most of the Chl, and three lower molecular weight peptides at approx 18, 19 and 22 kDa. These PS I preparations have no EPR-detectable cytochrome, soluble spinach [2Fe-2S] ferredoxin or Rieske Fe-S center and very little g=4.3 Fe (much less than one atom per reaction center). The EPR spectra of both PS I preparations had signals due to centers A, B and X similar to those previously reported (Evans, 1982). Samples prepared from the two organisms showed no significant differences in g values or linewidths of the EPR signals.

Fe X-ray absorption edge spectra of PS I preparations in which A, B and X are oxidized are shown in Figure IV-2, along with edge spectra for three reference compounds: $(Et_4N)_2$ Fe_4S_4(S-benzyl)$_4$, $(Et_4N)_2Fe_2S_2(S_2$-o-xyl$)_2$ and spinach $[2Fe\text{-}2S]^{2+(1+,2+)}$ ferredoxin (Nomenclature Committee of the I. U. B., 1979). Note that the shapes of the PS I edges and the edge positions are remarkably similar to that of the soluble spinach [2Fe-2S] ferredoxin, and are generally similar to all of the Fe sulfur spectra. In particular, the 1s to 3d transition in the pre-edge region is at least one tenth of the total edge height in all cases. The data from *Synechococcus* and spinach PS I are also remarkably similar to one another. Octahedral or distorted octahedral Fe complexes with mainly oxygen or nitrogen ligands have edge spectra which are very different from those of

PS I from Spinach

60 kDa

20 kDa

16 & 18 kDa

Figure IV-1. SDS polyacrylamide gel of PS I preparations from spinach. The band at ca. 60 kDa contains two distinct polypeptides which bind the primary reactants of PS I and probably also bind center X. Their true molecular weights are approximately 80 kDa, much higher than the apparent weight on this gel. Acrylamide concentration: 15%. The binding site of centers A and B is an 8 kDa polypeptide that either does not stain well or is not resolved well in this gel. (XBB 879-7428)

Fe-S complexes, and the presence of such a complex is obvious even when it constitutes a small fraction (10 - 15%) of the Fe. This is illustrated in Fig IV-3.

In our hands, the K-edge spectra of reduced ferredoxins and Fe-S clusters were not substantially different from those of the oxidized clusters when the reduction was conducted anaerobically (data not shown). The edge position shifted by a small amount (< 0.5 eV) to lower energy but no distinguishable changes were observed in edge shape. When the ferredoxins were irreversibly destroyed by oxidative damage, we saw dramatic changes in edge shape similar to those previously attributed to reduction (Teo & Shulman, 1982).

The k^3-weighted Fe EXAFS spectra of PS I preparations containing A, B and X in the oxidized state are shown in Fig IV-4. The envelope and beat pattern clearly indicate the presence of more than one frequency component in the data. The modulus and the real part of the Fourier transforms of these spectra are shown in Fig IV-5.

The Fourier transformed EXAFS spectra of PS I provide evidence for the presence of two classes of neighbor atoms with peak positions (or bond lengths) characteristic of Fe-S clusters. Curve fitting of the EXAFS spectra indicated that the closest neighbor is likely to be sulfur and the other neighbor is Fe. Although EXAFS simulations cannot distinguish between Fe and some other transition metals, we have analyzed our PS I preparation for all of the other transition metals necessary for growth (Mo, Mn, Zn, Cu and Co) by atomic absorption analysis and find less than 0.4 atom per P700 in all cases. Table I lists the Fe-S and Fe-Fe bond lengths and the Debye-Waller parameters determined by simulating our EXAFS data. The bond lengths for the PS I preparations are nearly identical to those we determined for the [2Fe-2S] and [4Fe-4S] ferredoxins and the inorganic clusters. The data do not indicate any additional neighbors other than the Fe and S. In particular we found no evidence for nitrogen or oxygen ligands, or for additional Fe or sulfur neighbors at unusual bond distances. There are no significant differences between the *Synechococcus* and the spinach PS I EXAFS spectra. There

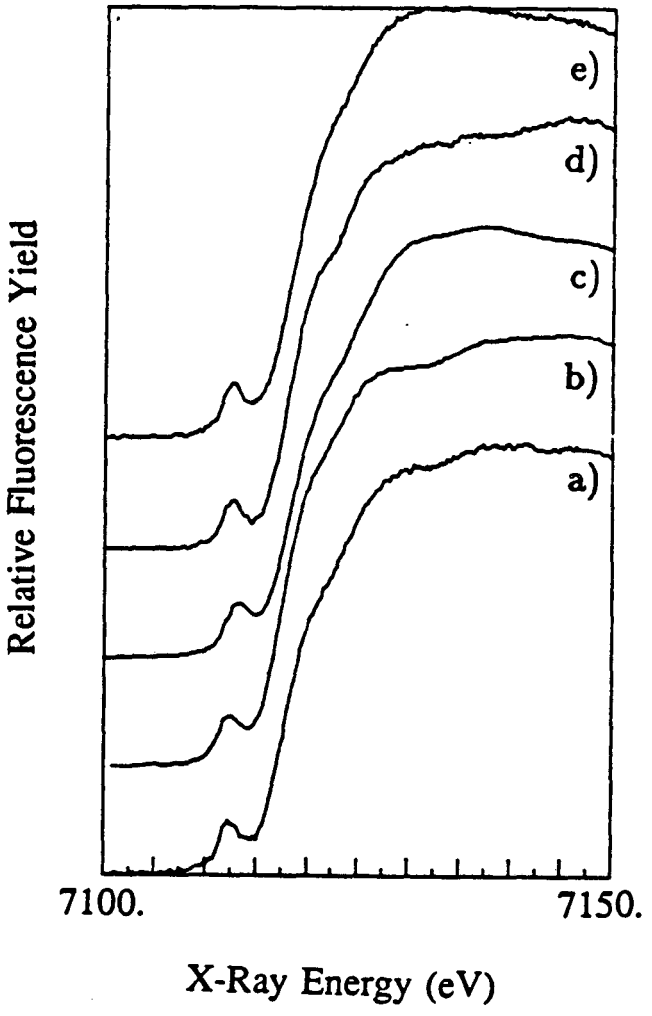

Figure IV-2. X-ray absorption edge spectra of oxidized PS I and oxidized iron-sulfur compounds. From the bottom: a) PS I from spinach, b) PS I from *Synechococcus*, c) $(Et_4N)_2Fe_4S_4$ $(S\text{-benzyl})_4$, d) Spinach $[2Fe\text{-}2S]^{2+(2+,1+)}$ ferredoxin, e) $(Et_4N)_2Fe_2(S_2\text{-o-xyl})_2$. A linear background has been removed from all spectra. The pre-edge feature at approximately 7112 eV has been assigned as a 1s-3d transition and is a good indicator of non-centrosymmetric environments. The PS I from spinach and *Synechococcus* are quite similar to each other and to the soluble spinach [2Fe-2S] ferredoxin.

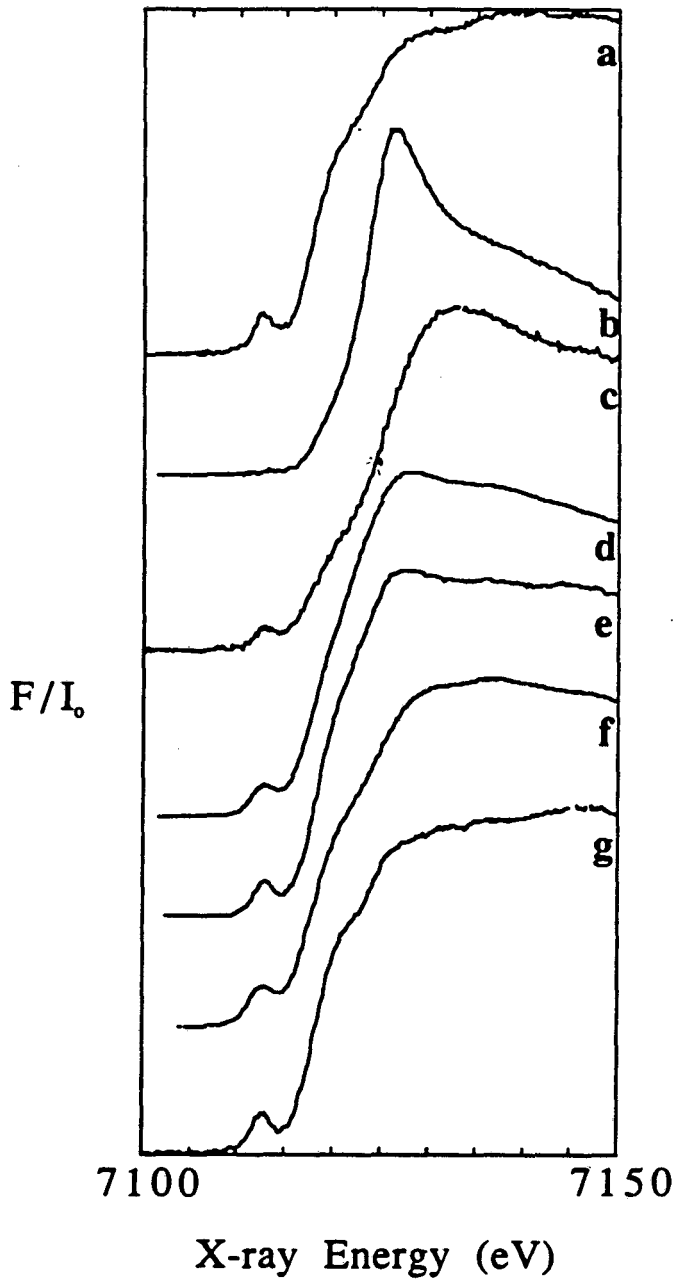

Figure IV-3. Fe X-ray absorption edge spectra of oxidized PS I and other iron complexes. The spectra are: a) PS I from spinach, b) octahedral iron, c) Clostridial ferredoxin containing 15% octahedral iron, d) $(Et_4N)_2Fe_4S_4(S\text{-benzyl})_4$ with 15% octahedral iron, e) spinach [2Fe-2S] ferredoxin with 15% octahedral iron, f) $(Et_4N)_2Fe_4(S\text{-benzyl})_4$ and e) spinach [2Fe-2S] ferredoxin. The iron K-edge spectrum of PS I strongly resembles that of spinach ferredoxin, and is not so similar to any of the spectra containing 15% octahedral iron. This argues against a model for PS I in which an [8Fe-8S] ferredoxin (centers A and B) and one or more octahedral iron atoms are present.

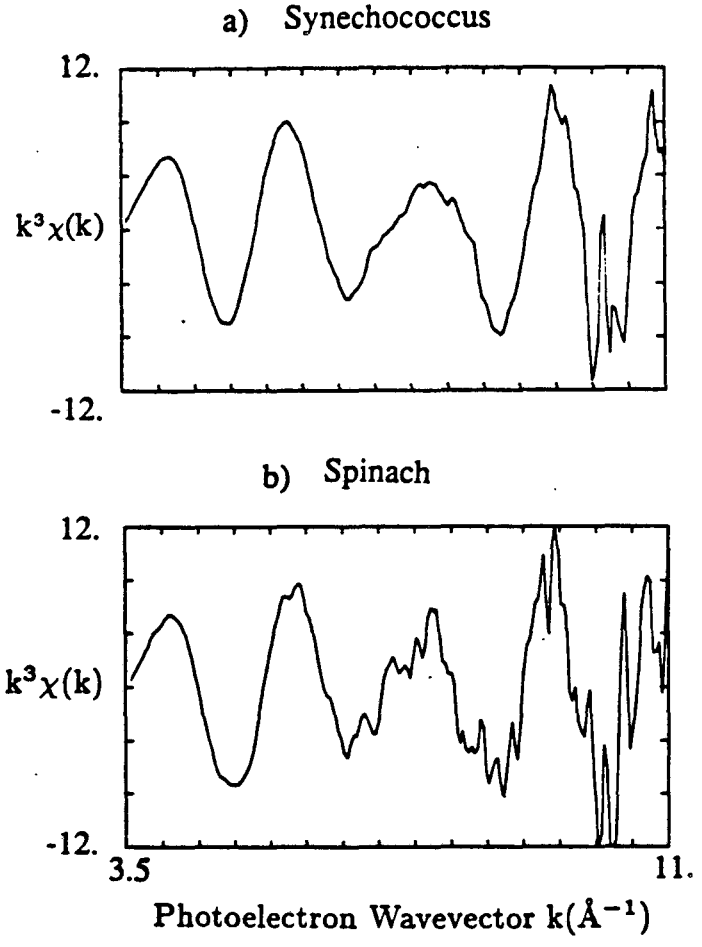

Figure IV-4. EXAFS spectra of PS I preparations, with background removed and weighted by k^3. The top spectrum (a) is PS I from *Synechococcus*; the bottom spectrum (b) is PS I from spinach. The spectra clearly contain more than one Fourier component.

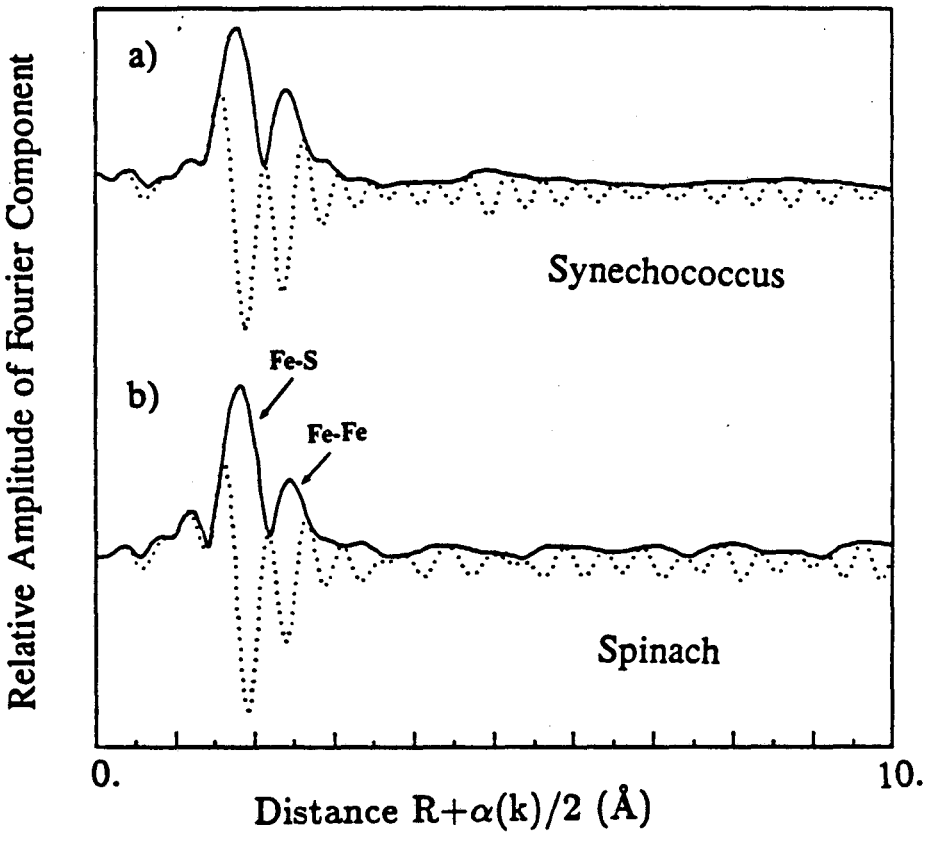

Fig IV-4. Fourier transformed EXAFS spectra of PS I: a) from *Synechococcus* (top) and b) from spinach (bottom). Solid line–modulus; dotted line–real component. The first peak is due to backscattering from sulfur at 2.27 Å, and the second is due to backscattering from iron at 2.75 Å.

were also no significant differences between oxidized and reduced *Synechococcus* PS I EXAFS spectra (data not shown).

Figure IV-6 shows the Fourier-filtered spinach PS I EXAFS data plotted over data from soluble spinach [2Fe-2S] ferredoxin and data from soluble Clostridial [4Fe-4S] ferredoxin. In the region of k=7.5 $Å^{-1}$ the [4Fe-4S] reference compound spectra differ from the PS I spectra. Around k=7.5 $Å^{-1}$ the dimer and tetramer oscillations are far out of phase, and the phase of the PS I spectrum resembles that of the dimer. Curve fitting analysis demonstrates that the spectrum is better explained by a sum of [2Fe-2S] ferredoxins and [4Fe-4S] ferredoxins than by a sum of all [4Fe-4S] ferredoxins. The best fits of the PS I data involved two Fe neighbors and Debye-Waller factors similar to those of our reference compounds (Table IV-1). We specifically addressed whether X might be a [4Fe-4S] ferredoxin, or [2Fe-2S] ferredoxins by attempting to fit the EXAFS data with specified numbers of Fe neighbors. Figure 6 shows fits to the spinach PS I (6 a and b) and to the *Synechococcus* PS I (6 c and d) data. In each case the number of Fe neighbors used in the fit was constrained to either 2.3 (6 b and d) or 3.0 (6 a and c) to simulate either a mixture of two [2Fe-2S] and two [4Fe-4S] ferredoxins or to simulate all [4Fe-4S] ferredoxins. The Debye-Waller disorder parameter was *not* fixed for any simulations, and the values used give optimal simulations. The central portions of these fits are the most informative, because the 'beat' region of the envelope is quite sensitive to the ratio of Fe and S backscattering. It is also the most reliable portion of the data, because the signal to noise is poor in the high k region, while the very low k region has features owing to processes other than EXAFS. For both the spinach and *Synechococcus* PS I spectra, the fits to a model with both [2Fe-2S] and [4Fe-4S] ferredoxins had lower least squares errors by a factor of more than two than did the fits for an all [4Fe-4S]; the former fits also match the data much better in the region of k=7.5$Å^{-1}$. Thus, even with larger Debye-Waller factors, fits using three Fe neighbors did not agree with the data. Parameters for simulations of the PS I Fe EXAFS to an assumed model of all [4Fe-4S] clusters and for the best simulations are included in Table IV-2. Assuming

that 10 or 15% of the Fe is in a non-ferredoxin and oxygen-coordinated environment did not change our essential conclusion that including [2Fe-2S] clusters as well as [4Fe-4S] clusters achieves a much better simulation than including [4Fe-4S] clusters alone (simulations not shown).

Figure IV-8 shows the Fourier transformed Fe EXAFS data of the LDS and Tiron-treated PS I preparations. The Fourier transformed data shows a very large feature at R + $\alpha/2$ of 4.4 Å. The large amplitude of this feature, despite the fact that it occurs at an apparent distance greater than 3 Å, is suggestive of a multiple scattering origin. The other unusual aspect of the EXAFS spectrum is that the features which we tentatively assign as Fe-S and Fe-Fe backscattering features at R+α < 3.0 Å are not so well resolved as in other Fe-S EXAFS spectra. We have been unsuccessful in simulating this spectrum to our satisfaction; this may be because our simulation routines include single scattering calculations only. Neither of these two unusual features is seen in the spectrum of control PS I preparations. Experiments are in progress to confirm this result, to attempt to prepare more native X samples, and to measure the EXAFS of the linear trimeric complex.

IV C. Discussion

The Fe K-edge spectra of PS I are almost identical to that of the soluble spinach [2Fe-2S] ferredoxin including the size of the 1s to 3d transition, which is an indicator of the amount of tetrahedral Fe. This feature is systematically larger in tetrahedral than in trigonal bipyramidal complexes, and smaller yet in octahedral complexes, as is predicted from symmetry considerations (Roe et al., 1984). We conclude that among the 10-14 Fe atoms per P700 there may be one octahedral Fe atom, but it is unlikely that there are two or more. This implies that there are additional Fe-S centers present besides A and B; it is *not* consistent with these X-ray absorption results that the iron in PS I consists of an [8Fe-8S] ferredoxin and one or more octahedral Fe atoms (as part of an Fe-Q complex). The additional Fe-S clusters are likely to be X on the basis of its EPR spectrum.

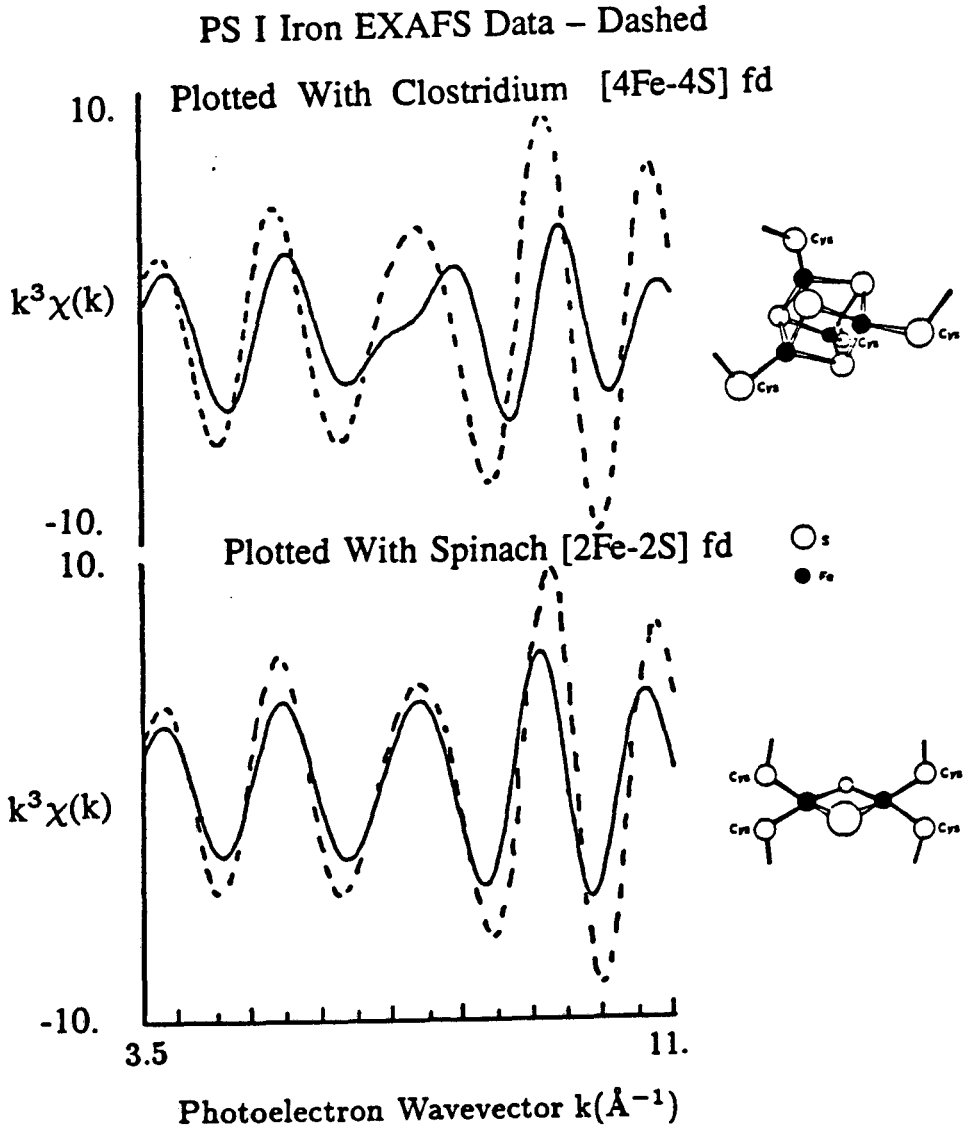

Figure IV-6. The Fourier filtered k^3-weighted spectrum of spinach PS I preparation (dotted spectrum) is plotted with the spectra of reference samples (solid spectrum). The top panel is a spectrum of $(Et_4N)_2Fe_4S_4(S\text{-benzyl})_4$, and the the bottom panel is a spectrum of $[2Fe\text{-}2S]^{2+(1+,2+)}$ ferredoxin. The strong beat in the region around k=7.5Å^{-1} is diagnostic of [4Fe-4S] ferredoxins. This region of the spectrum indicates that PS I is likely to contain some [2Fe-2S] ferredoxins.

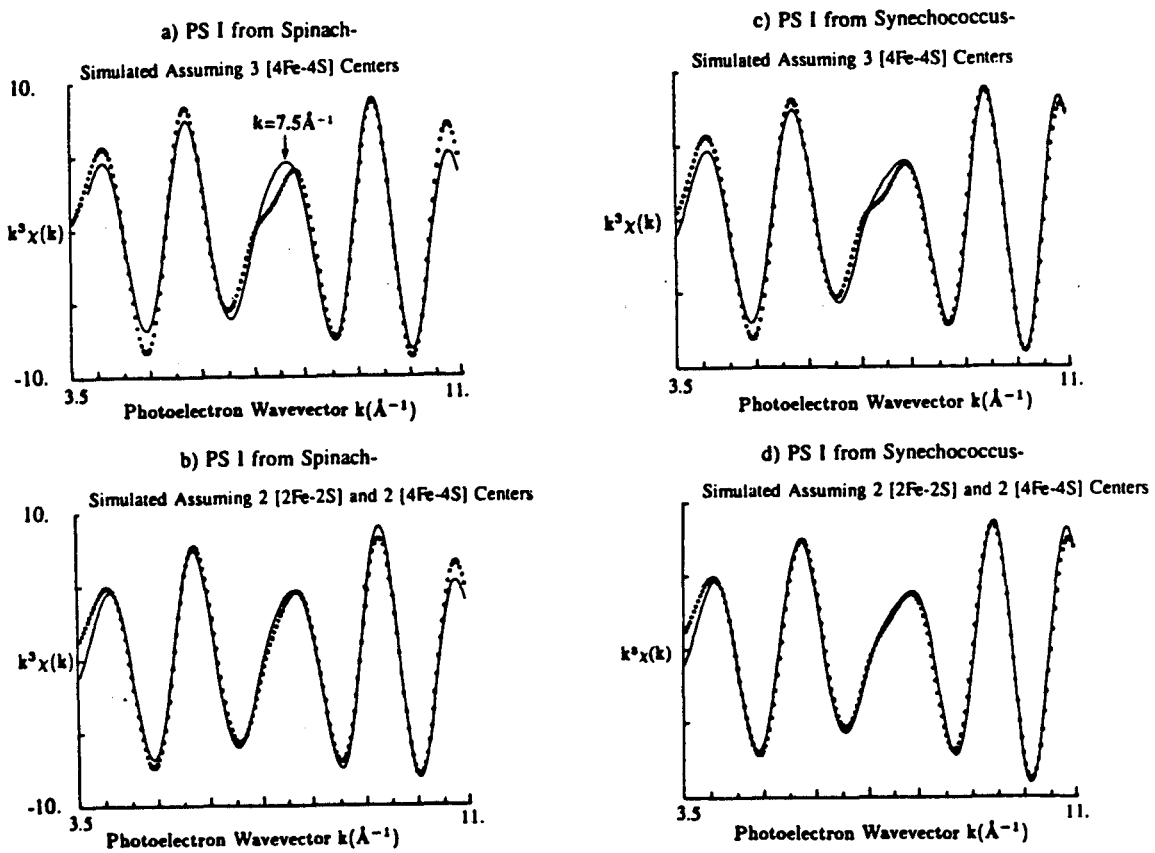

Figure IV-7. Fourier filtered, k^3-weighted EXAFS spectra of iron in PS I (solid lines), and calculated simulations of the spectra (dotted). The fits are as follows: a) fit of spinach data assuming all [4Fe-4S] ferredoxins, b) fit of spinach data assuming an equal number of [2Fe-2S] and [4Fe-4S] ferredoxins, c) fit of *Synechococcus* data assuming all [4Fe-4S] ferredoxins, d) a fit of *Synechococcus* data assuming an equal number of [2Fe-2S] and [4Fe-4S] ferredoxins. Note that the quality of fit in the beat region indicates that PS I is likely to contain [2Fe-2S] as well as [4Fe-4S] ferredoxins. However, other iron sulfur complexes in which there is one iron neighbor at 2.7 to 2.8 Å on average would also be consistent with these EXAFS data.

TABLE IV-1

Bond Distances and Coordination Numbers of Iron-Sulfur Compounds, Proteins, and PS I [a]

SAMPLE	$R_{Fe-S}(A)$	N_S	$\sigma_{Fe-S}(A)$	$R_{Fe-Fe}(A)$	N_{Fe}	$\sigma_{Fe-Fe(A)}$
Spinach [2Fe-2S] Fd.	2.26	4.1	.07	2.74	0.9	.05
$(Et_4N)_2Fe_4S_4$(S-benzyl)$_4$	2.25	4.0	.08	2.74	2.9	.08
Clost. Past. Fd.	2.23	4.	.08	2.75	2.8	.09
PS I from Spinach	2.27	3.9	.07	2.78	1.9	.08
PS I from *Synechococcus*	2.26	4.6	.07	2.76	2.1	.07

[a] Bond distances and Debye Waller parameters determined by the Teo-Lee method (Teo & Lee, 1979). Error in determination of R is .03 A, in σ is .02 A. The error in N is approximately 20% in all cases except for *Clostridium Pasturianum* ferredoxin for which it is 30%.

TABLE IV-2

EXAFS Simulation Parameters of PS I Data [a,b]

SIMULATION	N_{Fe}	$\sigma_{Fe\text{-}Fe(A)}$	Error[c]
PS I from Spinach Simulated assuming all [4Fe-4S]	3.0	.12	60.
PS I from Spinach Best Fit	1.9	.08	9.
PS I from *Synechococcus* Simulated assuming all [4Fe-4S]	3.0	.10	100.
PS I from *Synechococcus* Best Fit	2.1	.07	50.

[a] Values determined by the Teo-Lee method (Teo & Lee, 1979).

[b]The errors for the best fits are smaller by a factor of six for spinach and two for *Synechococcus* as compared with all-[4Fe-4S] simualtions. The Debye-Waller factors of 0.08 A and 0.07 A for the best fits are similar to the values obtained from reference Fe-S complexes.

[c] Error in fit is the sum of residuals.

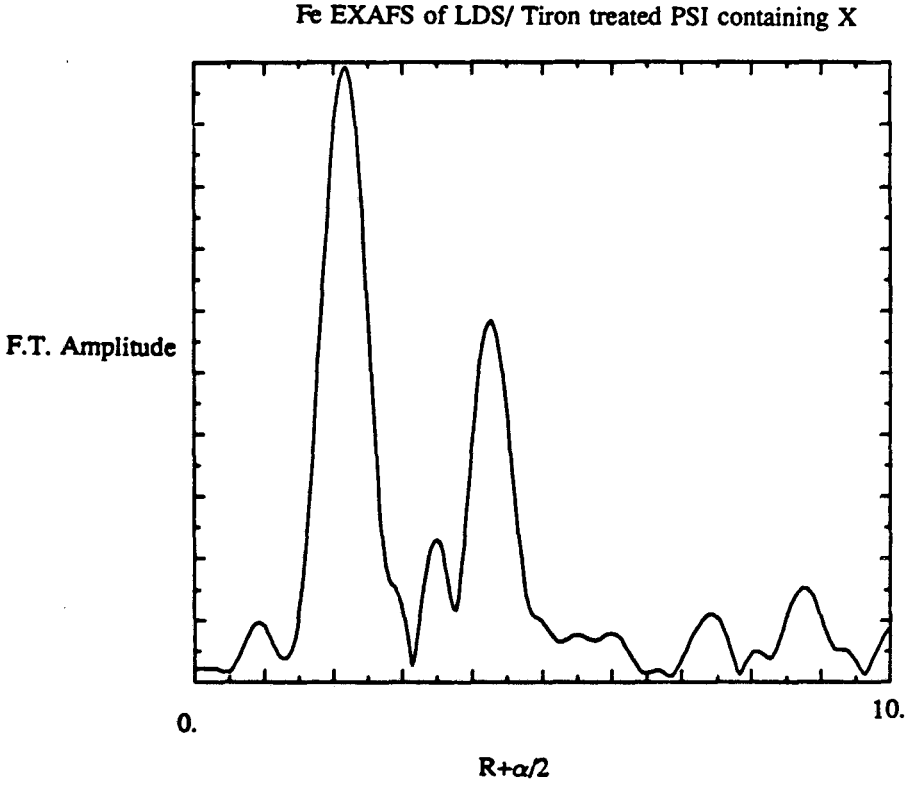

Figure IV-8. Fourier transformed Fe EXAFS spectrum of the LDS-treated X-enhanced PS I preparation. The feature at R + $\alpha/2$ of 4.4 Å is probably due to multiple scattering.

The EXAFS spectra have the characteristic features of an Fe-S cluster, with sulfur and Fe peaks at 2.27 Å and 2.74 Å and no other significant peaks. To discriminate between the two probable structures for X, [2Fe-2S] cluster(s) or a [4Fe-4S] cluster, we simulated the EXAFS spectrum to derive the average number of Fe neighbors. The [2Fe-2S] clusters and [4Fe-4S] clusters differ in the number of Fe neighbors by a factor of three, so that discriminating between all [2Fe-2S], half [2Fe-2S] and half [4Fe-4S] or all [4Fe-4S] clusters is within the capabilities of EXAFS. However, N is correlated with two of the parameters in our simulations: S_f, a scaling factor for the overall backscattering, and σ, the Debye-Waller disorder parameter. S_f was determined from analysis of spinach $[2Fe\text{-}2S]^{2+(1+,2+)}$ ferredoxin and other reference compounds, and agrees with determinations from previous studies (Teo et al., 1979). Because the soluble ferredoxins are structurally similar to the Fe in PS I, the determination of the number of neighbors is probably not subject to previously discussed systematic errors that arise from chemically dependent factors (Eisenberger & Lengeler, 1980). An erroneous value for σ can only partially compensate for an erroneous value for N, because the value of σ affects the envelope of the backscattering function while N affects the overall scaling of the backscattering. If an assumption is made that N_{Fe}=3.0, as in fig 5a and 5c, the best fits within this constraint involve an unusually high value for σ_{Fe-Fe} (ca. 0.12 Å), which partially compensates for the erroneously high value for N. These simulations are not satisfactory because they disagree with the data in the diagnostic 'beat region' near k=7.5 $Å^{-1}$. Our best fits for the PS I data had 2.0 ± .4 Fe neighbors, with Debye-Waller factors more typical of Fe-S clusters (0.07 to 0.08 Å). These simulations agree much better with the data than do those which assume an all [4Fe-4S] model for PS I. The parameters used in these simulations are given in Table IV-2. The EXAFS data indicate that there are fewer than three Fe neighbors at 2.75 Å on average and thus are not consistent with a model in which all of the Fe in PS I is in relatively symmetric, traditional [4Fe-4S] clusters.

Since centers A and B are probably [4Fe-4S] centers, the EXAFS data indicate that PS I includes in addition some [2Fe-2S] cluster(s) or some other Fe-S cluster in which on average each Fe has one Fe neighbor at 2.7 Å. It is logical to assign this Fe-S cluster(s) as X. One model for the Fe in PS I which we considered to be likely, based on biochemical precedent and previous evidence concerning PS I, is a mixture of two [2Fe-2S] clusters (which are X) and two [4Fe-4S] clusters (which are centers A and B). The simulation involving two [2Fe-2S] and two [4Fe-4S] ferredoxins is within the error of the parameters used for the best global fit, while the simulation using all [4Fe-4S] clusters is outside of that error range IV-7, Table IV-2). However, the EXAFS spectra may also be consistent with other assignments for X, as long as the structure is a four coordinate sulfur complex involving two to six Fe atoms. In addition the Fe atoms (on average) must have approximately one Fe neighbor at 2.7 Å. Some biologically unprecedented structures fit this description, such as the highly distorted tetranuclear or trinuclear Fe-S clusters (Hagen et al., 1983, Kanatzidis et al., 1983). The distorted tetranuclear is of particular interest because the addition of an extra thiolate ligand to one of the Fe atoms causes major changes in the Fe-Fe distances such that they might result in a reduced amplitude of Fe backscattering because of destructive interference of the EXAFS contributions. In addition, the extra S ligand causes the midpoint potential of the cluster to be lowered by approximately 0.5 V relative to those of other synthetic [4Fe-4S] clusters. It is unclear at present whether such structures would be consistent with the EPR spectra of X.

The EXAFS spectrum of the LDS-treated and X-enhanced preparations exhibits a very large feature at R + $\alpha/2$= 4.3 Å. This unusual feature is suggestive of a multiple scattering process. Very large multiple scattering peaks are seen in complexes that have linear arrays of three or more atoms. It is interesting that this feature in the spectrum of the X-enriched sample is found at approximately twice the apparent distance of the usual Fe-Fe backscattering feature. These data indicate a structure similar to the linear

trimeric Fe-S complex synthesized by Holm and coworkers (Hagen et al., 1983). Such a structure has not been observed previously in a biological sample.

As there is no indication of such a (presumably) multiple scattering feature in the EXAFS spectrum of control PS I particles, these EXAFS data indicate that a structural rearrangement of X occurs on removal of centers A and B. Bending the linear trimeric cluster so as to take the three Fe atoms out of alignment would be expected to reduce the multiple scattering feature. It is not simple to estimate what magnitude of structural rearrangement would be necessary to explain the change in the EXAFS spectrum. The synthesis of an extended linear structure such as the linear trimeric cluster would not be expected to occur during degradation of [2Fe-2S] or [4Fe-4S] clusters. Thus the existence of such a biologically unprecedented cluster is an interesting result *even if this cluster represents a structural rearrangement of X.*

The presence of [2Fe-2S] ferredoxins in PS I, as well as their assignment as X are suggested by recent core extrusion ^{19}F NMR characterizations (Golbeck et al., 1987). However, Mössbauer results were interpreted to indicate that X, A and B are all [4Fe-4S] ferredoxins (Evans et al., 1981). In this EXAFS study we analyzed a composite of all of the Fe in the sample, while in the Mössbauer study the reduced-minus-oxidized spectrum was analyzed. It is difficult to reduce X quantitatively by illumination in a concentrated sample. It is possible that the Mössbauer spectrum reflects mainly A and B, while 35% of Fe that on reduction and illumination had an unchanged Mössbauer spectrum may include X, as has been suggested (Bonnerjea & Evans, 1984).

As mentioned in Chapter I, the peptides that are thought to bind X, PSI-A1 and PSI-A2 have no apparent homology to other ferredoxin sequences. It is not known how many copies of each peptide per P700 are present, but it is clear that one copy of each peptide (i. e. two peptides total) would not provide the eight cysteines required for binding two [2Fe-2S] clusters (Fish et al., 1985). These peptides contain six cysteines, which would not be enough to bind two [2Fe-2S] clusters. It is possible that more than one copy each of PSI-A1 and PSI-A2 is involved, or that additional peptides are

involved. On the other hand, X may be bound by fewer than eight cysteines, either because it has nitrogen or oxygen ligands, or because it is not a pair of [2Fe-2S] clusters, but is an unusual Fe sulfur cluster. Due to inherent limitations, EXAFS and edge data do not address whether X may have one N or O ligand, but the involvement of ligands which are less electron donating than S is unlikely based on the unusually low midpoint potential of X.. The absence of these sequence elements lends support to the idea that X is an unprecedented type of Fe-S cluster.

We also conclude from this study that the structures of A, B and X are preserved across the estimated two billion year evolutionary gap separating spinach and *Synechococcus*. We have found no significant differences between the two complexes by EPR, EXAFS, X-ray absorption edge spectroscopy, SDS-PAGE or chemical analysis for Fe and sulfide. This conclusion, as well as the conclusion that A_0 and A_1 are similar in prokaryotes and eukaryotes, has also been reached by other workers (Smith et al., 1987). The structural similarity is not surprising based on the great degree of homology for PS I peptides from the two classes of organisms (Bryant et al., 1987). The use of prokaryotes to accomplish genetic or isotopic substitutions which would be difficult in higher plant systems will probably become more common. The spectroscopic comparison of cyanobacterial and plant reaction centers validates the notion of generalizing results from prokaryotes to higher plant systems.

Chapter V:

Characterization of PS II from Cyanobacteria by EPR and XAS

V A. Introduction

The elucidation of the structure of the Mn-OEC has been advanced by primarily two spectroscopic techniques, EPR and XAS, in conjunction with the use of innovative biochemical preparations. To date, EPR signals have been seen only in the S_2 state, so a significant advantage of XAS is that it may be used to probe all of the S states that can be prepared. As mentioned in Chapter I, most of the XAS and EPR spectroscopy of the Mn-OEC has been done with plants, but many useful studies of the ligands require the use of prokaryotes or algae. This chapter concerns a comparison of the EPR spectra and XAS of samples in the S_1 and S_2 states from *Synechococcus* and spinach.

A detailed comparison of the spectral properties of the Mn complex in PS II between cyanobacteria and plants is lacking. Therefore, before beginning to do spectroscopic work on prokaryotic PS II, it is useful to conduct a systematic comparison of the EPR signals in the cyanobacteria and spinach. This is the focus of one of the chapters of this thesis. Previous to this work, differences in the proteins of the donor complexes of cyanobacteria and spinach had been reported, including: 1) the absence of 24 and 18 kDa proteins in cyanobacteria (Stewart et al., 1985) which in spinach PS II stabilize binding of two necessary cofactors of oxygen evolution, Ca^{2+} and Cl^- (Ghanotakis & Yocum, 1985), 2) different salt extraction properties of a 33 kDa protein (Koike & Inoue, 1985) which stabilizes binding of Mn but does not provide ligands for Mn (Miller et al. 1987, Cole et al., 1987b) and 3) differences in the gene sequences of D1 and D2 from eukaryotes and prokaryotes (Williams & Chisholm, 1987, Curtis et al, 1984, Mulligan et al, 1984). In addition to these differences in the proteins, different biochemical methods are generally used in preparing PS II from prokaryotic organisms and plant chloroplasts. A multiline EPR signal similar to that observed in the S_2 state

in spinach has been observed in cyanobacteria (Ke et al., 1982) indicating that at least part of the Mn complex is similar in the PS II preparations from the two classes of organisms.

In this chapter I describe 1) development and characterization of a preparation of PS II from *Synechococcus* with a homogeneous Mn content, 2) characterization of the S_1 to S_2 advance and protocol for preparing S_1 and S_2 state samples, and 3) characterization of the structure and oxidation states of the Mn cluster from *Synechococcus* in the S_1 (dark adapted) and S_2 states by EPR and X-ray absorption spectroscopy. The comparison of PS II prepared from the two classes of organisms yields a larger perspective on the salient and essential features of the Mn complex. More significantly, it leads the way for studies of the Mn-OEC that necessarily make use of a prokaryotic organism.

V B. Methods

Methods for preparing and analyzing samples are described in Chapter II.

EPR signal amplitudes were measured as peak-to-trough amplitudes in the first derivative spectrum for the Fe^{2+}-Q signals at g=1.8 and 1.6. The multiline amplitude was measured similarly, using the fourth and fifth hyperfine lines downfield from g=2. In spectra with both the g=1.8 and g=1.6 signals it is difficult to estimate their amplitudes because they overlap; in these cases the amplitudes were estimated by simulating the spectra with sums of spectra containing only one signal. The amplitudes were normalized to correct for variable sample concentrations and volume.

X-ray methods are described in Chapter II.

V C. Results

V C. 1. Characterization of the Preparation

This preparation of PS II from *Synechococcus* results in an improvement in the PS II to PS I ratio of approximately 50 and in a yield of greater than 80% of O_2 evolution activity relative to unfractionated thylakoid fragments. The stability of the steady state

O_2 evolution activity is excellent under the conditions of the preparation procedure and during data collection. Analysis of the preparation indicates 3.5 ± 0.5 Mn and 60 to 70 Chl per reaction center. Despite the fact that the preparation is largely stripped of its light harvesting system and resembles core preparations in peptide content (Figure V-1), the concentration of Mn in a dense pellet is not higher than in spinach Triton X-100 preparations (Yachandra et al., 1986a); both are approximately 700 μM in Mn. Our cursory evaluation of a recent O_2-evolving core preparation from spinach (Ghanotakis & Yocum, 1986) indicates that it also does not allow a significant improvement in reaction center concentration in a dense pellet.

V C.2. EPR Studies of the S_1 to S_2 Transition at 220 K

Figures V-2 and V-3 show the multiline signal generated during continuous illumination at several different temperatures. Figure IV-4 shows the multiline signal generated at 220 K from Synechococcus as compared with a multiline spectrum from spinach PS II illuminated at 190 K (courtesy of Ron Guiles). Spectra collected with 32 Gauss modulation exhibit a very similar lineshape, and both have a splitting in the major features of 88-90 G (figure V-4 A). An essential similarity of multiline signals between spinach and another cyanobacterium, *Anacystis Nidulans*, has also been reported (Aasa et al., 1987). Spectra collected with field modulation of 4 to 8 G show additional structure, as previously discussed for spinach PS II samples (Yachandra et al., 1986b). The first derivative lineshape at high resolution is similar for *Synechococcus* and spinach except for the region between 3550 and 3650 G, where differences are apparent (figures V-4 B and C).

The maximal amplitude of multiline signal is developed at approximately 220 K. Three observations suggest that the conversion from S_1 to S_2 in active centers is essentially complete when conducted at 220 K (data not shown): 1) the multiline signal amplitude is linear with concentration of PS II, 2) the multiline amplitude reaches a maximum with respect to illumination time by 15 sec and remains constant with longer

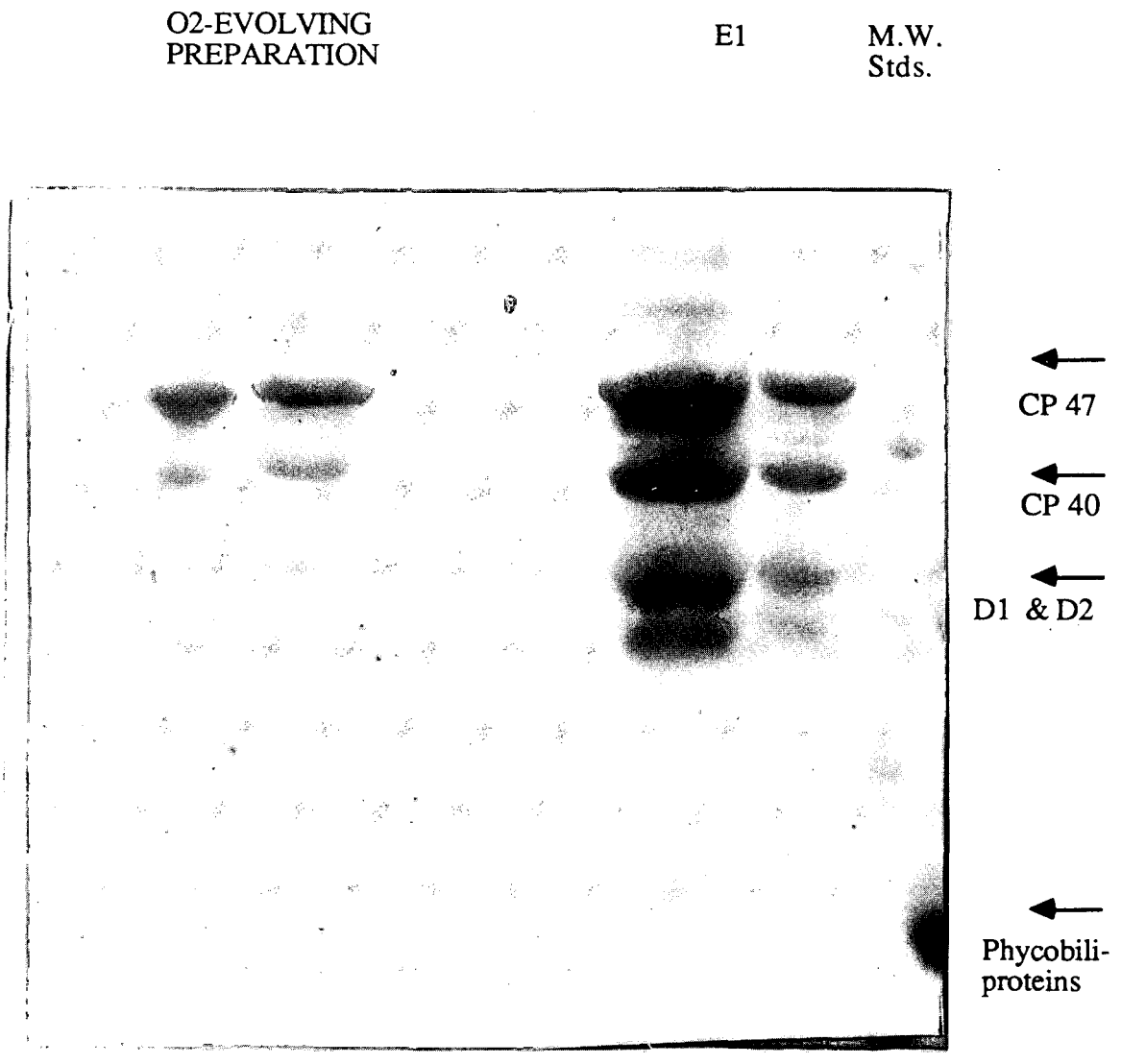

Figure V-1. SDS polyacrylamide gel of PS II from *Synechococcus*. For comparison, a sample of molecular weight standards (MW: 92.5, 66.2, 45.0, 31.0, 21.5, 14.4 KDa, from top) and a sample of the E-1 preparation, a non-oxygen evolving PS II reaction center preparation (Yamagishi et al., 1985; sample courtesy of Dr. Akihiko Yamagishi). (XBB 879-7429)

illumination and 3) the same amplitude of the multiline signal is generated by continuous illumination at 215 K as by illumination at ice temperature in the presence of DCMU, which leads to single turnover photochemistry (Joliot, 1974). Our sample preparation protocols involve resuspending the PS II in a buffer containing 50% glycerol for illumination and EPR measurements. In our experience, the glycerol is necessary to observe the multiline EPR signal.

The g=1.8 and g=1.9 acceptor signals which form upon illumination at 240 K, shown in Figures V-5 and V-6, are similar to the signals formed in spinach PS II (Rutherford & Zimmermann, 1984). The spectra in Fig V-5 and V-6 were measured at 5 K; at this temperature the multiline signal saturates at lower microwave power than do the iron-semiquinone signals, and spectra taken at 50 mW reflect mainly the iron-semiquinone species with little contribution from the multiline spectrum. Although there are two separate signals at g=1.9 and g=1.8, within our signal-to-noise ratio both signals vary in a similar fashion with illumination temperature. In estimating the amplitudes of these signals, we do not distinguish between them and we refer to the composite as 'the 1.8 signal'.

V C. 3. EPR Studies of the S_1 to S_2 Transition at 140 K

Figure V-2 shows that when the illumination is conducted at temperatures below 190 K the amplitude of the multiline EPR signal produced is smaller. In PS II preparations from spinach, the loss of the multiline signal amplitude at lower illumination temperatures is paralleled by the growth of an EPR signal at g=4.1 (Casey & Sauer, 1984, de Paula et al., 1985) which has been assigned to Mn in the S_2 state (Zimmermann & Rutherford, 1986; Cole et al., 1987a). In our preparations, no light-induced signal at g=4.1 is seen. We have extensively and unsuccessfully searched for a Mn signal or other donor species signal from the samples illuminated at 140 K, using microwave powers ranging from 10 μW to 50 mW, measurement temperatures from 4.3 to 25 K and field values ranging from g=8 to g=1.5. In particular we do not see a substantial

Figure V-2. Illuminated-minus-dark EPR spectra of PS II from *Synechococcus*. Spectra were taken at 8K following continuous illumination for 1.5 min at the indicated temperature. A section of the spectrum near g=2 has been removed from the spectrum. Spectrometer conditions were: 9.21 GHz, 50 mW, 32 G and 100 kHz field modulation and a gain of 5000. The observation temperature (8 K) and microwave power were chosen for optimal observation of the multiline signal. The broad multiline signal centered at g=2 strongly resembles the multiline signal observed in spinach PS II particles in the S_2 state. The maximum amplitude of the multiline signal is seen in samples illuminated at 220 ± 10 K.

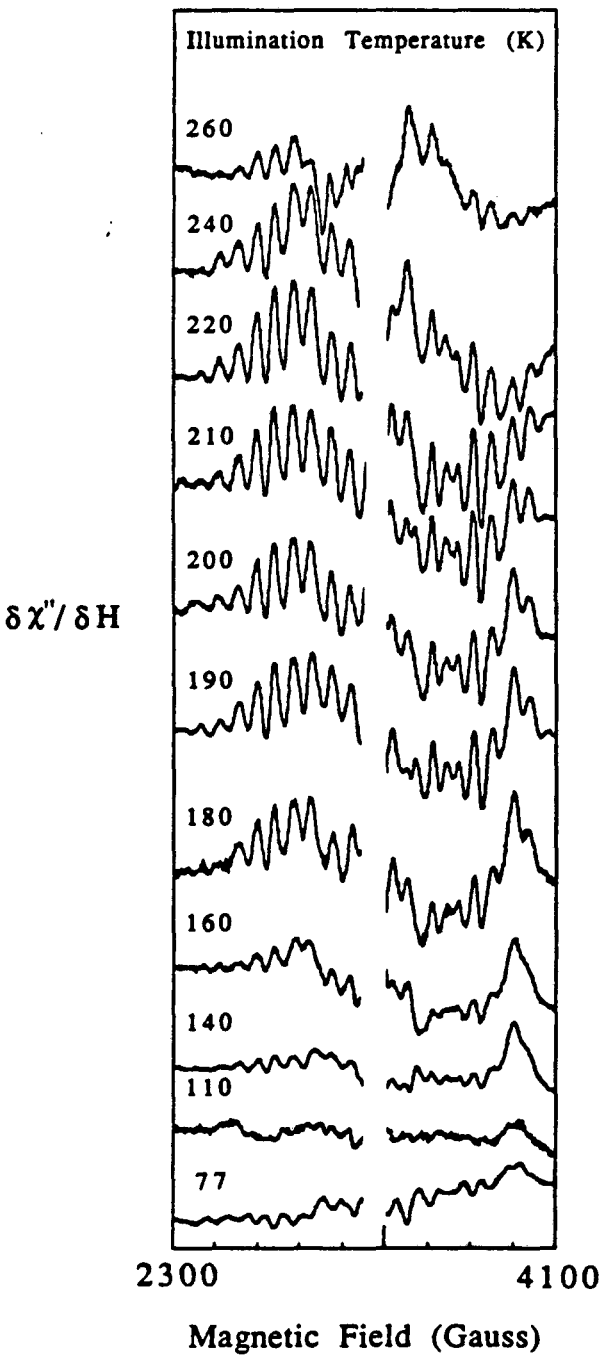
Illumination Temperature (K)
260
240
220
210
200
190
180
160
140
110
77
δχ''/δH
2300
4100
Magnetic Field (Gauss)

Figure V-3. Illuminated-minus-dark EPR Spectra at 8K of PS II from *Synechococcus*. Spectra were taken after continuous illumination for 1.5 min at the indicated temperature. Spectrometer conditions were 50 mW, 32 G of 100 kHz field modulation, microwave frequency 9.21 GHz, gain 5000. The high field portions of these same spectra are shown in Fig V-2, where the multiline signal generation is discussed. The low field portions of these spectra show the lack of g=4.1 signal or any other EPR signals at 8 K following illumination. The cytochrome signals at g=3 and the features at ca. 1000 G are due to a subtraction artifacts resulting from slight variation in sample temperature.

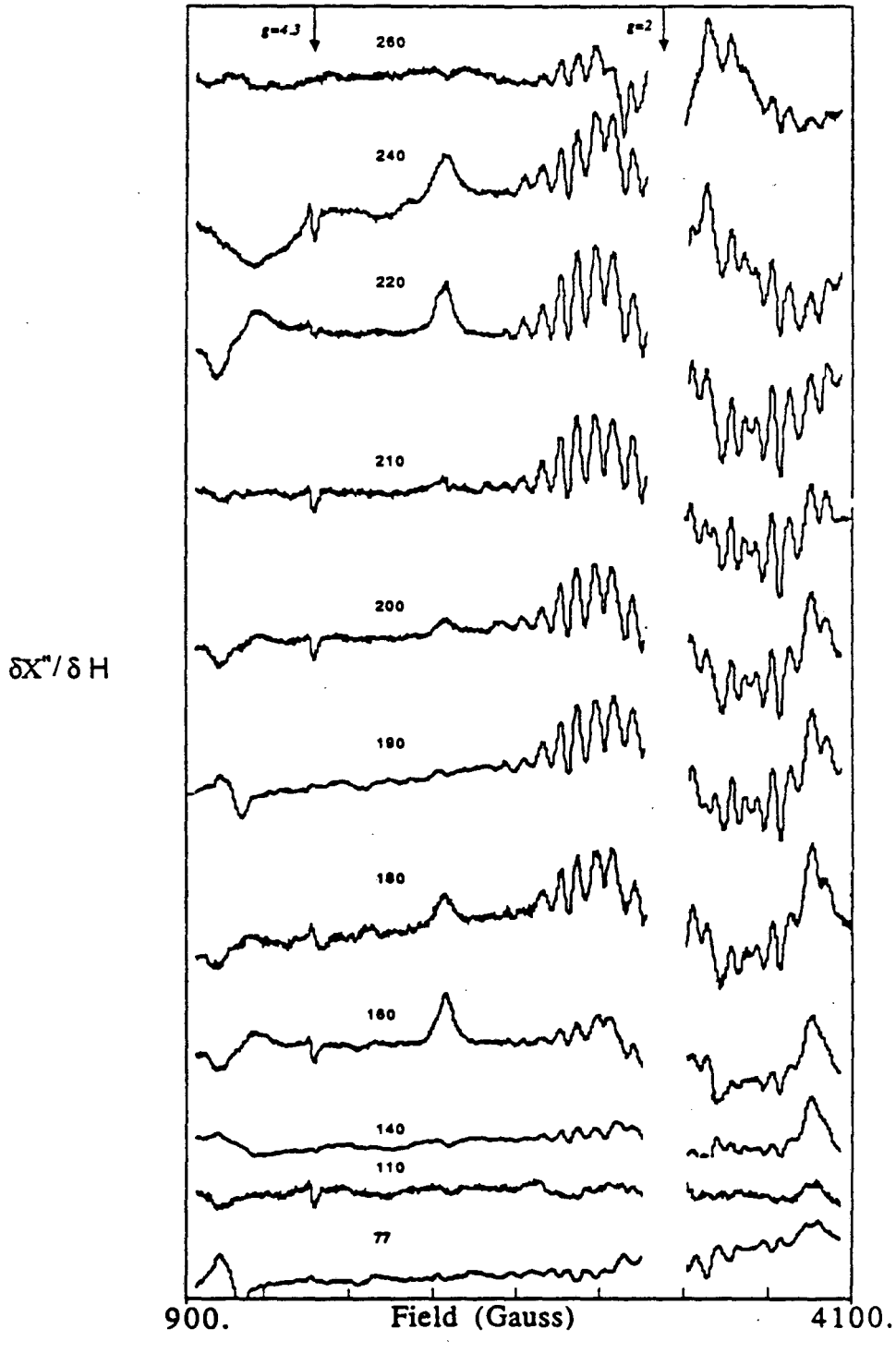
g=4.3
g=2
260
240
220
210
200
190
180
160
140
110
77
δX''/δH
900.
Field (Gauss)
4100.

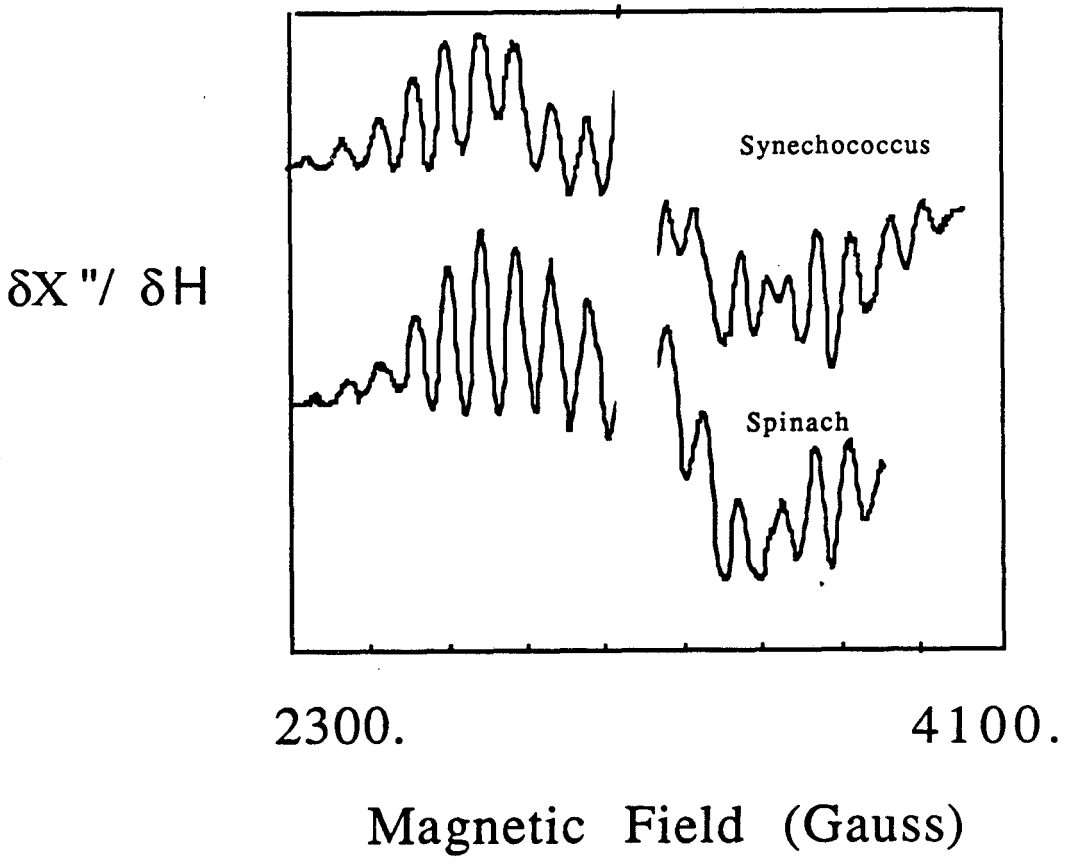

Figure V-4 A. Illuminated-minus-dark EPR spectra at 8 K of PS II from *Synechococcus* illuminated at 215 K and PS II from spinach illuminated at 190 K. Spectrometer conditions as in Fig V-2. The hyperfine splitting in the multiline signal, 88 G, is the same for PS II preparations from the two organisms when the signals were measured with 32 G modulation. Higher resolution spectra are shown in Figures V-2 B and C. (The spectrum from spinach is courtesy of Ron Guiles).

Figure V-4 B. Multiline EPR spectra of PS II from *Synechococcus* and spinach at high resolution. Top panel: three spectra from *Synechococcus*; Bottom Panel: two spectra from spinach. Spectrometer conditions: microwave power, 25 mW; Field modulation 4 Gauss, except for middle *Synechococcus* spectrum, which is 8 Gauss; otherwise as in Fig V-2. Both the *Synechococcus* and the spinach multiline spectra show additional structure at higher resolution. For the higher field region the two samples show similar structure, but between 3550 and 3650 G there is an apparent difference in structure. The field range was chosen to avoid a large contribution from the Fe-Q acceptor signal.

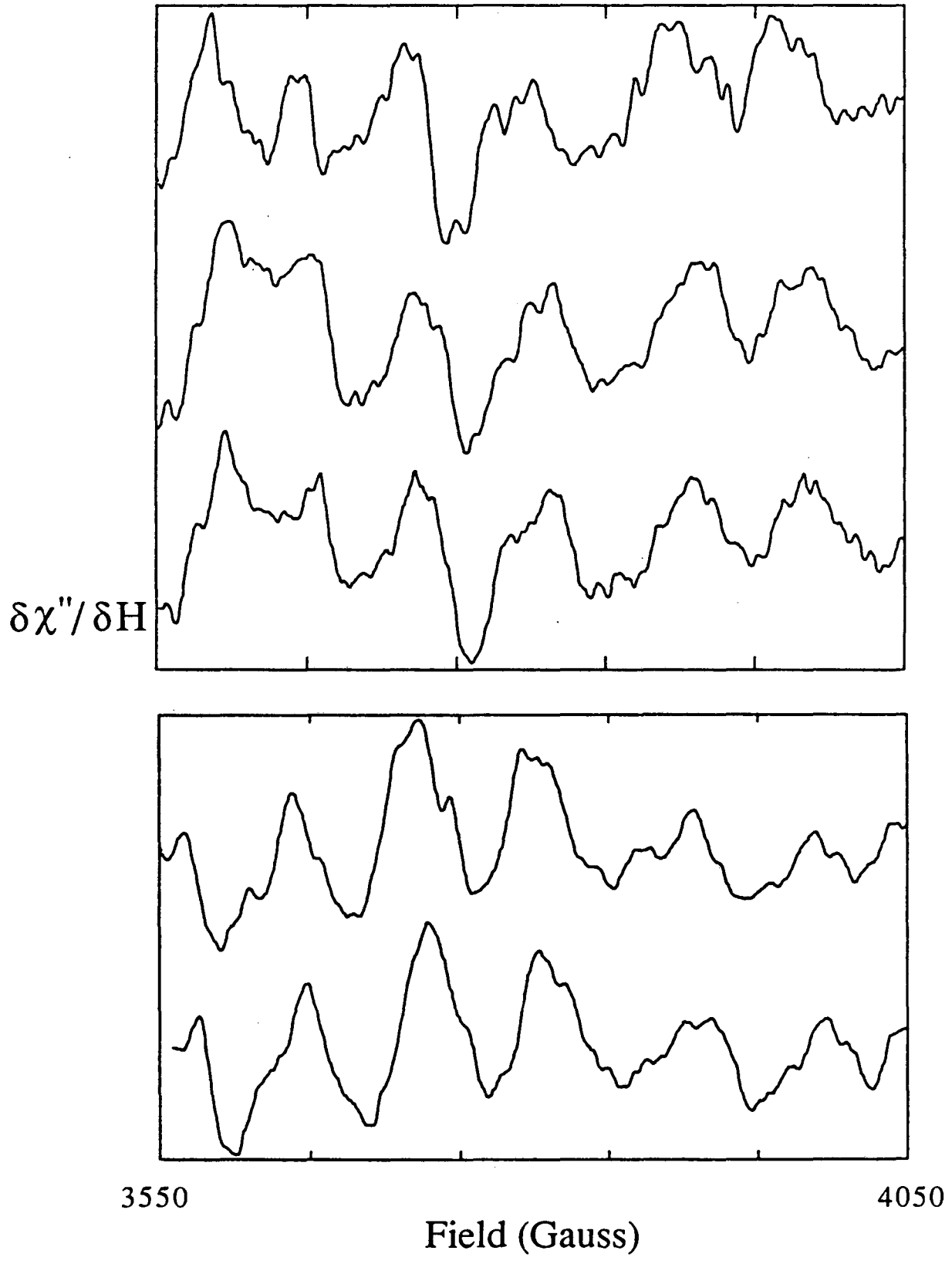
δχ''/δH
3550
4050
Field (Gauss)

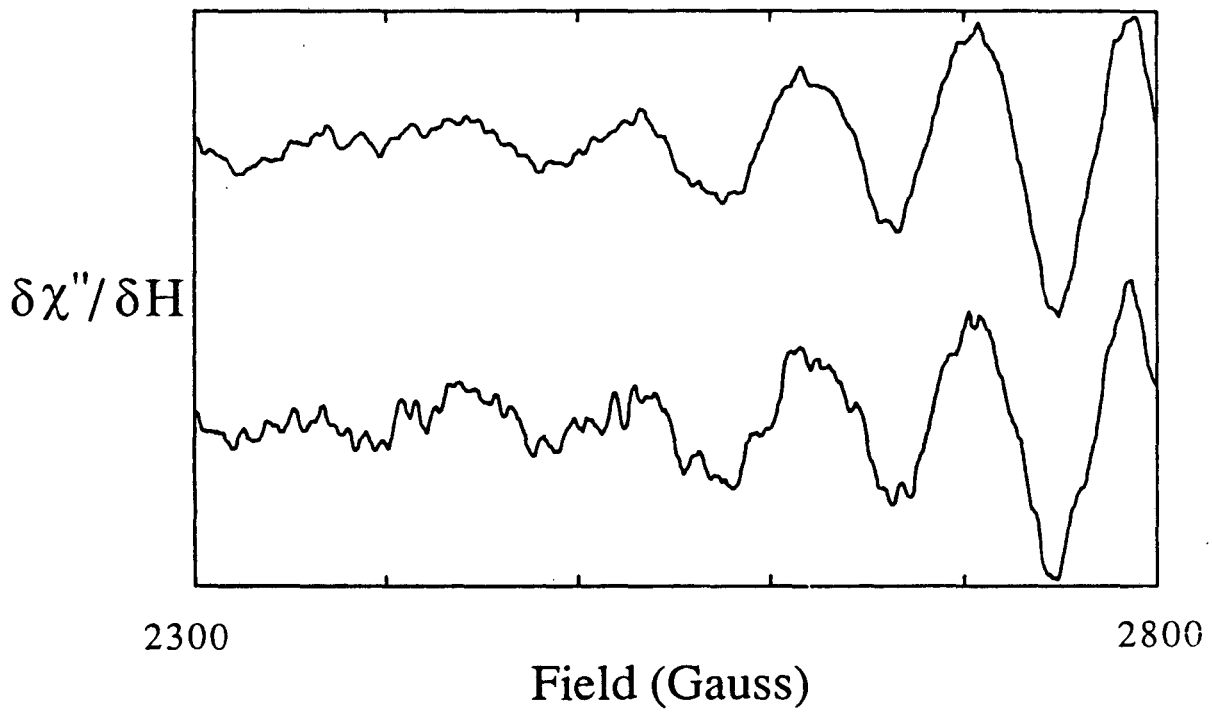

Figure V-4 C. Multiline EPR spectra of PS II from *Synechococcus* at high resolution. The lower field portion shows relatively less structure than does the high field portion. The field range was chosen to avoid a large contribution from the cytochrome signals.

Figure V-5. Illuminated-minus-dark EPR spectra of PS II from *Synechococcus*. Spectra were taken at 5 K following continuous illumination at the indicated temperature for 1.5 min. The observation temperature (5 K) was chosen for optimal observation of the Fe^{2+}-Q_A^- signal with minimal interference from the multiline signal. The signals at g=1.8 and 1.9 generated at 240 and 260 K are due to Fe^{2+}-Q_A^- and Fe^{2+}-Q_B^-; at 180 K and below, the signal due to Fe^{2+}-Q_A^- appears at g=1.6 instead. The smaller amplitude of the signal generated by illumination at 110 and 140 K, as compared with the signal generated by illumination at 180 K, is due to nonsaturating illumination at that temperature. The spectra collected after illumination at 200, 210 and 220 K reflect the g=1.6 signal together with the g=1.8 and 1.9 signals. Other spectrometer conditions as in Fig V-2.

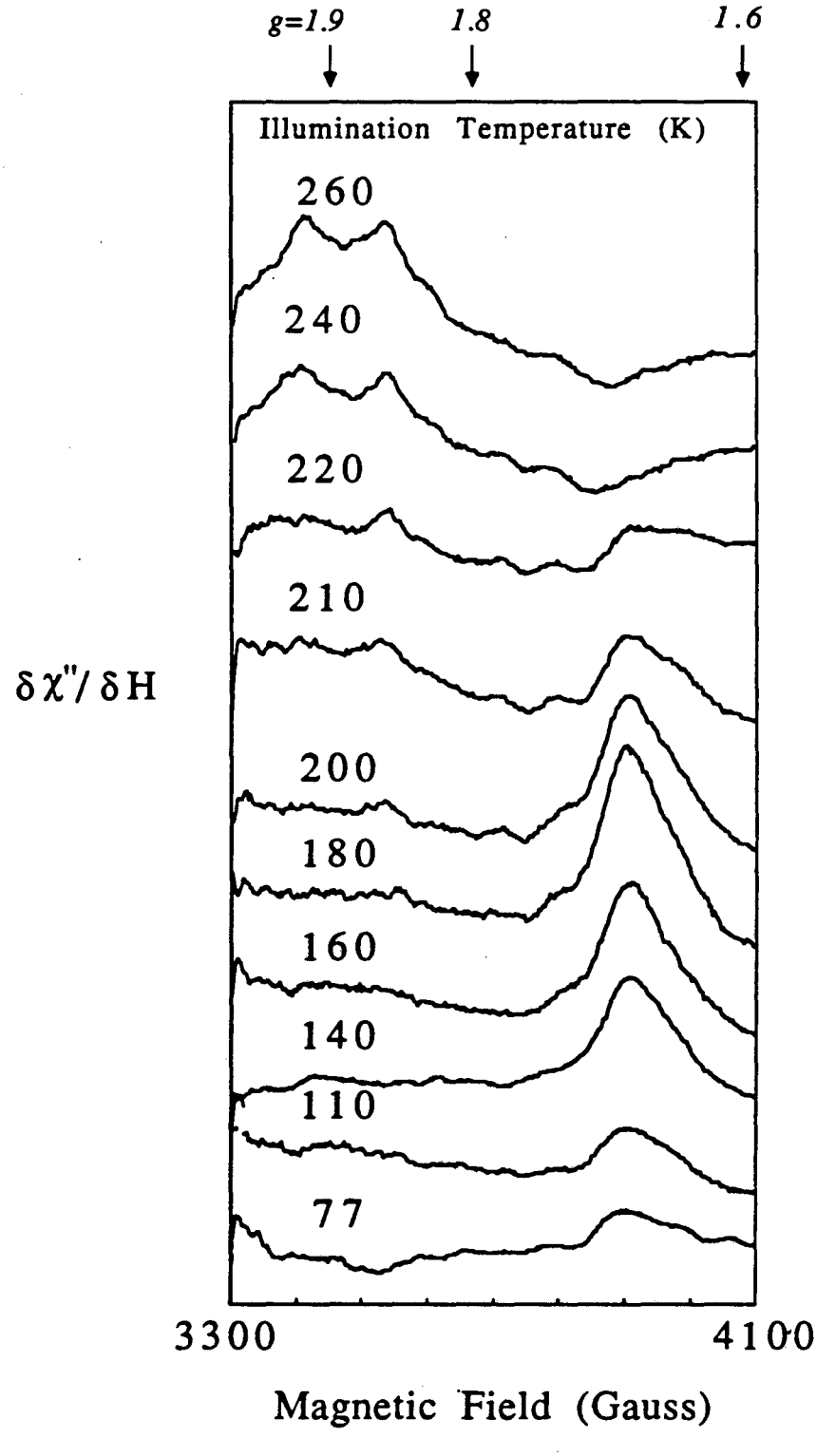
g=1.9
1.8
1.6
Illumination Temperature (K)
260
240
220
210
200
180
160
140
110
77
δχ''/δH
3300
4100
Magnetic Field (Gauss)

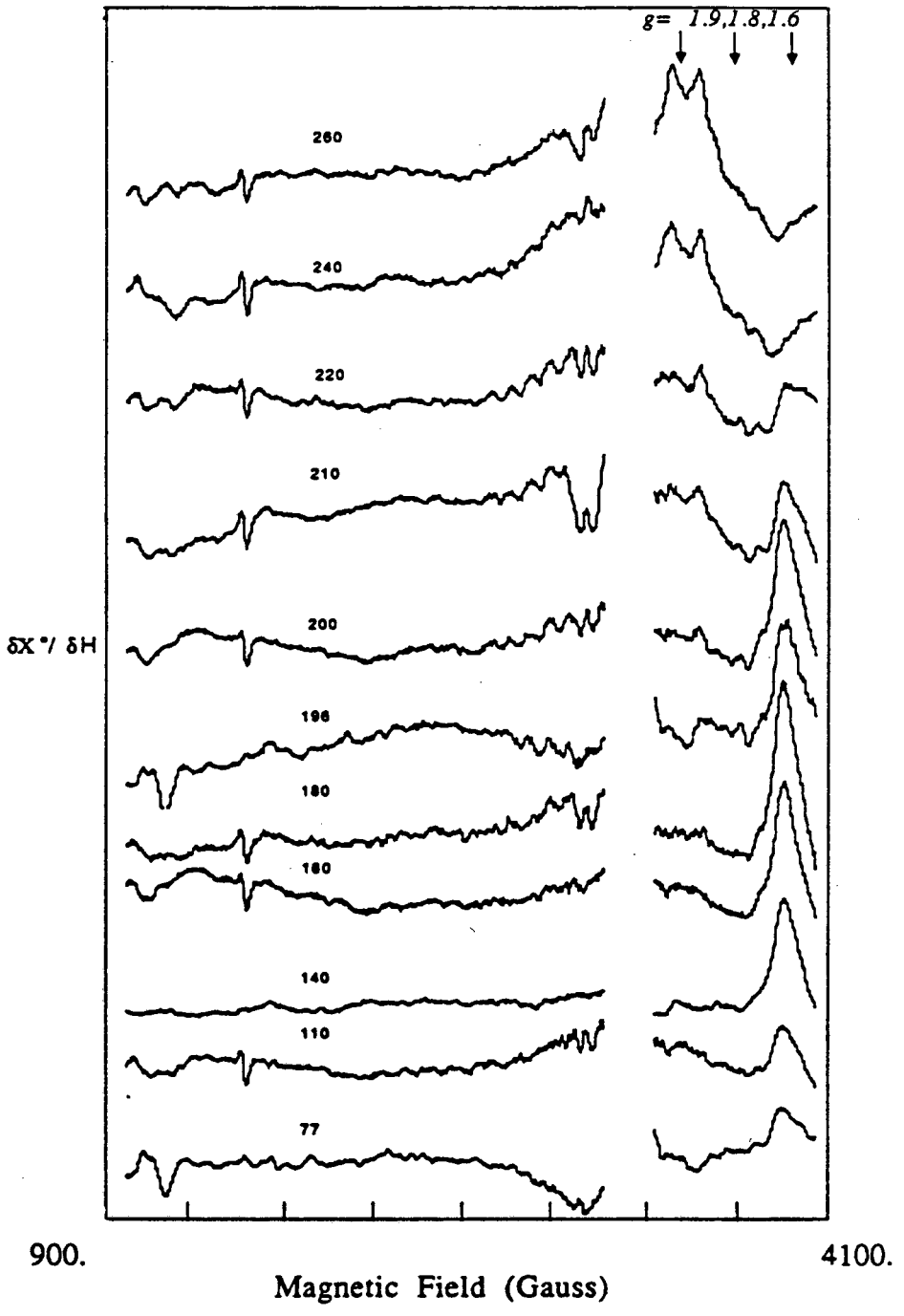

Figure V-6. Illuminated-minus-dark EPR spectra at 5 K of PS II from *Synechococcus*. Spectra were taken following continuous illumination at the indicated temperature for 1.5 min. Spectrometer conditions as in Fig V-2. High field portions of these spectra are shown in Fig V-3, to emphasize the Fe^{2+}-Q_A^- signals. No other light-induced EPR signals were seen at 5 K following illumination.

light-induced g=2 radical signal or a light-induced cyt b_{559} signal. In addition, warming the 140 K illuminated sample to 215 K for 2 min does not result in a donor signal.

Figure V-5 shows that at lower illumination temperatures the g=1.9 and g=1.8 signals assigned to Fe^{2+}-Q_A^- are absent. Upon illumination in the range of 110 to 180 K, we observe a previously unreported signal near g=1.6 (Fig V-5). Figure V-7 illustrates the first derivative lineshape of this signal, which has a broad absorption; the separation between the first derivative maximum and minimum is 300 ± 50 G. The rising edge of this signal is relatively sharper than the falling edge, and its maximum (i.e. the zero-crossing of the first derivative) corresponds to a g-value of 1.64 ± .03. Measurements at 9.19 GHz and 8.87 GHz indicate a change in the first derivative maximum from 3920 G to 3780 G, confirming that the resonance field position reflects the g value of the signal and not zero-field splittings (Figure V-8). This signal is not saturated at microwave powers up to 100 mW at 5 K indicating a very rapid spin relaxation pathway, and the temperature dependence of the amplitude between 5 and 20 K is consistent with a ground state species.

The dependence of the EPR signal amplitudes on temperature of illumination is shown in Figure V-9. The amplitude of the g=1.6 signal is complementary to that of the g=1.8 signal, suggesting that it is an acceptor species (Fig V-9 a). Spectra at 220 K reflect an admixture of the g=1.6 and the g=1.8 signals as shown in Figure V-10.

A likely assignment is an alternative configuration of the Fe^{2+}-Q complex. The sensitivity of this signal to various chemical treatments supports this assignment. Treatment with 25 mM sodium formate at pH 6.0 followed by dark adaptation and illumination at 140 K does not produce the g=1.6 signal, but a signal at g=1.8 appears, which is shown in Figure V-11. This signal has a first derivative lineshape similar to an Fe^{2+}-Q_A^- signal seen in formate-treated spinach PS II (Vermaas and Rutherford, 1984). Treatment with DCMU inhibits O_2 evolution in the preparation from *Synechococcus*. Illumination of DCMU-treated PS II preparations at 140 K does not result in formation of the signal at g=1.6, but results in signals at g=1.8 and 1.9 (Figure V-12).

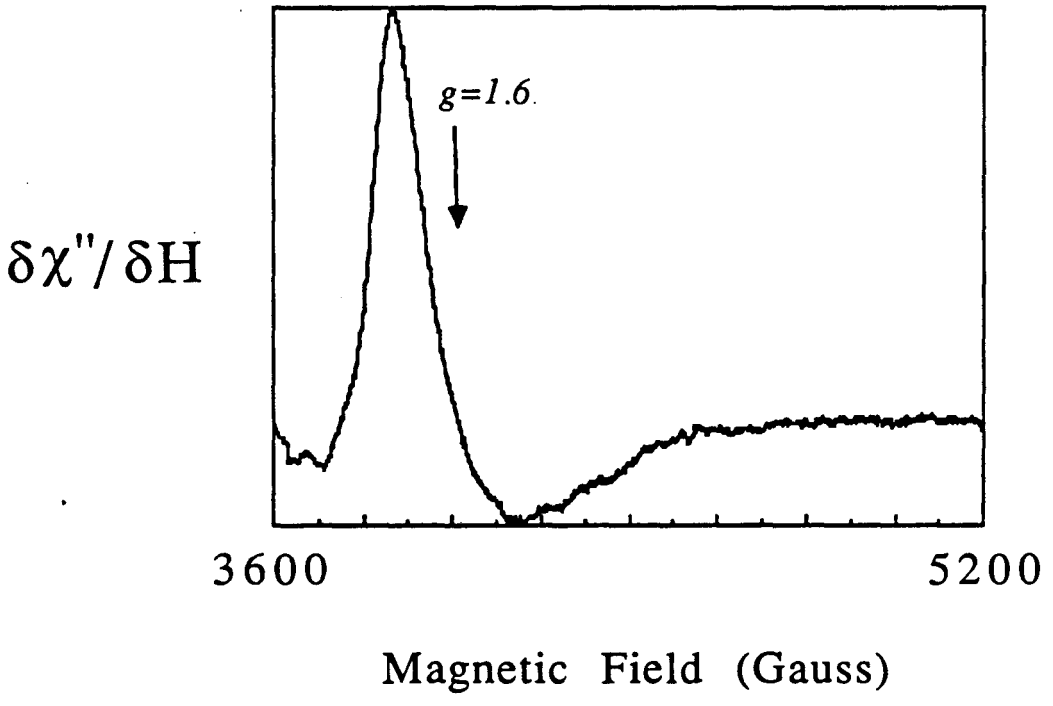

Figure V-7. Illuminated-minus-dark EPR spectra at 5 K of PS II from *Synechococcus*. The spectrum was taken following continuous illumination at 140 K for 2 min. This spectrum illustrates the lineshape of the g=1.6 EPR signal, which is less symmetric than those of the g=1.8 or 1.9 signals. Spectrometer conditions as in Fig V-5.

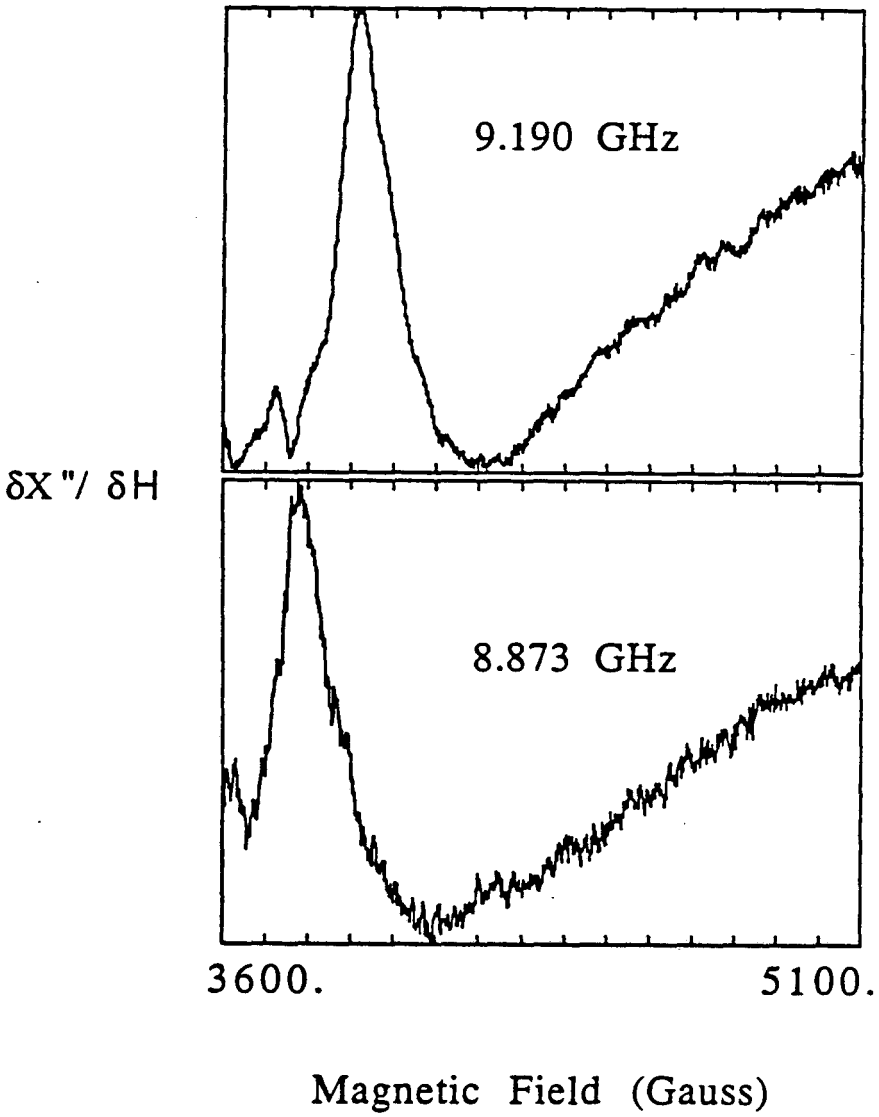

Figure V-8. EPR spectra at 4.3 K of PS II from *Synechococcus* following illumination at 140 K. Spectrometer conditions as in Fig V-2 except that the spectrometer frequency was varied by intruding a lucite rod in the microwave cavity resulting in the indicated indicated measurement frequencies. The change in the field position of first derivative maximum from 3920 G to 3780 G with a change in measuring frequency from 9.19 GHz to 8.87 GHz indicates that the resonance field position results from a g-value with little contribution from zero field splittings.

Figure V-9.

Signal amplitudes for EPR signals generated by illumination of *Synechococcus* PS II particles as a function of the illumination temperature.

In the spectra of samples illuminated at 200, 210 and 220 K the g=1.8 and g=1.6 signals overlap and cancel. Therefore their amplitudes were estimated by simulations using sums of the 240 K and 180 K spectra. The amplitude of the multiline signal was measured using the fourth and fifth hyperfine lines downfield from g=2. Fig V-9 a shows that the amplitude of the g=1.6 signal is complementary to that of the g=1.8 signal between 180 and 240 K, while Fig V-9 b shows that the amplitude of the multiline signal is not complementary to that of the g=1.6 signal.

a

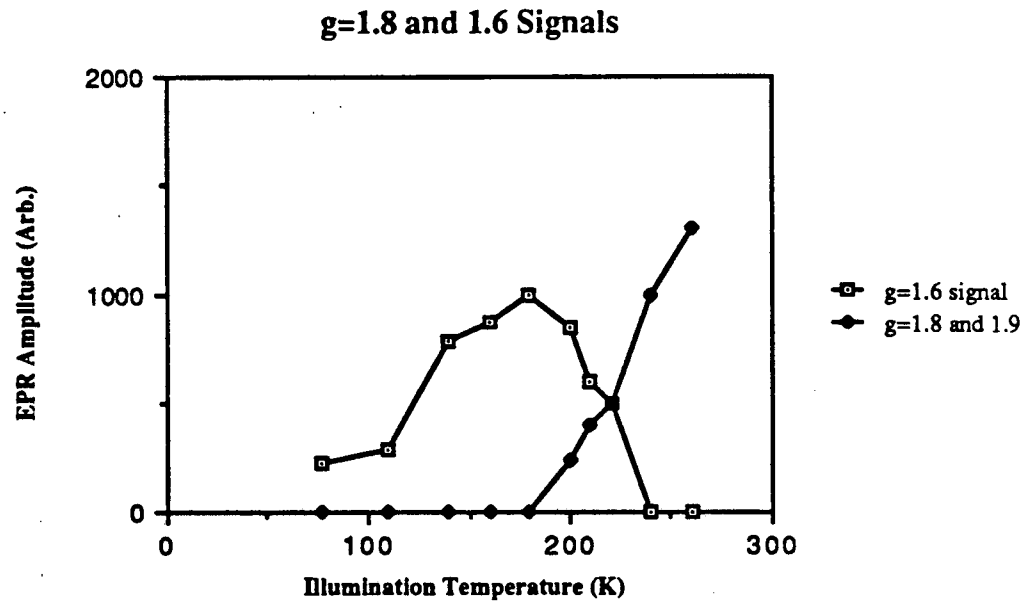
g=1.8 and 1.6 Signals
2000
1000
0
EPR Amplitude (Arb.)
0
100
200
300
Illumination Temperature (K)
g=1.6 signal
g=1.8 and 1.9

b

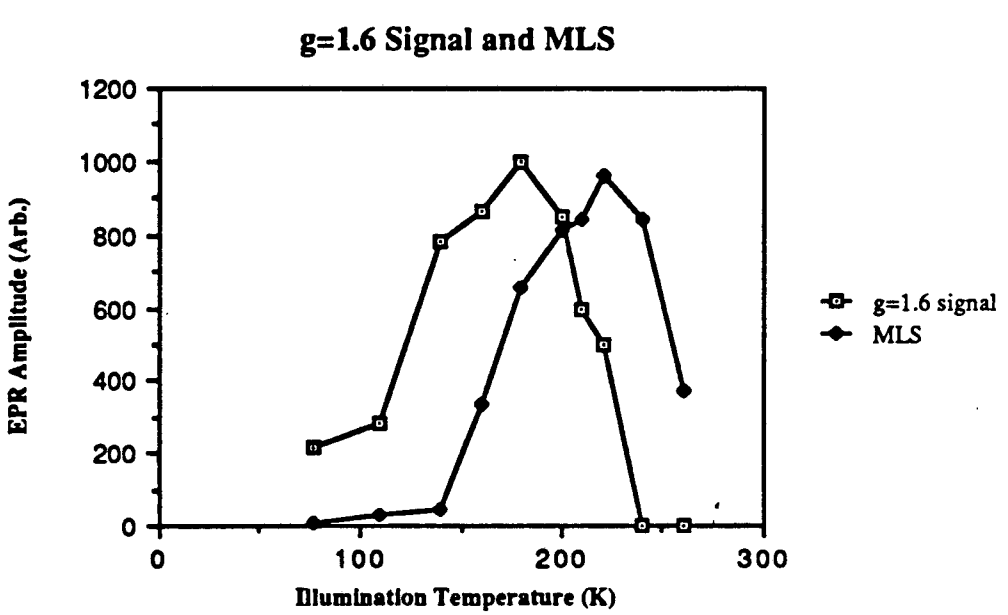
g=1.6 Signal and MLS
1200
1000
800
600
400
200
0
EPR Amplitude (Arb.)
0
100
200
300
Illumination Temperature (K)
g=1.6 signal
MLS

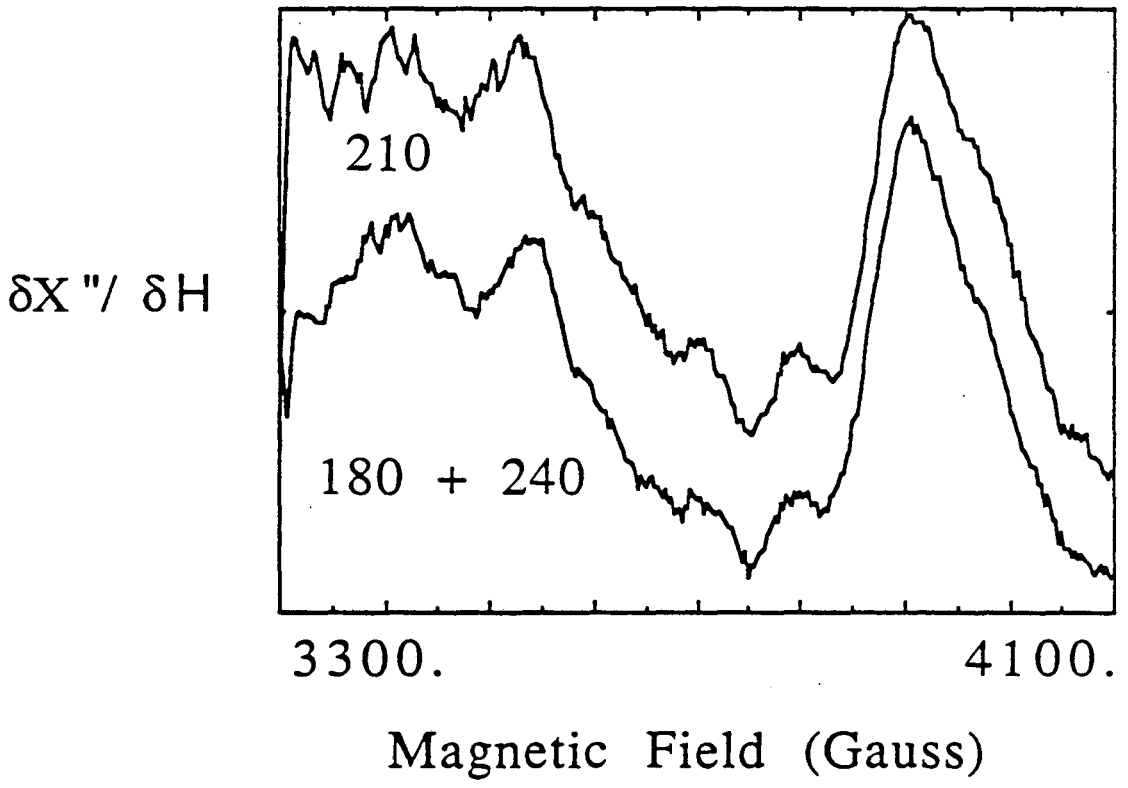

Figure V-10. Illuminated-minus-dark Fe^{2+}-Q spectra from *Synechococcus* PS II. The top spectrum, resulting from illumination at 210 K, is plotted with a sum of the spectra resulting from illumination at 180 K and at 240 K. The 180 K and 240 K spectra were both multiplied by 0.5. These spectra indicate that at 210 K an equal amount of the g=1.6 and the g=1.8 and 1.9 forms are produced. Spectrometer conditions as in Fig V-2.

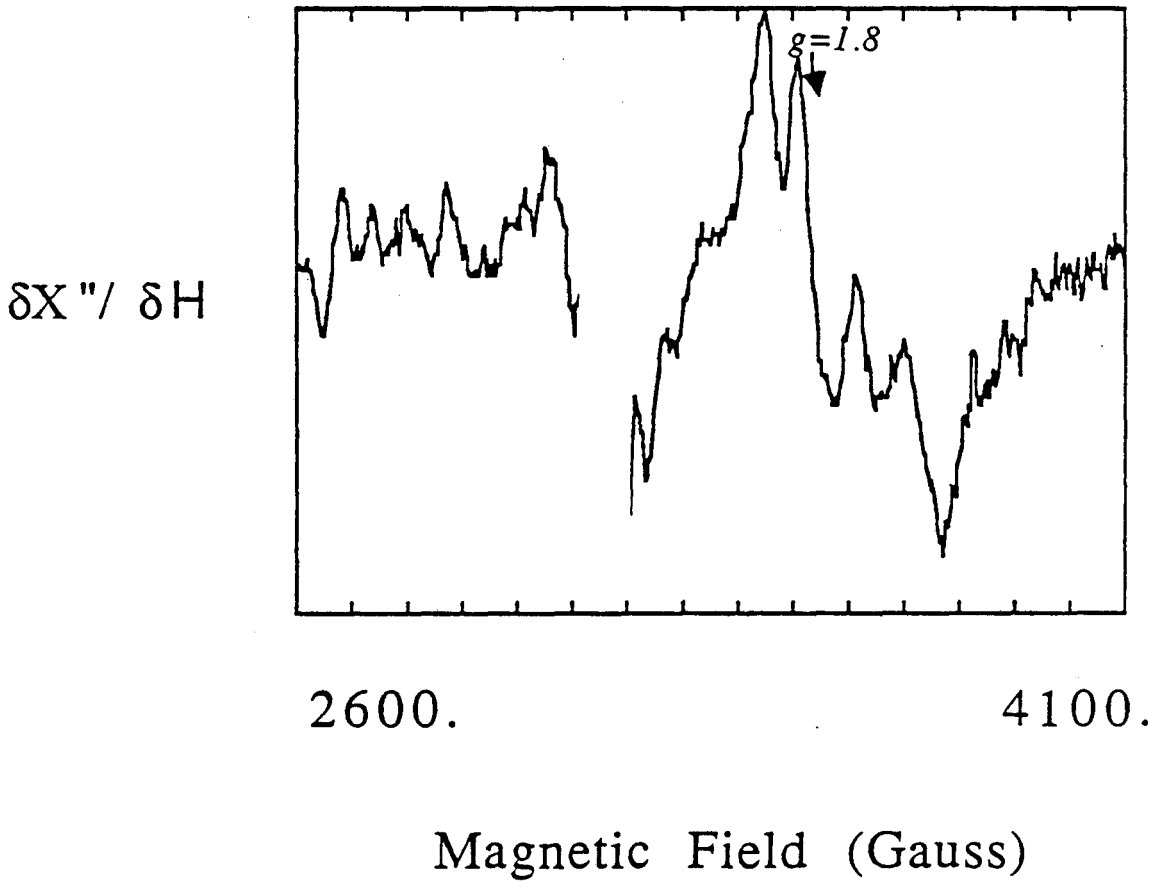

Figure V-11.

Light-minus-dark EPR spectrum of PS II from *Synechococcus* after treatment with 25 mM sodium formate. Illumination was conducted at 140 K. The signal at g=1.8 had a g-value and lineshape similar to that of a signal observed in formate treated PS II from spinach (Vermaas & Rutherford, 1984). No g=1.6 signal was seen.

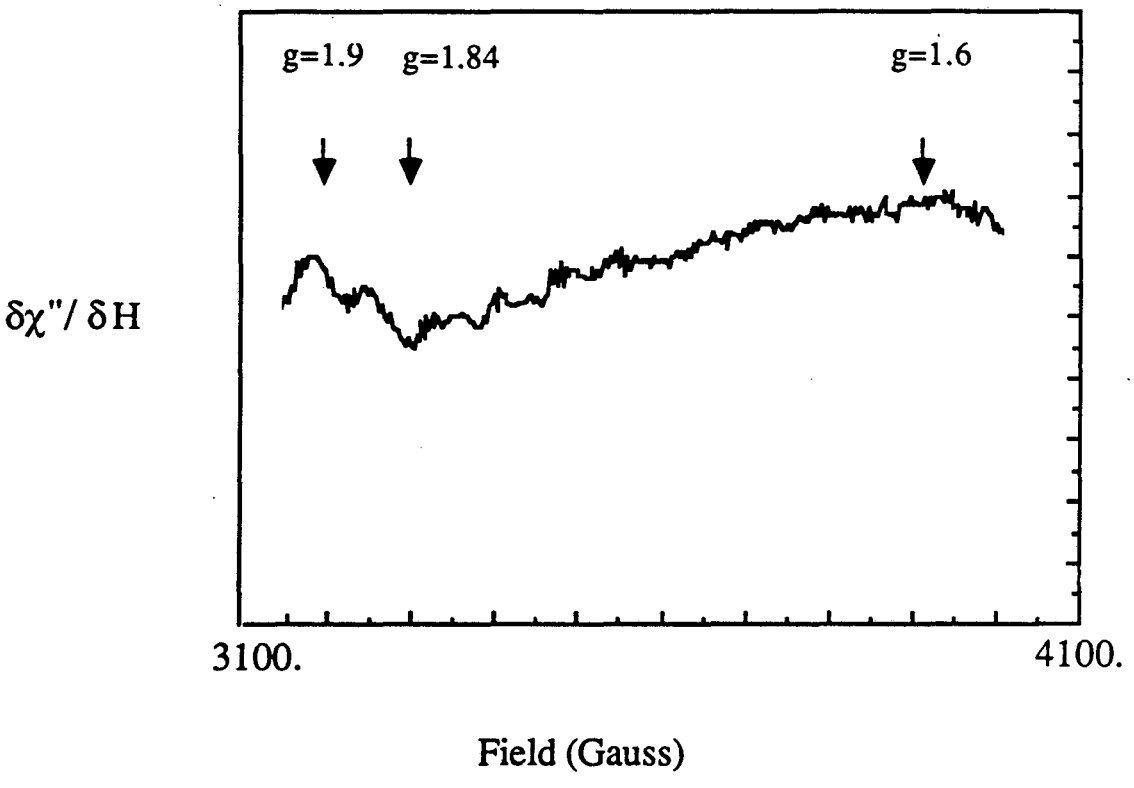

Figure V-12. Illuminated-minus-dark EPR spectra of DCMU-treated PS II particles, following illumination at 140 K.

Two treatments that remove Mn and extrinsic PS II proteins, incubation in 0.8 M Tris at pH 8.5 or treatment with 0.5 mM NH_2OH, cause a decreased amplitude of the g=1.6 signal induced by 140 K illumination to 30% of the control amplitude (Figure V-13).

V C. 4. X-Ray Absorption Edge Studies of Manganese

Figure V-14 compares the Mn X-ray absorption edge spectra of PS II prepared in the S_1 state and in the S_2 state by 215 K illumination. Upon illumination the edge inflection shifts by 0.8 ± 0.2 eV from approximately 6550 to 6551 eV, indicating an oxidation of Mn. In the K-edge spectra of Mn in the S_1 and the S_2 states, transitions at 6541 eV ("pre-edge features") are apparent. The spectrum of the S_2 sample has a trough between the pre-edge feature and the main edge transition in which the absorbance is less than half that of the maximum of the pre-edge feature (Figure V-14 B.). In contrast, the spectrum of the S_1 sample has only a small decrease in absorbance between the pre-edge maximum and the main edge transition. Thus, the S_1 to S_2 transition is accompanied by not only a shift in Mn K-edge inflection energy, but also a change in Mn K-edge structure. The shape of the pre-edge features is very similar in the Mn K-edge spectra of PS II from *Synechococcus* and spinach. Furthermore, the change in pre-edge structure from the S_1 to the S_2 state is seen in preparations from both organisms. For both S_1 and S_2 samples, the Mn K-edge inflection energy is 0.5 ± 0.3 eV lower for Mn in PS II from *Synechococcus* as compared with Mn in PS II from spinach (Yachandra et al., 1987).

Figure V-15 compares the Mn K-edge spectra of S_2 states prepared by illumination at 215 K and by illumination at 140 K. A similar edge position is seen in the two samples, indicating that Mn was oxidized upon illumination at 140 K. The pre-edge region in the spectrum of the 140 K illuminated sample exhibits a trough between the pre-edge maximum and the main edge transitions as does the spectrum of the sample illuminated at 215 K, while the amplitude of the pre-edge feature is higher in the spectrum of the 140 K illuminated sample.

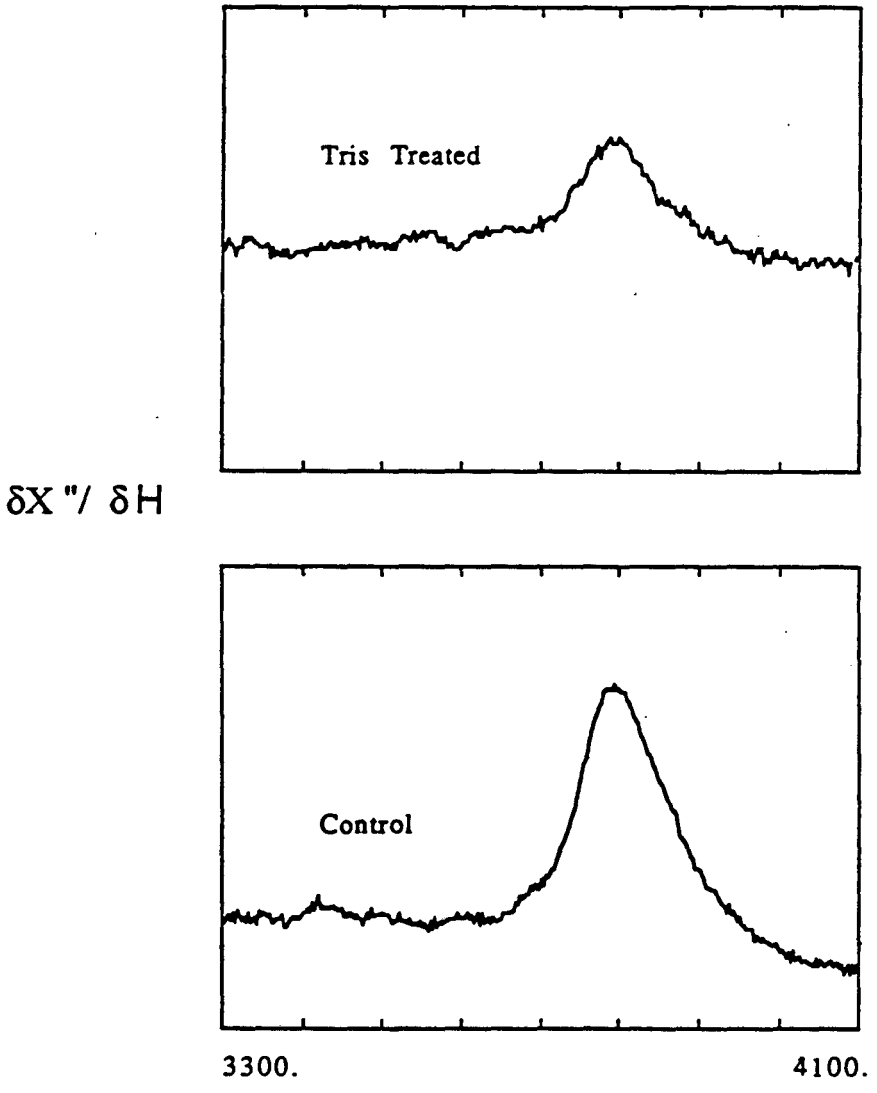

Figure V-13.

Illuminated-minus-dark EPR spectra at 4.5 K of PS II from *Synechococcus* illuminated at 140 K showing the amplitude of the g=1.6 signal following Tris treatment of the PS II. The amplitude of the of the g=1.6 signal following inhibition of the Mn donor complex by Tris or hydroxylamine treatment was approximately 30% of the control for a 2 min illumination.

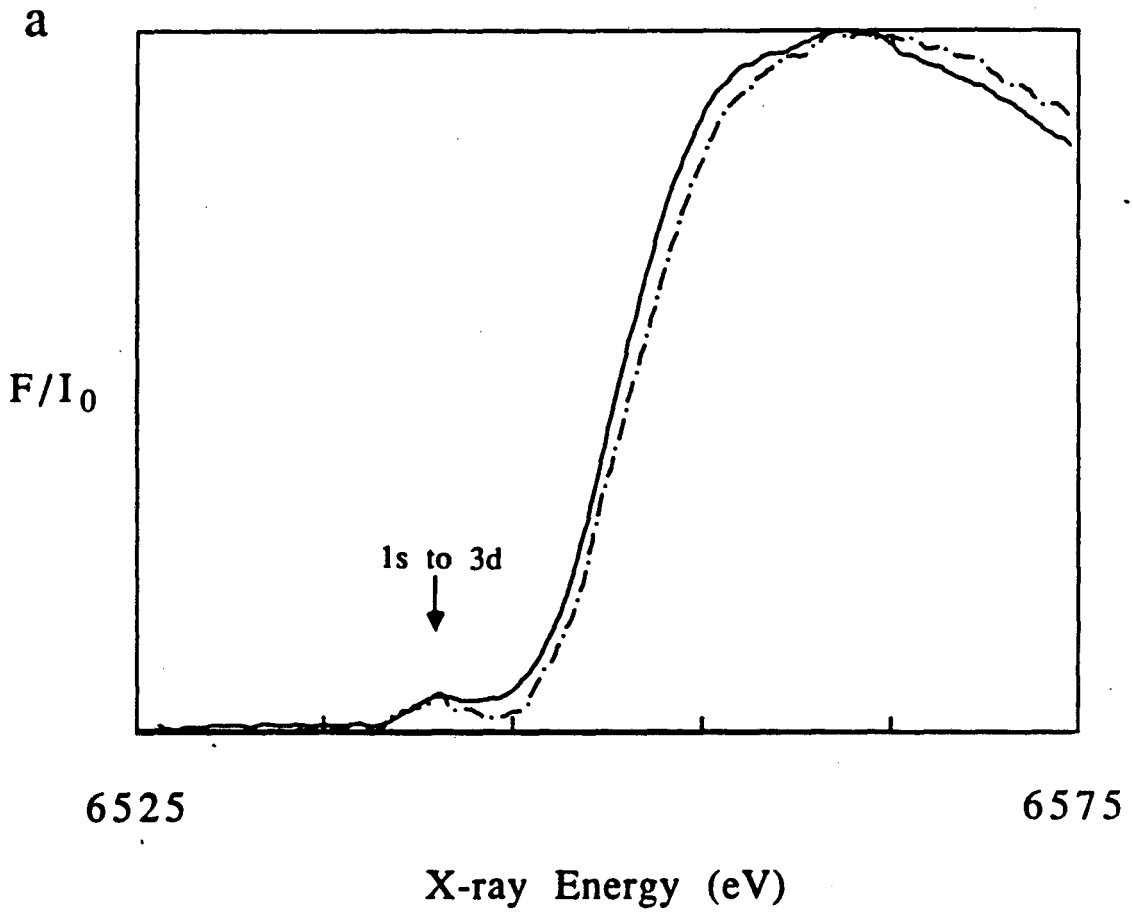

Figure V-14. Mn K-edge X-ray absorption spectra of *Synechococcus* PS II particles. Samples were prepared in the S_1 state by dark adaptation (solid line) and the S_2 state by continuous illumination at 215 K following dark adaptation (dashed line). The data were smoothed with a domain of approximately 1 eV. The edge inflection energy of the S_2 sample is 0.7 eV higher than that of the S_1 sample (Fig V-14 A). The features at approximately 6541 eV (just before the edge) are due to semiforbidden 1s-3d transitions, and are expanded in Fig V-14 B. These features resemble, respectively, those of Mn(III) complexes in the S_1 state and those of Mn(IV) complexes in the S_2 state (Sauer et al., 1987).

b

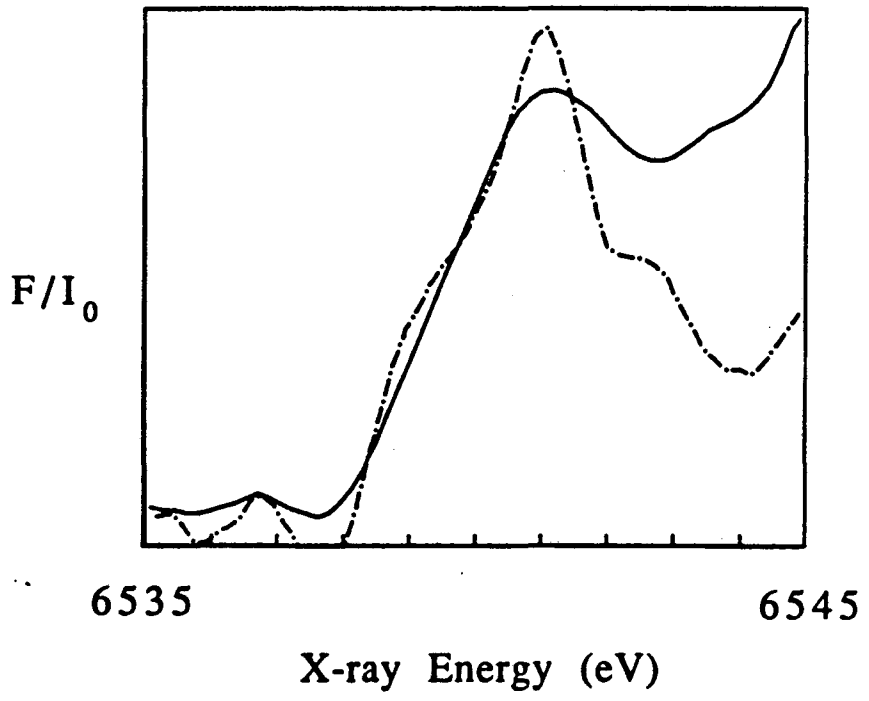

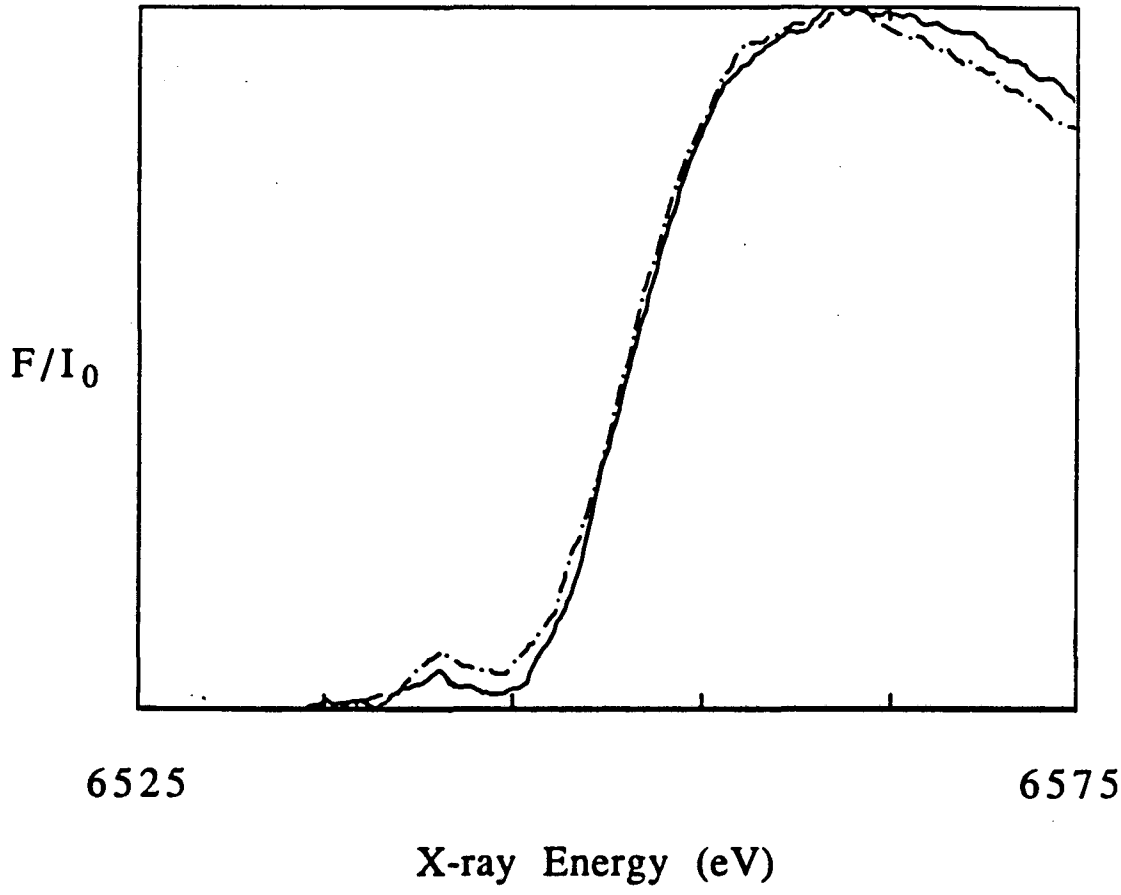

Figure V-15. Mn K-edge X-ray absorption spectra of *Synechococcus* PS II particles. Samples were prepared in the S_2 state by dark adaptation followed by continuous illumination at 215 K (solid line) and at 140 K (dashed line). The data were smoothed with a domain of approximately 1 eV. The two edge inflection energies are indistinguishable from each other, indicating that the oxidation states are the same, and both are oxidized relative to S_1. The structure of the pre-edge for the 140 K illuminated sample also resembles those of Mn(IV) complexes, but has a higher intensity than that of the 215 K illuminated sample.

V C. 6. X-Ray Absorption Fine Structure Studies of Manganese

Figure V-16 shows Fourier transforms of the Mn EXAFS data of the 215 K-illuminated S_2 state of PS II from *Synechococcus*. The k-space data were multiplied by k^1 or k^3 to emphasize first row ligands or transition metal neighbors, respectively. The Fourier transforms have two main features: a peak at $R + \alpha/2 = 1.2$ Å which is due to O or N (peak I), and a peak at approximately $R + \alpha/2 = 2.2$ Å which is due principally to a transition metal (Peak II). The third peak at $R + \alpha/2 = 3$ Å is barely above the noise level and is somewhat variable; we have been unable to determine whether this peak is due to a transition metal or a first row element(s) or both.

Figure V-17 shows simulations by the Teo-Lee method (Teo & Lee, 1979) of k^2-weighted Fourier-filtered data. An extensive search for acceptable simulations of these data indicates that it is essential to include a first row transition metal neighbor at 2.7 Å and C N or O at 1.75 Å. The transition metal neighbor at $R+ \alpha/2 = 2.2$ Å is very likely to be another Mn atom, since simulations of the multiline EPR spectrum indicate that at least two Mn are required to explain the hyperfine structure (Dismukes & Siderer, 1981; Dismukes et al., 1982; Hansson & Andréasson, 1982). Based on chemical precedent, we assume that the bridging atom(s) are oxygen.

Simulations of peak II suggest that a symmetric tetranuclear structure is unlikely (Fig V-17). The best simulations involved one Mn neighbor at 2.7 Å, together with O, C or N neighbors at 3.2 Å (Fig V-17 c, Table V-1). The simulation of the Mn peak assuming three Mn neighbors does not adequately reproduce the amplitude or the shape of the envelope (Fig V-16 b) *regardless of what value for the Debye-Waller factor is used.*

Simulations of peaks I and II together leads to the same conclusion. Figure V-17 c shows a best fit to the data for three types of neighboring atoms which had parameters corresponding very closely to binuclear structures, including one to two μ-oxo ligands at 1.75 Å, 3 to 4 additional O neighbors in a range of distances between 1.9 and 2.3 Å and 1 to 1.5 Mn neighbor(s) at 2.75 Å. The S_1 data (not shown) can be simulated

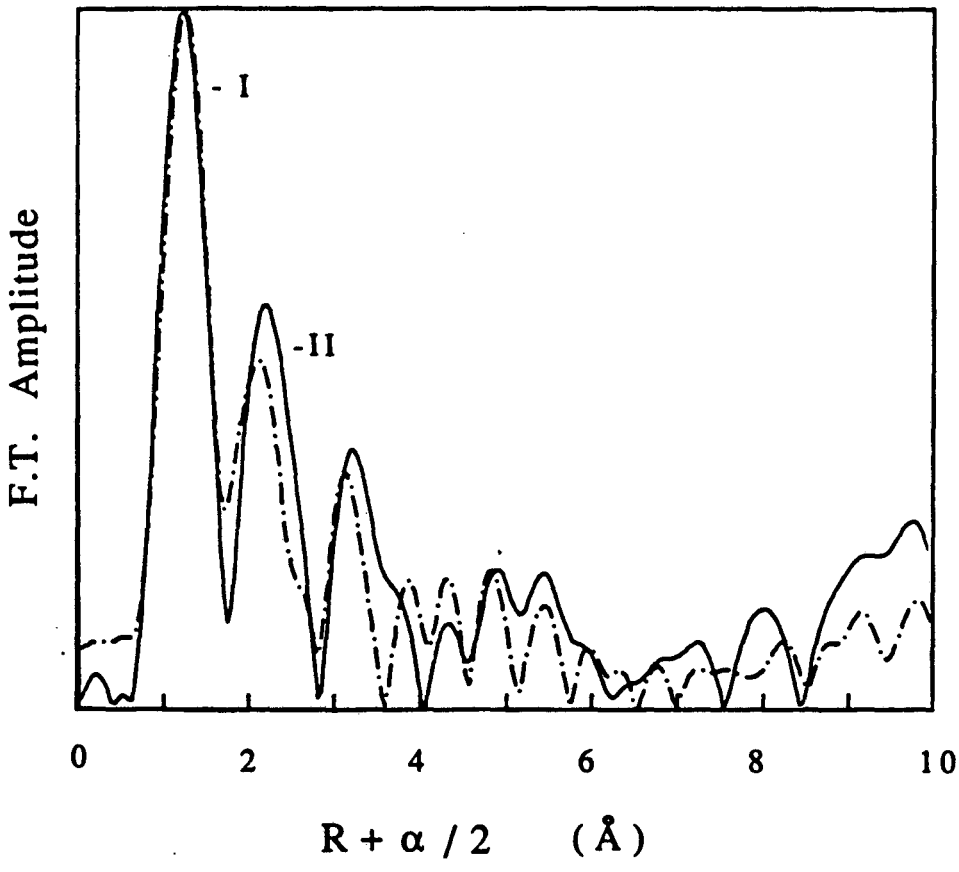

Figure V-16. Fourier transforms of the k^1 (dashed line) and k^3 (solid line) weighted Mn EXAFS data of *Synechococcus* in the S_2 state. The first peak is due primarily to bridging O (or N) ligands at 1.75 Å and terminal ligands at 2 to 2.4 Å. The second peak is due primarily to transition metal neighbor(s) at 2.7 Å. These peaks are characteristic of a di-μ-oxo bridged Mn cluster. The peaks appear at an apparent distance which is shorter than the internuclear distance by an amount related to the photoelectron phase shift, $\alpha(k)$. The high-resolution MLS EPR spectrum of this sample is shown in Figures V-4 B and C.

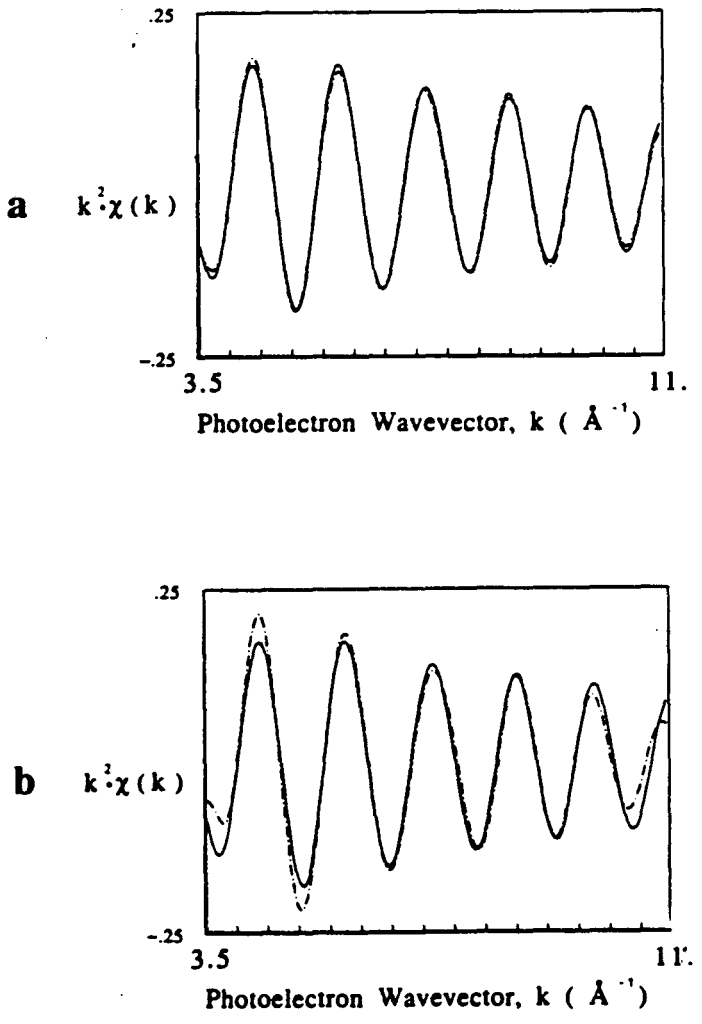

Figure V-17. Simulations of Fourier filtered Mn EXAFS data of PS II from *Synechococcus*. The data were weighted by k^2, including only peak II (a and b) or peaks I and II (c, d and e). The data (solid line) are shown with the best simulation with no assumptions about numbers of neighboring atoms (dotted line, a and c) or with an optimized simulation using numbers of neighbors characteristic of tetranuclear clusters (dotted line, b, d and e). The Debye-Waller parameters were optimized for quality of fit in each case. Fig V-17 d is a simulation of a relatively symmetric adamantane-like tetranuclear cluster which would involve four-coordinate Mn, while Fig V-17 e is a simulation of a cube-like tetramer which would involve six-coordinate Mn. The simulations suggest that both of these structures are unlikely. The best simulations (a and c) had numbers of ligands similar to those of dimeric clusters. The parameters of the simulations are listed in Table V-1.

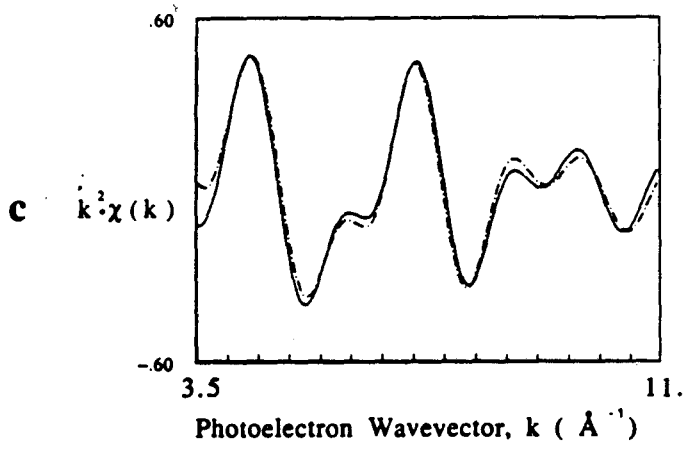
c
k²·χ(k)
.60
-.60
3.5
11.
Photoelectron Wavevector, k (Å⁻¹)

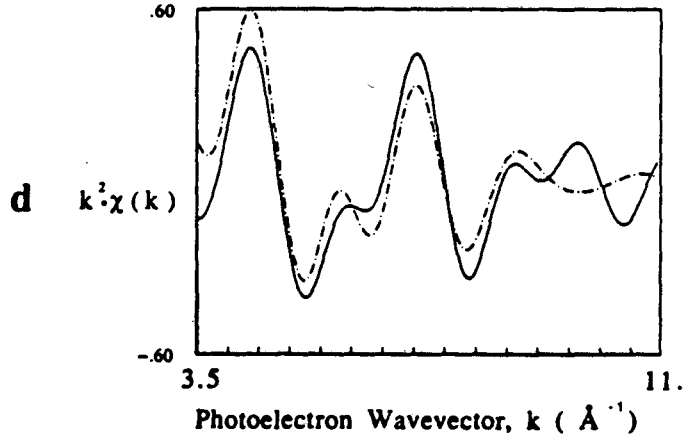
d
k²·χ(k)
.60
-.60
3.5
11.
Photoelectron Wavevector, k (Å⁻¹)

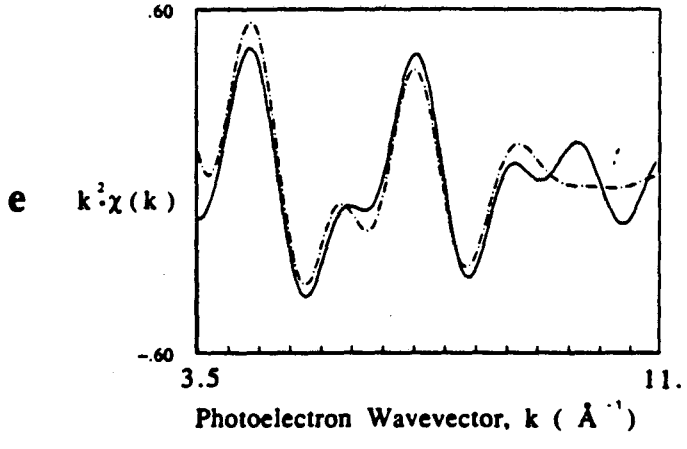
e
k²·χ(k)
.60
-.60
3.5
11.
Photoelectron Wavevector, k (Å⁻¹)

by very similar parameters. For comparison, two less satisfactory simulations of peaks I and II of the S_2 data are shown in Fig V-17 d and V-17 e. In these simulations each Mn is assumed to have three Mn neighbors, three μ-oxo ligands and one (Fig V-17 d) or three (Fig V-17 e) terminal ligands to mimic four coordinate and six coordinate symmetric tetranuclear clusters. Again, regardless of the Debye-Waller factor used in the simulations, we cannot obtain better agreement for a symmetric tetranuclear simulation than those shown in Figs V-17 d and V-17 e.

The full set of parameters used in these simulations is presented in Table V-1.

V D. Discussion

V D. 1. The S_1 to S_2 Transition at 220 K

Illumination at 210-240 K results in a charge separation involving Mn as the electron donor and Q_A as the acceptor, and the oxidized donor gives rise to a multiline EPR spectrum with 88 G splittings, quite similar to that seen in spinach. The acceptor signal includes the g=1.8 and 1.9 signals previously reported for spinach PS II, together with a new EPR signal at g=1.6. Illumination at temperatures above 240 K leads to a smaller amplitude of the multiline signal when no DCMU is included. These data demonstrate that the temperature at which a maximal multiline signal is formed is higher for *Synechococcus* (220 K) than for spinach (190 K), possibly because in *Synechococcus* S-state conversion rates or Q_A to Q_B electron transfer rates are different from those of spinach.

V D. 2. A New EPR Signal at g=1.6

After illumination at 110-160 K, the multiline EPR spectrum of the Mn donor and the g=1.8 and 1.9 EPR spectra of the Q_A acceptor are absent, but a new signal at g=1.6 appears. Presumably this signal is due to an oxidized donor or a reduced acceptor. The amplitude of the g=1.6 signal is complementary to the amplitude of the g=1.8 and 1.9 signals in the temperature range from 180 to 240 K (Fig V-9 a). In the same range of illumination temperatures the multiline signal amplitude varies by less than 20% from

TABLE VI-1
EXAFS SIMULATION PARAMETERS[a]

Figure	Neighboring Atom	R(A)[b]	N[c]	σ(A)[d]	Fit Error[e]
Figure 8a.	Mn	2.76	1.3	0.1	.006
(Best fit of Peak II)	O	3.27	2.0	0.10	
Figure 8b.	Mn	2.75	3.0	0.10	.08
(Three Mn fit of Peak II)	O	3.23	1.4	0.01	
Figure 8c.	O	1.74	1.6	0.08	.1
(Best fit of Peaks I and II)	O	2.21	3.4	0.22	
	Mn	2.69	1.3	0.13	
Figure 8d.	O	1.78	3.0	0.18	1.4
(Adamantane fit of Peaks I and II)	O	2.18	1.0	0.09	
	Mn	2.70	3.0	0.22	
Figure 8e.	O	1.80	3.0	0.16	.76
(Cube fit of Peaks I and II)	O	2.18	3.0	0.16	
	Mn	2.68	3.0	0.19	

a. Simulations were done by the method of Teo and Lee (1979) and are shown in Fig 8. In addition to the parameters listed, these simulations vary the E_o value for each shell separately. The range for ΔE_o was restricted to -10 eV to 10 eV where E_o was 6550. eV.
b. R is the internuclear distance between the absorbing Mn and the neighbor.
c. N is the number of neighboring atoms, which is adjusted from the value determined in the simulation by a factor of 2 as described (Teo & Lee, 1979).
d. σ is the Debye-Waller parameter, equal to the r.m.s. sum of static and dynamic disorder in the internuclear distance, R.
e. The fit error is a relative measure of the sum of residuals of the simulation.

the maximal value, and is not complementary to the amplitude of the g=1.6 signal (Fig V-9 b). These observations are suggestive that the g=1.6 signal and the g=1.8 signal are both acceptor signals. Electron transfer from P to Q_A proceeds at temperatures as low as 5 K in spinach PS II preparations and in purple non-sulfur bacteria (Nugent et al., 1980; Butler et al., 1984). Q_A to Q_B electron transfer is blocked below 190 K in spinach (de Paula et al., 1985) and probably below 220 K in *Synechococcus*. Therefore it is very likely that Q_A is the acceptor in this preparation at 140 K.

Two treatments that are thought to affect the acceptor complex specifically have a dramatic effect on the g=1.6 signal. Addition of formate followed by illumination at 140 K results in a signal with a g-value and lineshape like the altered Fe^{2+}-Q_A^- signal seen in formate-treated spinach PS II particles (Vermaas & Rutherford, 1984), while the g=1.6 signal is no longer present. Formate is thought to bind in the acceptor complex at the same site as bicarbonate. A recent review of the mechanism of the formate effect is available (Govindjee & Eaton-Rye, 1986). The conversion of the g=1.6 signal to a g=1.8 signal on formate addition indicates that that the acceptor species at 140 K is Q_A and that it gives rise to the g=1.6 signal. Further, the g=1.6 signal is affected by binding of DCMU at the Q_B site, while the donor side is not affected, as evidenced by the presence of the multiline signal. In this respect it is noteworthy that binding of quinones and quinone analogs at the Q_B site alters the Fe^{2+}-Q_A^- signals in cyanobacteria and higher plants (Atkinson & Evans, 1983; Rutherford et al., 1984).

In contrast, treatments that are specific to the donor complex have relatively less effect on the g=1.6 signal. In particular, 30% of the g=1.6 signal appeared following abolition of O_2 evolution activity with hydroxylamine or Tris treatment. The decreased amplitude of the g=1.6 signal on release of Mn by Tris or hydroxylamine treatment is suggestive that the efficiency of stable electron transfer decreases in the absence of a competent donor.

These data indicate that the Fe^{2+}-Q_A^- species exhibits two different EPR signals depending on the temperature of illumination. It is possible that the g=1.6 form is

a conformationally excited form of the Fe^{2+}-Q_A^- complex that cannot relax at lower temperatures. Upon incubation with formate, only one form of the Fe^{2+}-Q_A^- signal is seen in *Synechococcus*; it resembles the Fe^{2+}-Q_A^- signal seen in spinach PS II following formate treatment. Formate may bind at the iron in a site analogous to the glutamate (M232) ligand in bacterial reaction centers (Deisenhofer et al., 1985). We speculate that the conversion from the g=1.6 to the g=1.8 form of the Fe^{2+}-Q_A^- complex could involve changes in the iron carboxy ligand, and that the existence of the g=1.6 signal in *Synechococcus* but not plants could signify differences in the iron carboxy ligands present in the two organisms. There are many differences between the region of the glutamate ligand in the M subunit and the analogous region of D2, (Hearst, 1986); this region of D2 also differs between cyanobacteria and plants (Williams & Chisholm, 1987).

The signal from Fe^{2+}-Q_A^- in purple nonsulfur bacteria at g=1.8 has been modeled in terms of the S=2 states of the Fe^{2+} system coupled to the S=1/2 semiquinone radical (Butler et al., 1980; 1984; Dismukes et al., 1984); this treatment may be useful for describing the g=1.6 signal as well. A second-order perturbation treatment describing the exchange interaction between the semiquinone and the iron yields an expression for the resulting g value: $g=g_Q[1-2(J/\Delta E_{1,2})^2]$, where g is the observed g-value of the coupled iron semiquinone system, J is the exchange coupling between the semiquinone and the iron, g_Q is the g-value of an isolated semiquinone and $\Delta E_{1,2}$ is the splitting between the two lowest M_S states in the S=2 manifold of the Fe^{2+} (Butler et al., 1984). If the g=1.6 signal is due to Fe^{2+}-Q_A^-, the g-value of 1.6 may result from a large decrease in $\Delta E_{1,2}$ or a large increase in J as compared with the g=1.8 signal. The lineshape of the g=1.6 signal shows a relatively steep low field rising edge and a shallower high field falling edge as compared with the g=1.8 signal. Based on higher order perturbation terms, Butler et al. (1984) discuss the effects of J and $\Delta E_{1,2}$ on signal lineshapes as well as g values. Their results indicate that changing the zero field splitting parameters

is not likely to explain the lineshape of the g=1.6 signal, but increasing J_z relative to that of the g=1.8 form may explain the lineshape and g-value.

V D. 3. Illumination at 140 K Results in Mn Oxidation but No MLS or g=4.1 EPR Signal

At 140 K an apparent acceptor signal is seen, but we are unable to observe a donor signal. The absence of a g=4.1 signal following illumination at 140 K raises the question as to whether Mn is oxidized upon illumination at 140 K. To address this point we monitored the Mn K-edge changes upon illumination at 140 K. Our edge study confirms that Mn is the donor at 140 K but that it is EPR silent under the conditions of our experiment. Mn(IV) and Cr(III), which are both d^3 ions, show EPR signals from the S=3/2 ground state with g-values near g=4 if they have large zero-field splittings. A monomeric Mn(IV) species has been proposed as an assignment for the light-induced g=4.1 S_2 signal (Hansson et al., 1987). A study of Cr(III) EPR signals indicates that, depending on the relative energies of the microwave quantum and the zero field splitting (between the $M_S=\pm 3/2$ and the $M_S=\pm 1/2$ Kramers pairs), the lineshape can vary from 1) a somewhat broad g=4 signal for large zero field splitting, to 2) a broad unresolved signal from zero field to beyond g=2 when the zero field splitting is comparable to the microwave quantum, to 3) a rather sharp g=2 signal for octahedral complexes with negligible zero field splitting (Singer, 1955). Some examples of Mn(IV) monomeric species have been reported that may correspond to case 2) described above, in that they possess approximate octahedral symmetry and show very broad EPR signals (Hartman et al., 1984; Kessissoglou et al., 1986; 1987). If the g=4 signal in spinach is due to a Mn(IV) species with a large zero-field splitting, our Mn K-edge and EPR data may be explained by proposing that a similar oxidation occurs at 140 K in the *Synechococcus* preparation, but the zero-field splitting is smaller and the EPR signal is too broad to be observed. If the g=4.1 signal in spinach is due to a multimeric Mn cluster, a similar change in zero-field splitting parameters might also broaden the signal

in *Synechococcus*. This EPR silent state also does not give rise to a multiline signal upon warming, indicating that associated with the structural difference in the Mn site are differences in conformational or electron transfer dynamics.

The apparent differences in Mn structure between the two organisms may reflect changes in PS II proteins due to the large evolutionary gap between cyanobacteria and plants, or they may reflect differences in the preparation procedure. The most striking evolutionary change is that the *Synechococcus* complex lacks the 18 and 24 kDa proteins found in spinach PS II. These peptides can be removed from spinach PS II by washing with high concentrations of NaCl (Ghanotakis & Yocum, 1985). The basic structure of the Mn complex is similar in the absence of the 18 and 24 kDa proteins. In contrast to control preparations from spinach or these preparations from *Synechococcus*, illumination of the salt washed preparations at 140 K resulted in a g=2 donor species (de Paula et al., 1986), possibly because the salt-washing procedure causes an irreversible decreased rate of electron transfer from the Mn complex (Dekker et al., 1984; Cole et al., 1986; Cole & Sauer, 1987). Thus it is difficult to compare the results from these salt-washed preparations to our results from *Synechococcus*.

V D. 4. X-Ray Absorption Edge Structure Indicates Mn Valences

The Mn X-ray absorption K-edge position and the structure of the K-edge offer a method of valence identification. The edge inflection energies of 6550 to 6551 eV for S_1 and 6551 to 6552 eV for S_2 samples are similar to those of Mn(III/IV) mixed valence complexes, Mn(IV) complexes and some Mn(III) complexes (Kirby et al., 1981; Sauer et al., 1987). The 0.5 to 1.0 eV change in edge inflection observed on advance from S_1 to S_2 is consistent with a one electron or a two electron change per four Mn by comparison with inorganic complexes (Kirby et al., 1981; Guiles, manuscript in preparation). The pre-edge region, in which semi-allowed 1s to 3d transitions are present, also yields information about the oxidation state. These transitions are formally unallowed by dipole selection rules, and generally become 'dipole-allowed' by mixing

with 4p orbitals. The structure of the pre-edge region of the Mn K-edge transitions is systematically different in Mn(III) and Mn(IV) complexes, most notably in that for Mn(IV) the pre-edge transitions are resolved from the main edge transition while for Mn(III) complexes they are not (Sauer et al., 1987). These differences in the edge spectra are presumably related to systematic symmetry differences between Mn(III) and Mn(IV) complexes which give rise to differences in the energies of the d electron levels and/or differences in matrix elements for 1s to 3d transitions. The pre-edge region of the K-edge spectra of S_1 samples resembles to those of many Mn(III) complexes while for S_2 samples this region of the spectrum resembles those of Mn(IV) complexes. These results are strongly suggestive that in the the S_1 to S_2 transition Mn(III) atom(s) are oxidized to Mn(IV).

The K-edge structure is quite similar in spinach and *Synechococcus* preparations. This suggests that the oxidation states are probably the same for the two organisms, and that the lower edge inflection edge energy for *Synechococcus* as compared with that for spinach may be due to a difference in the Mn ligands in the two organisms and/or a small amount (< 10%) of nonspecifically bound Mn(II). We are unable to account for the structure in the Mn K-edge spectra and the edge position in *Synechococcus* by adding K-edge spectra of octahedral Mn(II) to the K-edge from spinach, as shown in Figure V-18. In addition, our preparations from *Synechococcus* systematically have less Mn per reaction center (3.5 ± 0.5) than our preparations from spinach (4.8 ± 0.5; Cole et al., 1987b), and we have not observed the characteristic six-line Mn(II) signal in our preparations from *Synechococcus*. Therefore, we think it likely that the difference in the K-edge position for the two organisms results from some change in the ligand environment of the Mn.

V D. 5. The EXAFS Indicate a μ-Oxo Bridged Cluster

The EXAFS results, particularly the 2.7 Å Mn-Mn distance, offer convincing evidence for a di-μ-oxo bridged structure in *Synechococcus*. This conclusion was also

Figure V-18. X-ray absorption K-edge spectra of Mn in PS II particles from *Synechococcus* (solid line) and spinach (dotted line, panel a). The K-edge inflection energy is approximately 1 eV higher for Mn in spinach PS II as compared with *Synechococcus* PS II. Whether the lower edge energy in *Synechococcus* could be due to contaminating hexaquo Mn(II) is addressed in Figs V-18 b and V-16 c, where the Mn K-edge spectrum of Mn from spinach PS II (dotted line) is plotted with the Mn K-edge of *Synechococcus* PS II minus 10% (Fig V-18 b) or 20% (Fig V-18 c) of a Mn K-edge spectrum of hexaquo Mn(II). The subtracted Mn edge spectra mimic the edge position but not the shape of the edge spectrum of Mn from PS II of spinach, indicating that contaminating octahedral Mn(II) is not a likely explanation for the difference in the edge positions. This is also confirmed by the facts that no characteristic six-line EPR spectrum of hexaquo Mn(II) is seen in our samples from *Synechococcus* and that the Mn content per reaction center is systematically lower in *Synechococcus* than in spinach.

a.

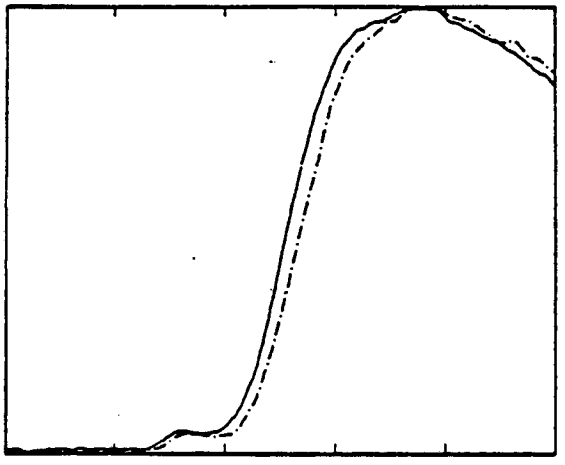
F/I$_o$
6525.
6575.
X-Ray Energy (eV)

b.

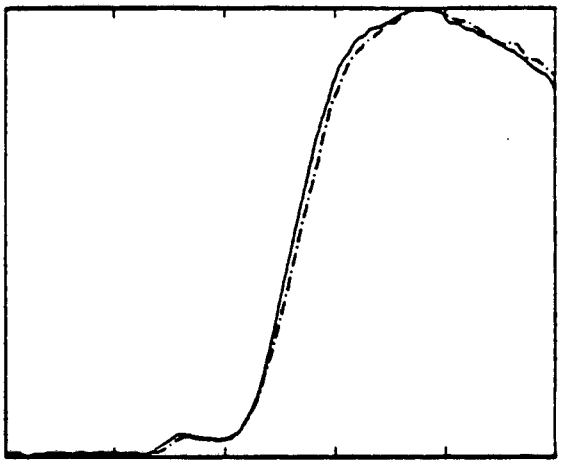
F/I$_o$
6525.
6575.
X-Ray Energy (eV)

c.

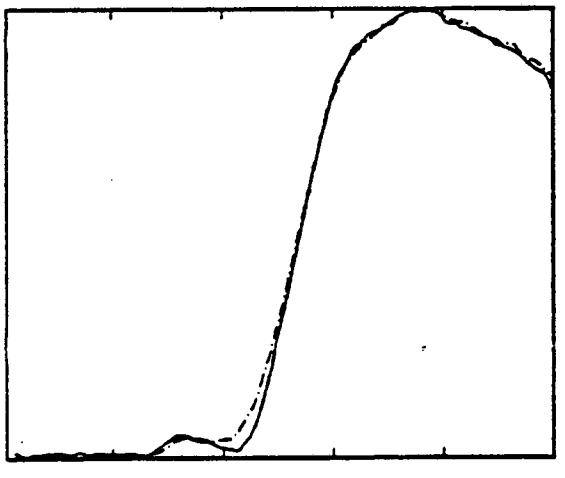
F/I$_o$
6525.
6575.
X-Ray Energy (eV)

reached in our previous studies of Mn in PS II from spinach (Yachandra et al., 1987). The use of an energy resolving detector in this work allowed us to collect EXAFS data that were relatively free from background artifacts and that can be simulated with excellent agreement. We are able to retrieve more detailed information from the EXAFS data than was previously possible, especially with regard to the O and N ligands and with regard to determination of the number of ligands and the Debye-Waller factors.

We tested the proposal of relatively symmetrical tetranuclear structures with mostly μ-oxo bridges, such as those illustrated in a recent discussion of the chemistry of H_2O oxidation (Brudvig & Crabtree, 1986). Simulations of the Mn peak at 2.7 Å alone (Fig V-17 a and b) show that each Mn is μ-oxo bridged to approximately one (and not three) Mn neighbor(s). These simulations include a freely adjustable Debye-Waller parameter to account for the possibility that there are various Mn-Mn distances that are not resolved in the 2.7 Å Mn peak.

One may expect differences between symmetrical tetranuclear complexes and binuclear complexes in the distribution of μ-oxo bridging and terminal ligands as well as in the number of Mn neighbors. In binuclear complexes, each Mn has two μ-oxo bridging O atoms which generally have short Mn-O bond lengths (1.7-1.9 Å) and four terminal ligands which generally have longer bond lengths (2.0 Å or greater). For symmetric tetranuclear structures, each Mn would have three bridging ligands. The 2.7 Å Mn-Mn distance and the 1.7 to 1.8 Å Mn-O distance have implications with respect to the bond angles and therefore the coordination numbers at the Mn center for tetrameric structures. An adamantane-like tetranuclear structure with these bond distances should involve O-Mn-O bond angles of approximately 114° which is typical of four-coordinate complexes, while a cube-like tetranuclear structure with these bond lengths would require O-Mn-O bond angles of approximately 90°, as found in six-coordinate complexes. This observation led us to simulate an adamantane cluster as a four coordinate cluster, including *one* terminal ligand (O, N, Cl or S) three μ-oxo ligands and three Mn neighbors (Fig V-17 d). We simulated a cube as a six coordinate cluster by including

three terminal ligands, three μ-oxo ligands and three Mn neighbors (Fig V-17 e). (We note that among multinuclear Mn complexes Mn is almost always found to be six co-ordinate.) Both the cube-like and the adamantane-like simulations show much poorer agreement than do simulations with fewer Mn neighbors. Our best simulation (Fig V-17 c) includes 1.5 to 2 μ-oxo ligands, 3 to 4 terminal ligands and 1 to 1.5 Mn neighbors. These parameters are consistent with a complex with two binuclear clusters possessing similar Mn-Mn distances, a binuclear cluster with nearby monomeric Mn atoms or with trinuclear structures or distorted tetranuclear clusters in which each Mn atom has approximately one Mn neighbor at 2.7 Å. There may be additional Mn neighbors at longer distances which are not resolved with the current signal-to-noise ratio. However, considering the amplitude of Mn backscattering in the 2.7 Å peak, it is probably not appropriate to picture all four Mn as μ-oxo-bridged in a single symmetric cluster. These conclusions about the Mn environment are quite similar to those derived from studying Mn in PS II from spinach (Yachandra et al., 1987).

It has been suggested that a peroxo-bridged structure is an intermediate for either the S_2 or the S_3 state (Renger, 1977). This proposal has been made on the basis that two-electron oxidation of H_2O to form a peroxo compound is thermodynamically favored over sequential one-electron oxidations. It is unlikely that Mn atoms which are 2.7 Å apart are bridged by peroxo moieties in either S_1 or S_2, since peroxo-bridged structures are characterized by a longer Mn-Mn distance (Mabad et al., 1985). One may propose that at the S_1 or S_2 stage the oxidizing equivalents are still stored on Mn and therefore the peroxo bridge has not yet formed; this is supported by the edge shifts in the S_1 to S_2 transition together with the absence of structural change in the EXAFS spectrum. On the other hand, one may picture peroxo bridges *between* two binuclear clusters or between a cluster and a monomer. If the resulting Mn-Mn distance were characterized by a large Debye-Waller factor, it would be difficult to observe with our current EXAFS analysis.

Because of the high degree of disorder in the terminal ligands, it is difficult to assign them in the EXAFS spectrum. The nature of these ligands may be addressed in other experiments, many of which will be facilitated by the use of a prokaryote.

V E. Conclusions

1 The S_1 to S_2 transition occurs on continuous illumination of the PS II preparation from the thermophilic cyanobacterium, *Synechococcus* sp., at illumination temperatures between 140 and 220 K, probably involving a formal oxidation state change from Mn(III) to Mn(IV) and reduction of Q_A.

2 The salient structural features of the Mn in the O_2-evolving complex, as evidenced by EXAFS, are similar in the preparations from *Synechococcus* and spinach. They indicate the presence of a di-μ-oxo bridged structure, with Mn-O bond length of 1.75 ± .05 Å and a Mn-Mn distance of 2.71 ± .05 Å in the S_1 and S_2 states. The data are not consistent with a symmetric tetranuclear cluster.

3 Significant differences in the Fe^{2+}-Q_A^- and in the Mn structure between spinach and *Synechococcus* are evident by EPR when the complexes are illuminated at 140 K. We interpret the new signal at g=1.6 in *Synechococcus* to result from the Fe^{2+}-Q_A^- complex in a different conformation which probably has a larger exchange coupling between the iron and the semiquinone as compared with the species giving rise to the g=1.8 signal, possibly due to differences in the carboxy ligand of the iron. We suggest that the oxidation of Mn but absence of the g=4.1 signal on illumination at 140 K may be explained by a change in the zero-field splitting parameters of a Mn(IV) monomeric species or a Mn cluster (relative to spinach) resulting in an extremely broadened EPR signal.

Chapter VI: Future Work

VI A. Photosystem I and Center X

In the studies of the structure of center X of PS I, I did not reach a unique answer, but obtained an indication that a current model for X, a [4Fe-4S] ferredoxin, was inadequate. Our ongoing experiments, in collaboration with Prof. John Golbeck's group in Portland State University, are likely to yield a unique answer to this question. The preliminary results from these experiments suggest a rather unusual structure for X. Mössbauer experiments, particularly those of center X isolated from centers A and B and other Fe complexes, and prepared from an organism grown on Fe^{57}, will be very useful in defining its structure. Such experiments are already in progress elsewhere. We have considered measuring sulfur X-ray absorption spectra of X. The X-ray absorption edge spectra of sulfur are much better resolved than those of Fe because the resulting core hole lifetime is considerably longer. Therefore much more detailed information can be garnered concerning symmetry and oxidation state. One potential difficulty in such an experiment is that PS I contains numerous methionines (Table VI-1); the sulfurs from these methionines will contribute an undesirable background to the S K-edge spectrum. In addition, sulpholipids are found in thylakoids and are probably associated with PS I (Harwood, 1980).

Using S^{33} and Fe^{57}-grown *Synechococcus*, one may measure the hyperfine coupling of these nuclei in X. One may then use pulsed EPR measurements to determine the stoichiometry of Fe atoms, S atoms, and unpaired electrons involved in reduced center X relative to P700. These measurements may be very useful for determining the structure of X.

The number of copies of PSI-A1 and -A2 polypeptides associated with PS I is of interest because their primary sequence is known. Thus one can begin to address what cofactors are associated with what amino acids. In particular, since center X

seems to be bound on PSI-A1 and PSI-A2, the number of copies of these polypeptides determines the maximum number of cysteines that might be ligands to X. One copy of each polypeptide would contribute 5 or 6 cysteines total. The number of cysteines per P700 determines whether X may consist of two [2Fe-2S] clusters, since 8 cysteines are required for binding two clusters. One approach to measuring the number of copies of these polypeptides involves C^{14}-grown cyanobacteria (Lundell et al., 1985; Bruce & Malkin, 1987). One can then use autoradiography on SDS-polyacrylamide gels to measure the relative amounts of the polypeptides present in PS I. If one assumes that the simplest integral ratio between the concentrations yields the stoichiometries, then the number of each polypeptide per reaction center can be determined. This method is most useful if one knows that the subunits are functionally related to each other and are present in fixed ratios regardless of growth conditions and throughout the purification procedure, and one must have an estimate of the mass of the entire complex, and an accurate measure of the masses of all the subunits. This approach has resulted in values between one and two copies of each of the PSI-A polypeptides per P700, with one being more likely (Bruce & Malkin, 1987). It would be desirable to use a method that directly compares the concentration of PSI-A1 and-A2 to the concentration of P700, so that no assumptions need be made. Perhaps this could be done by growing cyanobacteria on S^{35} of a known specific activity, and purifying CP1. Using a CP1 sample of known P700 concentration, one could remove the lipids by organic extraction, and the amount of radioactivity associated with the polypeptides could then be measured. As indicated in Table I, the S content is dominated by methionines with a small contribution from cysteines, and the acid-labile contribution is small. It should be straightforward to determine from the S-to-P700 ratio whether two copies or one copy of each polypeptide is associated with each P700. This information would be of great interest not just for understanding the structure of X, but generally for modelling PS I.

VI B. Photosystem II and the Mn-OEC

VI B. 1. EPR of Prokaryotes

Surprisingly, EPR spectra of the Fe-Q acceptor are different in spinach and *Synechococcus*. What is the cause of the differences among the Fe-Q acceptor EPR signals at g=1.9, 1.8 and 1.6? Lineshape simulations and Mössbauer spectra similar to the studies conducted on the Fe-Q complex from purple non-sulfur bacteria (Butler et al., 1980, 1984) would be informative. In addition, power saturation studies may provide insight and constraints for the EPR simulations.

The comparison of the structure of the Mn-OEC using XAS yielded the expected result, i.e. that the structures in cyanobacteria and plants are essentially similar. However, the g=4.1 EPR signal assigned to a donor species in spinach is absent in *Synechococcus*. It would be interesting to know whether the g=4.1 signal, or the F-induced g=4.2 signal can be formed under other experimental conditions. Could such signals be observed at other EPR spectrometer frequencies? Upon illumination of PS II at 140 K, in the absence of the g=4.1 signal or any other donor EPR signal, we observed a Mn K-edge shift. The K-edges of these samples seemed to have a different pre-edge structure from those that were illuminated at 215 K and had multiline signals. It may be interesting to confirm this difference in the pre-edge structure and try to understand its origin.

One reason for comparing the spectra of PS II from a eukaryotic and a prokaryotic organism was that we would like to study PS II samples from cyanobacteria grown on isotopically altered or enriched media. I will discuss some factors relevant to planning these experiments, including a tabulation of some chemical analyses of PS II, some observations concerning the growth medium generally used, and a list of some potentially interesting isotopes. I will mention some spectroscopy experiments that have already been done using isotopes and some which we can do.

In planning these experiments, the first question to consider is, what elements are likely to play interesting roles in the Mn-OEC? Ca, Cl and Mn are known to be cofactors

for oxygen evolution. These species are somehow bound by a protein, so we can expect that O, N, H, C and perhaps S are nearby. As mentioned in chapter V, the ligands of the Mn are likely to be mostly O, perhaps with some N also. C and H are likely to be present as 'second shell' ligands. Sulfide is unlikely to be a direct ligand because it would probably be oxidized by high-valent Mn. Table VI-1 lists selected chemical analyses of PS II. These analyses indicate that several additional metals besides Mn are present. With the exception of a portion of the Fe present, the role of these metals in unknown. It is of obvious interest to investigate all of these components, and naturally one should begin with the species already known to be essential for activity. Thus studies of Mn, Cl (or its analogue, Br), Ca, O, N, C and H are of primary interest. Additional experiments, such as XAS, might probe the structures and possible roles of the other metals. Table VI-2 lists selected isotopes of these elements that are radioactive or that have nuclear spin.

The terminal ligands of the Mn cluster are poorly defined in the EXAFS spectra because of their heterogeneity. EPR measurements of ligand hyperfine interactions have already been used to address the nature of these ligands. Ongoing ESE-NEM measurements (Britt et al., 1987) are probably the most direct method; these methods indicate that there might be a few N ligands to the cluster. Other CW EPR experiments address couplings to exchangeable ligands. A comparison of PS II from spinach prepared in Cl buffers with preparations washed free of halide and resuspended in Br- containing buffers showed that both preparations had identical multiline spectra at 4 G resolution. This indicates that the Mn is unlikely to have an exchangeable halide ligand. Studies of PS II preparations resuspended in H_2O^{17} exhibited a different multiline EPR signal lineshape (Hansson et al., 1986). The authors concluded that this was due to hyperfine coupling with O^{17} derived from water which bound at the S_0, S_1 or S_2 state. Similarly, studies of the multiline signal in PS II suspended in $H^2{}_2O$ showed a different hyperfine structure as compared with controls (Nugent et al., 1987).

Using a prokaryotic organism one could address the nature of intrinsic ligands, such as N atoms from protein ligands, or (hypothetical) non-exchangeable halide ligands. Intrinsic O or H ligands would be rather expensive to exchange isotopically because one would have to use gallons of isotopically labeled water. Similarly, C labeling is not simple; the primary source is CO_2 which is bubbled through and needed in great quantities. However, many elements are introduced in trace form and would be more easily exchanged. The concentrations and chemical forms of these elements in the growth medium are indicated in Table VI-3. It is of note that all of these elements (except Co) are present in gross excess of the concentration of reaction centers in a mature culture. (The concentration of reaction centers is only accurate to within a factor of two or three. It was estimated based on the concentration of Chl in a mature culture and the approximate P700/Chl ratios in thylakoids, and on reported PS I/ PS II rations (Manodori & Melis, 1986).)

Experiments are already in progress to measure the XAS and EPR of cyanobacteria grown in the presence of excess Br and trace Cl. A comparison of these spectra to those of control samples will address whether the halide is a ligand of Mn. Another experiment that we are beginning involves growing cyanobacteria on medium containing N^{15} to simplify the N hyperfine coupling (relative to coupling with the N^{14} nucleus). One may then look for changes in the CW-EPR lineshape of the multiline signal or other signals of interest, and one could measure the ESE-NEM spectrum. These experiments could determine the number of N ligands present in the multiline and g=4.1 species.

Radiolabeling experiments involving Cl^{36} (as suggested by V. DeRose), Ca^{45} or Ca^{48} could address the minimum stoichiometries of these cofactors per active PS II reaction center. Provided that one obtains a preparation that has a small number of these ions per reaction center, it would be of great interest to probe their structures with XAS.

Mn^{53} has I=7/2 while the naturally occurring isotope, Mn^{55}, has I=5/2. Measurement of the multiline spectrum with Mn^{53} may lend additional constraints for the

structure of the Mn complex especially in conjunction with computer simulations of the hyperfine structure.

These experiments range from relatively straightforward experiments that are already in progress to rather involved or maybe even unfeasible experiments. The tables in this chapter may be useful in planning additional experiments.

VI B. 2. Mn-XAS

In marked contrast with the situation of five or ten years ago, we now make Mn XAS measurements routinely, both K-edge and EXAFS, using a variety of PS II preparations. This advance has come about by a combination of improvements in biochemical preparations and instrumental improvements. The XAS measurements demonstrated a redox role for Mn in the OEC, established the average oxidation states of Mn in S_1 and S_2 in *Synechococcus* and spinach and of S_3 in spinach, and demonstrated the existence of a di-μ-oxo-bridged Mn cluster in PS II.

Despite these achievements, the structure of the Mn-OEC is not clear! The Mn atoms do not seem to be present in a symmetric tetranuclear cluster. In principle, EXAFS measurements may be capable of defining whether Mn is present in a distorted tetranuclear or trinuclear cluster, or a pair of binuclear clusters, however our data at present are not sufficient to make an assignment. Another disappointment in the Mn-EXAFS measurements has been the near invariance of the spectrum among preparations in various S-states. There probably are differences among these samples, but within our S/N they are difficult to characterize. To study possible Mn shells at longer distances, and subtle differences in Debye-Waller factors, it is apparent that we would like to have ideal data, i.e. minimal artifacts, a long data set, and a tremendous S/N. Perhaps we would benefit most now from improving *how* we collect the data, rather than emphasizing a wide variety of samples. The level of artifacts in the EXAFS data was dramatically improved by changing from a non-energy-resolving detector to an energy-resolving detector, as elaborated in chapter II and Appendix I. Although this detection

apparatus is a clear improvement over the previous scintillation array, there may be better methods for X-ray detection yet, with faster counting rates, better linearity or much better resolution of X-ray energies. A similar dramatic improvement is needed in the useful data length and the S/N, especially at high energy. This improvement can be made partly by changing to another data collection software package, based on an algorithm that emphasizes time-efficiency and collects more data at high energy where it is most needed. With such an algorithm we should easily collect good data to k=12 Å, while currently, even with extensive signal averaging using very bright beam line, the data beyond k=10 Å is generally of dubious quality. Thus both the resolution of the various backscattering shells, and the S/N of our measurements is compromised. Such an improvement in useful data length might allow us to determine whether the features which variably appear at R>3Å are due to C or Mn or are simply noise, and it might allow us to discern a small amount of Br bound to the Mn complex.

In contrast to the invariable EXAFS features, changes in the Mn X-ray K-edge spectrum are apparent from sample to sample, and ongoing studies of the effects of cofactors and inhibitors are likely to be quite fruitful. Improving the resolution of these measurements is an important priority, as this would aid in assigning the transitions and interpreting these edge changes more quantitatively. We have considered measuring Mn L-edges. Due to the longer lifetime of a 2 p or 2 s hole as compared with a 1 s hole, these spectra are likely to be much better resolved than the Mn K-edges. Based on the exciting changes in the K-edge spectra, the L-edge spectra are likely to provide a wealth of information. Unfortunately these measurements would require having the sample in a vacuum. Additionally, the measurement of K-edges of lower-Z elements such as Ca, S and Cl is of great interest, provided that they are catalytically significant and that there is little nonspecific ions present. These measurements are technically much simpler than Mn L-edges in that they can be done in a He atmosphere rather than in a vacuum.

One set of experiments we have considered is to prepare very thin samples for XAS, and advance the S-states in the sample by saturating illumination. Using a YAG laser, a PS II preparation of concentration 3 mg Chl $(mL)^{-1}$ with a path length of 3 mm can be saturated with respect to S-state advance (Dr. J.-L. Zimmermann, personal comm.). This is consistent with estimations made using an extinction coefficient of 10 to 15 $mM^{-1}cm^{-1}$ for Chl, and assuming an energy per pulse of 250 mJ. PS II samples used for XAS measurements have a concentration of approximately 30 mg Chl $(mL)^{-1}$, so a path length of approximately 0.2 to 0.5 mm may be saturated, depending on whether the sample is illuminated on one side or on two sides during each pulse. This is an extremely thin sample!

We would like to know what Mn fluorescence count rates would be obtained from such a sample. In Appendix I, calculations of the Mn fluorescence rate as a function of sample depth are described. The calculated rates for various sample thicknesses are plotted in Table VI. These data indicate that with 0.4 mm samples we can expect count rates approximately half of those obtained with an infinitely thick sample. It is of note that the transmitted beam intensity in these experiments would be over 50% of the incident intensity, so that there would be an acceptable flux 'left over' for another dilute sample.

TABLE VI-1: SELECTED CHEMICAL ANALYSES OF PS II AND PS I

Constituent	Stoichiometry
	PS II: Stoichiometry per Z or D^+
Chl	50 - 90
Mn	3 - 4
Fe	10 - 14
Co	.3
Cu	.7 - 1.
Zn	1-2
Mo	.2 - 1.0
Cl	unk. conc., necc. cofactor
Ca	unk. conc., necc. cofactor

	PS I Particles	CP1 Only
Fe	11 - 14 per P700	ca. 5 per P700
Acid Labile S	10 - 13 per P700	ca. 4 per P700
Known Cysteines in: PS I-A1 and PSI-A2 for CP1; 8kDa , PSI-A1 and PSI-A2 for PS I Particles.	15 total per 1 copy ea.	6 per 1 copy ea.
Known Methionines (as for Cys)	24 total per 1 copy ea.	22 per 1 copy ea.
Other Metals (Mn, Co, Cu, Zn, Mo)	n.d.	

TABLE VI-2: GROWTH MEDIUM COMPONENTS

Component	Concentration
NH_4	0.1 mM as $(NH_4)_6Mo_7O_{24}\cdot 4\ H_2O$
NO_3	11 mM (as K and Na salts) 0.1mM as $Co(NO_3)_2$
Mg	1.2 mM as Mg SO_4
Na	6 mM (as NO_3- and EDTA salts)
PO_4	3 mM as KH_2PO_4 and K_2HPO_4
SO_4	1.2 mM as Mg SO_4 0.002 mM as Zn SO_4 0.076 mM as Cu SO_4
Cl	1 mM as $CaCl_2$, 0.1 to 0.2 mM as Fe Cl_3
K	10 mM (as PO_4 and NO_3 salts)
Ca	0.5 mM as Ca Cl_2
Mn	0.03 mM as $MnCl_2$
Fe	0.02 - 0.08 mM as $FeCl_3$
Co	.00005 mM or 50 nM as $Co(NO_3)_2$
Cu	0.08 mM as $CuSO_4$
Zn	0.0023 mM as Zn SO_4
Mo	0.1 mM as $(NH_4)_6Mo_7O_{24}\cdot 4H_2O$
PS I in a Mature Culture	ca. 30 nM
PS II in a Mature Culture	ca. 10 nM

TABLE VI-3: TABLE OF SELECTED ISOTOPES

Isotope	Abundance,%	Emission	Half-life	Nuclear Spin
$_1H^1$	99.9			1/2
H^2	.015			1
H^3	-	β-	12.5 y	1/2
$_6C^{13}$	1.11			1/2
C^{14}		β-	5730 y	
$_7N^{14}$	99.6			1
N^{15}	.37			1/2
$_8O^{16}$	99.8			
O^{17}	.037			5/2
O^{18}	.2			
$_9F^{19}$	100			1/2
$_{16}S^{33}$	.76			3/2
S^{35}		β-	88 d	3/2
$_{17}Cl^{35}$	76.			3/2
Cl^{36}		β	310,000 y	2
Cl^{37}	24.			3/2
$_{20}Ca^{43}$	.1			7/2
Ca^{45}		β-	165 d	
Ca^{48}		β-	$>10^{18}$ y	
$_{25}Mn^{52}$		EC, β+		6

Mn^{53}		EC, β+,γ	$2x10^6$ y	7/2
Mn^{54}		EC, γ	303 d	3
Mn^{55}	100			5/2
$_{26}Fe^{55}$		EC, Mn X-rays	2.6 y	
Fe^{57}	2.17			1/2
$_{27}Co^{59}$	100			7/2
Co^{60}		β-	5.2 y	
$_{29}Cu^{63}$	69			3/2
Cu^{65}	31			3/2
$_{30}Zn^{65}$		EC, β+	250 d	
Zn^{67}	4			5/2
$_{35}Br^{79}$	50			3/2
Br^{81}	49.			3/2
$_{42}Mo^{95}$	15.7			5/2
Mo^{97}	9.5			5/2

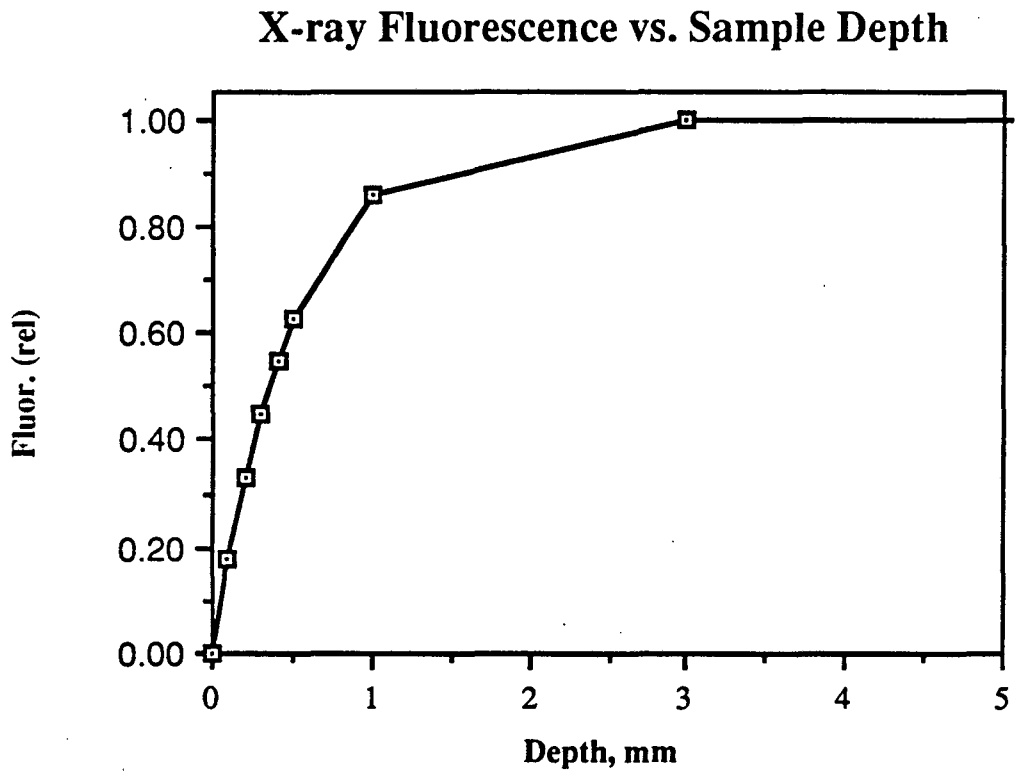

Figure VI-1. Dependence of fluorescence intensity on sample thickness. The fluorescence rates are relative to an infinitely thick sample. Calculations are analogous to those described in Appendix I. Note that an increase in sample depth from 1 mm to 3 mm yields a negligable increase in fluorescent count rate, but it will significantly reduce the intensity available for absorption measurement of the energy calibration standard.

Appendix I

In chapter II, two X-ray fluorescence detection methods are described and discussed. In that chapter I assumed Mn fluorescence rates of 1-6 K cps plus scattering and Cr fluorescence rates approximately twice that of the Mn fluorescence, with the exact rate depending on geometry and other factors. In this appendix, I will calculate the expected rates from the I_0 ion chamber reading to illustrate what determines our counting rates. These calculations were performed ostensibly to evaluate whether our detectors were receiving as may counts as we expect, and to estimate the S/N of the Si:Li and scintillation detectors before doing an experimental comparison.

The first step of the calculation is to estimate I_0 in cps. The flux in I_0 may be related to a current reading by the following approximate relation (personal comm., Dr. B. Hedman, SSRL staff):

$$I_0 = [Current(Amp.) \times (30eV)]/[1.6 \times 10^{-19} Coul \times E(eV) \times (1 - e^{-\mu x})].$$

In this equation E is the X-ray energy, μ is absorbance of the ion chamber gas which has a path length x, and 30 eV/ ion pair is an empirical factor determined for ionization of N_2 gas. Using $\mu = \rho\sigma$=1.25 g/L x 11 cm^2/g= .013 cm^{-1} (McMaster et al., 1969), and E=7000 eV we obtain I_0= 2 x 10 ^{17} x Current (Amp). A typical current for I_0 in our experiments is 2 x 10^{-7} Amp (this value was measured on BL VI-2, with the wiggler field at 5.5 KG, using Si< 400 > crystals, at 7000 eV, with a ring current of 46 mA). **Thus, I_0= 4 x10^{10} cps.**

Next we wish to calculate the Mn fluorescence yield and the scattering yield from the matrix. These may be calculated using the relation:

$$\phi = I/I_0 = \rho\sigma d$$

where ρ is the cross section (for Mn absorption and fluorescence, or matrix scattering), and σ is the density (of Mn or of the matrix, respectively). Since the sample is practically

opaque to the X-rays, the effective path length, d, must be replaced by an integral: $d = \int_0^b e^{-\mu x} e^{-\mu' x} \delta x$, where the optical densities μ and μ' refer to the attenuation of the incoming and outgoing X-rays by the matrix, respectively, and b is the actual sample depth. If we ignore the difference in cross section for absorbed and fluorescent photons, and replace μ with $\rho\sigma$ the integral may be approximated by $d = (1/2\rho\sigma)(1 - e^{-2\rho\sigma b})$. For $b >> \rho\sigma$, and assuming a carbon matrix of density 1g/cm^3 with a cross section of approximately 10 cm^2/gm at 7000 eV, (McMaster et al., 1969) we obtain d=.05 cm.

For Mn Kα fluorescence, ρ= 4x 10^{-5}g/cm^3 (equivalent to 700 μM), and the cross section for fluorescence is given $\sigma_{fl}=\sigma_{abs} \times \phi_{fl}$ =470 cm^2/g x 0.2 $\approx$ 100 cm^2/gm. **Thus $I_f=I_0$ x2x 10^{-4}.**

For scattering, ρ=1g/cm^3, and σ= 0.4 cm^2/gm, so $I_s=I_0$ x 2 x 10^{-2}.

The solid angle of the detectors is estimated to be $r^2/4R^2$, where r is the radius of the detector, and R is the distance from the sample to the detector. (This is actually a good approximation only when r/R<0.1, and is estimated for circular detectors.) For the Si:Li detector r=0.4 cm and R=10 cm, and the result is that 0.2% of the total fluorescence is captured. For the photomultiplier array, r=2.5 cm for each tube, and R=20 cm, which results in a 1.7% yield of fluorescence.

The effect of the Cr filter on scattering and fluorescence rates may also be calculated. For an 0.5 mil (or 0.0013 cm) filter, the transmittance for Mn Kα photons is approximately 0.5, but for scattered X-rays of energy 6550 eV is 0.01 and for X-rays of energy 7000 eV it is approximately 0.03. The fluorescence of the Cr filter is difficult to estimate. Empirically we have found it to be comparable to the transmitted scattering when using a 1 mil filter.

The transmittance of the air and the seven layers of mylar and/or kapton in the detectors and cryostat is a minor correction, probably much smaller than the uncertainty in the overall calculation. For example, if one assumes a 1 mil thickness for each of seven mylar or kapton windows, the transmittance is roughly 0.8 overall for either the fluorescence or the scattering. For 25 cm of air between the I_0 ionization chamber and

the sample, the transmittance would be .75. A final factor is that, for measurements using the photomultipliers, the monochromator was detuned such that I_0 was 50% of maximum. This detuning reduced some background artifacts. When using the Si:Li detector, the monochromator was not detuned.

Putting all of these corrections together, we can estimate the count rates incident at the detectors. Using the photomultiplier tubes, the center tube should receive 20,000 cps of Mn fluorescence and 40,000 cps scattering (and perhaps another 40,000 cps Cr fluorescence). At 7000 eV, the end of an EXAFS scan, the scattering will be considerably higher. These count rates predict a S/N of 63 at the top of the Mn K-edge edge in a scan collected for 1 second per point.

For the Si:Li detector, these corrections predict a Mn fluorescence rate of 4,800 cps and 9,600 cps of scattering and perhaps another 10,000 cps of Cr scattering. In the discriminator window we detect approximately 80% of the Mn fluorescence (since we get K-α fluorescence only) and 20% of the Cr fluorescence (the Cr Kβ fluorescence), thus we should expect the count rates in the discriminator window to be approximately 2 K background and 4 K Mn fluorescence. This would yield a S/N of 52 at the top of the Mn K-edge.

For 0.7 mM Mn samples the measured count rates are slightly different from those of these calculations. As measured, under the conditions assumed for this calculation, the photomultiplier tube receives approximately 20,000 cps of scattering and Cr fluorescence, and 5,000 cps of Mn fluorescence. In the discriminator window, the Si:Li receives approximately 2 K of Cr fluorescence and 5 K of Mn fluorescence. The discrepancies are probably due to the fact that I have no real estimate of Cr fluorescence rates, and I have not accounted for the Soller slits, nor have I corrected for the nonspherical spatial distribution of the scattering. The fact that the calculated count rate estimates agree with the experiment to better than an order of magnitude indicates that the calculations are probably sound. These calculations are probably a reasonable guideline to illustrate where our losses are in the experiment. In addition the agreement indicates that our

detectors are reasonably efficient and that our alignment is apparently acceptable. Of course, there are more accurate ways to check the efficiency of the detectors!

Both the estimated and the experimental count rates imply that the S/N at the top of the Mn K-edge is comparable for the two detectors. However, as mentioned in Chapter II, the removal of scattering background is a great advantage with respect to artifacts. In addition, the S/N of data collected with the photomultipliers is considerably worse at the high energy end of the scan, while for the Si:Li the S/N does not deteriorate so quickly. Usually the S/N at the end of the scan, and not at the top of the edge, actually limits the EXAFS analysis.

References

Aasa, R., Andréasson, L.-E., Lagenfelt, G., & Vänngård (1987) *FEBS Lett 221,* 245-248..

Allen, J. P., Colvin, J. T., Stinson, D. G., Flynn, C. P., & Stapleton, H. J. (1982) *Biophys J. 38* 299-310.

Arnon, D. I. (1949) *Plant Physiol. 24,* 1-15.

Atkinson, Y. E., & Evans, M. C. W. (1983) *FEBS Lett. 159,* 141-144.

Babcock, G. T., Ghanotakis, D. F., Ke, B., & Diner, B. A. (1983) *Biochim. Biophys. Acta 723,* 276-286.

Barry, B. A. & Babcock, G. T. (1987) *Proc. Natl. Acad. Sci USA* in press.

Bearden, A. J., & Malkin, R. (1972) *Biochim. Biophys. Acta. 283,* 456-468.

Beardwood, P., Gibson, J. F., Bertrand, P., & Gayda, J.-P. (1983) *Biochim. Biophys. Acta 742,* 426-433

Beckmann, J. D., Ljungdahl, P. O., Lopez, J. L., & Trumpower, B. L. (1987) *J. Biol. Chem. 262,* 8901-8909.

Beinert, H., & Thomson, A. J. (1983) *Arch. Biochem. Biophys. 222,* 333-361.

Bertrand, P., & Gayda, J.-P. (1979) *Biochim. Biophys. Acta 579* 107-121.

Bertrand, P., & Gayda, J. P. (1982) *Biochim. Biophys. Acta. 680,* 331-335.

Bertrand, P., Guigliarelli, B., Gayda, J.-P., Beardwood, P. & Gibson, J. F. (1985) *Biochim. Biophys. Acta 831,* 261-266.

Blum, H., Salerno, J. C., Rich, P. R., & Ohnishi, T. (1979) *Biochim. Biophys. Acta 548* 139-146.

Bolton, J. R. (1977) in *Primary Processes of Photosynthesis* (ed. Barber, J.) Elsevier, Amsterdam, 187-200.

Bonnerjea, J. R., & Evans, M. C. W. (1984) *Biochim. Biophys. Acta 767*, 153-159.

Brettel, K., Sétif, P., & Mathis, P. (1986) *FEBS Lett. 20,* 220-224.

Britt, R. D., Sauer, K., & Klein, M. P. (1987) in *Progress in Photosynthesis Research* (Biggins, J., Ed.), Martinus Nijhoff, Dordrecht, vol 1, 573-576.

Bruce, B. D., & Malkin, R. (1987) in *Plant Membranes: Structure, Function, Biogenesis* Alan R. Liss, Inc., 47-63.

Brudvig, G., & Crabtree, R. H. (1986) *Proc. Natl. Acad. Sci. USA 83,* 4586-4588.

Bryant, D. A., De Lorimier, R., Gugliemi, G., Stirewalt, V. L., Cantrell, A., & Stevens, S. E. Jr. (1987) in *Progress in Photosynthesis Research* (Biggins, J., Ed.), Martinus Nijhoff, Dordrecht, vol. 4, 749-755.

Bunker, G., Stern, E. A., Blankenship, R. E., & Parson, W. W. (1982) *Biophys. J. 37,* 539-551.

Butler, W. F., Johnston, D. C., Shore, H. B., Fredkin, D. R., Okamura, M. Y., & Feher, G. (1980) *Biophys. J. 32,* 967-992.

Butler, W. F., Calvo, R., Fredkin, D. R., Isaacson, R. A., Okamura, M. Y., & Feher, G. (1984) *Biophys. J. 45,* 947-973.

Casey, J. L., & Sauer, K. (1984) *Biochim. Biophys. Acta 767,* 21-28.

Castner, T. G. (1959) *Phys. Rev. 115* 1506-1515.

Chamorovsky, S. K., & Cammack, R. (1982) *Photobiochem. Photobiophys. 4,* 195-200.

Cole, J., Boska, M., Blough, N., & Sauer, K. (1986) *Biochim. Biophys. Acta 848,* 41-47.

Cole, J., Yachandra, V. K., Guiles, R. D., McDermott, A. E., Britt, R. D., Dexheimer, S. L., Sauer, K., & Klein, M. P. (1987a) *Biochim. Biophys. Acta 890,* 395-398.

Cole, J. L., Yachandra, V. K., McDermott, A. E., Guiles, R. D., Britt, R. D., Dexheimer, S. L., Sauer, K., & Klein, M. P. (1987b) *Biochem. in press.*

Cole, J., & Sauer, K. (1987) *Biochim. Biophys. Acta 891,* 40-48.

Cooper, S. R., Dismukes, G. C., Klein, M. P., & Calvin, M. (1978) *J. Am. Chem. Soc. 100,* 7248-7252.

Cramer, S., Eccles, T., Kutsler, F., Hodgson, K. & Mortenson, L. (1976) *J. Am. Chem. Soc. 98,* 1286-1287.

Curtis, S. E., & Haselkorn, R. (1984) *Plant Mol. Biol. 3,* 249-258.

Deisenhofer, J., Epp, O., Miki, K., Huber, R., & Michel, H. (1985) *Nature 318,* 618-624.

Dekker, J. P., Ghanotakis, D. F., Plijter, J. J., Van Gorkom, H. J., & Babcock, G. T. (1984) *Biochim. Biophys. Acta 767,* 515-523.

de Paula, J. C., Innes, J. B., & Brudvig, G. W. (1985) *Biochem. 24,* 8114-8120.

de Paula, J. C., Li, P. M., Miller, A.-F., Wu, B. W., & Brudvig, G. W. (1986) *Biochem. 25,* 6487-6494.

Dismukes, G. C., & Siderer, Y. (1980) *FEBS Lett. 121,* 78-80.

Dismukes, G. C., & Siderer, Y. (1981) *Proc. Natl. Acad. Sci. USA 78,* 274-278.

Dismukes, G. C., Ferris, K., & Watnick, P. (1982) *Photobiochem. Photobiophys. 3,* 243-256.

Dismukes, G. C., Frank, H. A., Friesner, R., & Sauer, K. (1984) *Biochim. Biophys. Acta 764,* 253-271.

Dörnemann, D. & Senger, H. (1986) *Photochem. Photobiol. 43,* 573-581.

Dyer, D. L., & Gafford, R. D. (1961) *Science 134,* 616-617.

Eisenberger, P., & Lengeler, B. (1980) *Phys. Rev. B 22,* 3551-3562.

Eisenberger, P., Okamura, M. Y., & Feher, G. (1982) *Biophys. J. 37,* 523-538.

Evans, E. H., Rush, J. D., Johnson, C. E., & Evans, M. C. W. (1979) *Biochem. J. 182,* 861-865.

Evans, E. H., Dickson, D. P. E., Johnson, C. E., Rush, J. D., & Evans, M. C. W. (1981) *Eur. J. Biochem. 118,* 81-84.

Evans, M. C. W., Reeves, S. G., & Cammack, R. (1974) *FEBS Lett. 49,* 111-114.

Evans, M. C. W. (1982) in *Iron-Sulfur Proteins* (Spiro, T. G., Ed.) John Wiley & Sons, New York, 249-284.

Fee, J. A., Findling, K. L., Yoshida, T., Hill, R., Tarr, G. E., Hearshden, D. O., Dunham, W., Day, E. P., Kent, T. A. & Münck, E. (1984) *J. Biol. Chem. 259,* 124-133.

Fish, L. E., Kück, U., & Bogorad, L. (1985) *J. Biol. Chem. 260,* 1413-1421.

Fogo, J. K., & Popowski, M. (1949) *Anal. Chem. 21,* 732-734.

Gabellini, N., & Sebald, W. (1986) *Eur. J. Biochem. 154,* 569-579.

Gayda, J.-P., Gibson, J. F., Cammack, R., Hall, D. O., & Mullinger, R. (1976) *Biochim. Biophys. Acta 434,* 154-163.

Gayda, J.-P., Bertrand, P., More, C., Le Gall, J. & Cammack, R. C. (1981) *Biochem. Biophys. Res. Comm. 99* 1265-1270.

Gayda, J.-P., Bertrand, P., Deville, A., More, C., Roger, G., Gibson, J. F., & Cammack, R. (1979) *Biochim. Biophys. Acta 581* 15-26.

Gayda, J.-P., Bertrand, P., More, C., LeGall, J. & Cammack, R. C. (1981) *Biochem. Biophys. Res. Comm. 99,* 1265-1270.

Ghanotakis, D. F., & Yocum, C. F. (1985) *Photosyn. Res. 7,* 97-114.

Ghanotakis, D. F., & Yocum, C. F. (1986) *FEBS Lett. 197,* 244-248.

Gibson, J. F., Hall, D. O., Thornley, J. H. M., Whatley, F. R. (1966) *Proc. Natl. Acad. Sci. USA 56,* 987-990.

Ginsberg, A. P. (1971) *Inorg. Chim. Acta. Rev.* 45-68.

Golbeck, J. H., McDermott, A. E., Jones, W. K & Kurtz, D. M. (1987) *Biochim. Biophys. Acta 891,* 94-98.

Golbeck, J. H., & San Pietro, A. (1976) *Anal. Biochem. 73,* 539-542.

Golbeck, J. H. (1980) *Methods Enzymol. 69,* 129-141.

Golbeck, J. H., & Cornelius, J. M. (1986) *Biochim. Biophys. Acta 849,* 16-24.

Goodin, D. (1983) Ph.D. Dissertation, Univ. of Calif., Berkeley, CA, USA, Lawrence Berkeley Laboratory Report, LBL-16901.

Goodin, D. B., Falk, K.-E., Wydrzynski, T., & Klein, M. P. (1979) *6th Annual Stanford Synchrotron Radiation Laboratory Users Group Meeting,* SSRL Report No. 79/05, 10-11, Stanford University, Stanford, CA.

Goulding, F. S. & Landis, D. A. (1978) *IEEE Transaction, Nuclear Science, 25* 896-920.

Goulding, F. S. & Landis, D. A. (1983) *IEEE Transaction, Nuclear Science, 30* 301-310.

Goulding, F. S., Landis, D. A. & Madden, N. W. (198?) LBL Report No. 14464.

Govindjee, & Eaton-Rye, J. (1986) *Photosyn. Research 10,* 365-369.

Hall, D. O., Rao, K. K. & Mullinger, R. N. (1975) in *Protein Structure and Evolution* (Ed., Fox, & Deyl) 233-259.

Hansson, Ö., & Andréasson, L.-E. (1982) *Biochim. Biophys. Acta 679,* 261-268.

Hansson, Ö., Aasa, R., & Vänngård, T. (1987) *Biophys. J. 51,* 825-832.

Harnisch, U., Weiss, H., & Sebald, W. (1985) *Eur. J. Biochem. 149,* 95-99.

Hartman, J. R., Foxman, B. M., & Cooper, S. R. (1984) *J. Am. Chem. Soc. 106,* 1380-1387.

Hearst, J. E. (1986) in *Encyclopedia of Plant Physiology, vol 19, Photosynthesis III* (eds. L. A. Staehelin and C. J. Arntzen) 382-388, Springer Verlag, Berlin.

Heathcote, P., Williams-Smith, D. L., & Evans, M. C. W. (1978) *Biochem. J. 170,* 373-378.

Hill, C. L., Renaud, J., Holm, R. H. & Mortenson, L. E. (1977) *J. Am. Chem. Soc. 99,* 2549-2557.

Hiyama, T., & Ke, B. (1972) *Biochim. Biophys. Acta 267,* 160-171.

Hiyama, T., Watanabe, T., Kobayashi, M. & Nakazato, M. (1987) *FEBS Lett. 214,* 97-100.

Ho, K. K. & Krogmann, D. W. (1982) *Botanical Monographs, vol 19, The Biology of Cyanobacteria* (Ed., Carr, N. G. & Whitton, B. A.) U. C. Press, Berkeley, CA 191-214.

Jaklevic, J., Kirby, J. A., Klein, M. P., Robertson, A. S., Brown, G. S., & Eisenberger, P. (1977) *Solid State Commun. 23,* 679-682.

Johnson, R. E., Papaefthymiou, G. C., Frankel, R. B., Holm, R. H. (1983) *J. Am. Chem. Soc. 105,* 7280-7287.

Kanatzidis, M. G., Ryan, M., Coucouvanis, D., Simpoulos, A., Kostikos, A. (1983) *Inorg. Chem. 22,* 179-181.

Joliot, P. (1974) *Biochim. Biophys. Acta 357,* 439-448.

Joliot, P., Barbieri, G., & Chabaud, R. (1969) *Photochem. Photobiol. 10,* 309-329.

Ke, B., Hansen, R. E., & Beinert, H. (1973 a) *Proc. Nat. Acad. Sci. USA 70,* 2941-2945.

Ke., B., Sugahara, K., & Shaw, E. R. (1973 b) *Biochim. Biophys. Acta 408,* 12-23.

Ke, B., Inoue, H., Babcock, G. T., Fang, Z.-X., & Dolan, E. (1982) *Biochim. Biophys. Acta 682,* 297-306.

Kessissoglou, D. P., Butler, W. M., & Pecararo, V. L. (1986) *J. Chem. Soc., Chem. Commun.* 1253-1255.

Kessissoglou, D. P., Li, X., Butler, W. M., & Pecararo, V. L. (1987) *Inorg. Chem., 26* 2487-2492.

Kirby, J. A., Robertson, A. S., Smith, J. P., Thompson, A. C., Cooper, S. R., & Klein, M. P. (1981 a) *J. Am. Chem. Soc. 103,* 5529-5537.

Kirby, J. A., Goodin, D. B., Wydrzynski, T., Robertson, A. S., & Klein, M. P. (1981 b) *J. Am. Chem. Soc. 103,* 5537-5542.

Kirby, J. A. (1981) Ph. D. Dissertation, Univ. of Calif., Berkeley, CA, USA, Lawrence Berkeley Laboratory Report, LBL-12705.

Koike, H., & Inoue, Y. (1985) *Biochim. Biophys. Acta 807,* 64-73.

Kok, B., Forbush, B., & McGloin, M. (1970) *Photochem. Photobiol. 11,* 457-475.

Kutzler, F. W., Natoli, C. R., Misemer, D. K., Doniach, S., & Hodgson, K. (1980) *J. Chem. Phys. 73,* 3274-3288.

Laemmli, U. K. (1970) *Nature 227,* 680-685.

Laskowski, E. J., Reynolds, J. G., Frankel, R. B., Foner, S., Papaefthymiou, G. C. & Holm, R. H. (1979) *J. Am. Chem. Soc. 101,* 6562-6570.

Lundell, D. J., Glazer, A. N., Melis, A., & Malkin, R. (1985) *J. Biol. Chem. 260,* 646-654.

Lynch, M. W., Hendrickson, D. N., Fitzgerald, B. J., & Pierpont, C. G. (1984) *J. Am. Chem. Soc. 106,* 2041-2049.

Mabad, B., Tuchagues, J.-P., Hwang, Y. T., & Hendrickson, D. N. (1985) *J. Am. Chem. Soc. 107,* 2801-2802.

Magers, K. D., Smith, C. G., & Sawyer, D. T. (1980) *Inorg Chem. 19,* 492-496.

Malkin, R. (1986) *FEBS Lett 208,* 343-346.

Mansfield, R. W., & Evans, M. C. W. (1986) *FEBS Lett. 203,* 225-229.

Manodori, A., & Melis, A. (1986) *Plant Physiol. 82,* 185-189.

Mauzerall, D. (1978) in *The Photosynthetic Bacteria* (Ed., Clayton, R. & Sistrom, W. R.) Plenum Press, N. Y. 223-229.

McDermott, A. E.; Yachandra, V. K.; Guiles, R. D.; Britt, R. D.; Dexheimer, S. L.; Sauer, K.; Klein, M. P. (1987) *Progress in Photosynthesis* (Ed., Biggins, J.) Martins Nijhoff, Dordrecht vol I 249-252.

Metz, J. G., Pakrasi, H. B., Seibert, M., & Arntzen, C. J. (1986) *FEBS Lett. 205,* 269-274.

Miller, A.-F., de Paula, J. C., & Brudvig, G. W. (1987) *Photosyn. Res. 12,* 205-218.

Mulligan, B., Schultes, N., Chen, L., & Bogorad, L. (1984) *Proc. Natl. Acad. Sci. USA 81,* 2693-2697.

Nanba, O., & Satoh, K. (1987) *Proc. Natl. Acad. Sci. USA 84,* 109-112.

Natoli, C. R., Misemer, D. K., Doniach, S., & Kutzler, F. W., (1980) *Phys. Rev. A 22,* 1104-1108.

Nechushtai, R., Muster, P., Binder, A., Liveanu, V., & Nelson, N. (1983) *Proc. Natl. Acad. Sci. U.S.A. 80,* 1179-1183.

Nigam, H. L., & Srivastava, U. C. (1971) *Chem. Comm. 14,* 761-763.

Nitschke, W., Feiler, U., Lockau, W. & Hauska, G. (1987) *FEBS Lett. 218,* 283-285.

Nomenclature Committee of the International Union of Biochemistry (1979) *Biochim. Biophys. Acta 549,* 101-105.

Noodleman, L. (1981) *J. Chem. Phys. 74,* 5737-5743.

Noodleman, L. & Baerends, E. (1984) *J. Am. Chem. Soc. 106,* 2316-2327.

Nugent, J. H. A., Diner, B. A., & Evans, M. C. W. (1981) *FEBS Lett. 124,* 241-244.

Oh-oka, H., Takahashi, Y., Wada, K., Matsubara, H., Ohyama, K., & Ozeki, H. (1987) *FEBS Lett. 218,* 52-54.

Olson, J. M. (1981) *Biosystems 14,* 89-94.

Orme-Johnson, W. & Orme-Johnson, N. (1982) in *Iron Sulfur Proteins* (Ed. Spiro, T. G.) 67-98.

Padan, E. & Cohen, Y. (1982) *Botanical Monographs, vol 19, The Biology of Cyanobacteria* (Ed., Carr, N. G. & Whitton, B. A.) U. C. Press, Berkeley, CA 215-235.

Palace, G. P., Franke, J. E., & Warden, J. T. (1987) *FEBS Lett. 215,* 58-62.

Pake, G. E¿ & Estle, T. L. (1973) *Physical Principles of Electron Paramagnetic Resonance* W. A. Benjamin, Reading, MA.

Pfefferkorn, B., & Meyer, H. E. (1986) *FEBS Lett. 206.* 233-237.

Pfenning, N. (1978) in *The Photosynthetic Bacteria* (Ed., Clayton, R. & Sistrom, W. R.) Plenum Press, N. Y. 3-18.

Pfister, K., Steinback, K. E., Gardner, G., & Arntzen, C. J. (1981) *Proc. Natl. Acad Sci. USA 78,* 981-985.

Plaksin, P. M., Stoufer, R. C., Mathew, M., & Palenik, G. J. (1972) *J. Am. Chem. Soc. 94,* 2121-2122.

Powers, L., Chance, B., Ching, Y., & Angiolillo, P. (1981) *Biophys. J. 34,* 465-498.

Powers, L. (1983) *Biochim. Biophys. Acta 683*, 1-38.

Renger, G. (1977) in *Photosynthetic Oxygen Evolution* (Metzner, H., Ed.) Academic Press, London, 229-248.

Richens, D. T., & Sawyer, D. T. (1979) *J. Am. Chem. Soc. 101,* 3681-3683.

Robertson, A. S. (1979) Ph. D. Dissertation, University of California, Berkeley, Lawrence Berkeley Laboratory Report No. LBL-9840.

Roe, A. L., Schneider, D. J., Mayer, R. J., Pryz, J. W., Widom, J., & Que, L., Jr. (1984) *J. Am. Chem. Soc. 106*, 1676-1681.

Rupp, H., De La Torre, A., & Hall, D. O. (1979) *Biochim. Biophys. Acta 548*, 552-564.

Rupp, H., Rao, K. K., Hall, D. O. & Cammack, R. (1978) *Biochim. Biophys. Acta 537* 255-269.

Rupp, H., De La Torre, A., & Hall, D. O. (1979) *Biochim. Biophys. Acta 548*, 552-564.

Rutherford, A. W., & Heathcote, P. (1985) *Photosyn. Res. 6*, 295-316.

Rutherford, A. W., & Heathcote, P. (1985) *Photosyn. Res. 6*, 295-316.

Rutherford, A. W., & Zimmermann, J. L. (1984) *Biochim. Biophys. Acta 767,* 168-175.

Rutherford, A. W., Zimmermann, J. L., & Mathis, P. (1984) *FEBS Lett. 165,* 156-161.

Salerno, J. C., Ohnishi, T., Blum, H., & Leigh, J. S. (1977) *Biochim. Biophys. Acta 494*, 191-197.

Satoh, K., Ohno, T., & Katoh, S. (1985) *FEBS Lett. 180,* 326-330.

Sauer, K. (1980) *Acc. Chem. Res. 13,* 249-256.

Sauer, K., Guiles, R. D., McDermott, A. E., Cole, J. L., Yachandra, V. K., Dexheimer, S. L., Britt, R. D., Zimmermann, J. L., & Klein, M. P. *Chemica Scripta* in press.

Schepler, K. L. (1975) Ph. D. Dissertation, University of Michigan.

Schoeder, H.-U., & Lockau, W. (1986) *FEBS Lett. 199,* 23-27.

Schwartz, R. M. & Dayhoff, M. (1981) *Ann. N.Y. Acad. Sci.* 260-269.

Shopf, J. W. (1978) *Sci. Am. 239,* 110-138.

Sheats, J. E., Czernuszewicz, R. S., Dismukes, G. C., Rheingold, A. L., Petrouleas, V., Stubbe, J., Armstrong, W. H., Beer, R. H., & Lippard, S. J. (1987) *J. Am. Chem. Soc. 109,* 1435-1444.

Shulman, R. G., Yafet, Y., Eisenberger, P. & Blumberg, W. *Proc. Natl. Acad. Sci. USA 73,* 1384-1388.

Singer, L. S. (1955) *J. Chem. Phys. 23,* 379-388.

Smith, N. S., Mansfield, R. W., Nugent, J. H. A., & Evans, M. C. W. (1987) *Biochim. Biophys. Acta. 892,* 331-334.

Srivastava, U. C., & Nigam, H. L. (1972) *Coord. Chem. Rev. 1,* 275-310.

Stern, E. A. & Heald, S. M. (1979) *Rev. Sci. Instrum. 50,* 1579-1582.

Stewart, A. C., Ljungberg, U., Åkerlund, H.-E., & Andersson, B. (1985) *Biochim. Biophys. Acta 808,* 353-362.

Stohr, J. (1986) *Journal de Phys., EXAFS IV* C8-173.

Stout, C. D. (1982) in *Iron-Sulfur Proteins* (Ed., Spiro, T. G.), John Wiley & Sons, New York, 97-146.

Takahashi, Y., Hirota, K., & Katoh, S. (1985) *Photosyn. Res. 6,* 183-192.

Teo, B. K., & Lee, P. A. (1979) *J. Am. Chem. Soc. 101*, 2815-2832.

Teo, B. K., Shulman, R. G., Brown, G. S., & Meixner, A. E. (1979) *J. Am. Chem. Soc. 101*, 5624-5631.

Teo, B. K., & Shulman, R. G. (1982) in *Iron-Sulfur Proteins* (Spiro, T. G., Ed.), John Wiley & Sons, New York, 343-366.

Teo, B. K. (1986) *Inorg. Chem. Concepts, 9* (Ed. Jorgensen et al.) Springer-Verlag, N.Y.

Teo, B.-K., & Lee, P. A. (1979) *J. Am. Chem. Soc. 101,* 2815-2831.

Thurnauer, M. C. & Gast, P. (1985) *Photochem. Photophys. 9,* 29-38.

Thurnauer, M. C., Gast, P., Peterson, J., & Stehlik, D. (1987) in *Progress in Photosynthesis Research* (Biggins, J., Ed.), Martins Nijhoff, Dordrecht, vol. 1, 237-240.

Trebst, A. (1986) *Z. Naturforsch. 41C,* 240-245.

Valentine, J. W. (1978) *Sci. Am. 239,* 140-158.

Vermaas, W. F. J., & Rutherford, A. W. (1984) *FEBS 175,* 243-248.

Warden, J. T., & Golbeck, J. H. (1986) *Biochim. Biophys. Acta 849*, 25-31.

Wasielewski, M. R. , Norris, J. R., Shipman, L. L., Lin, C. P., Svec, W. A. (1981) *Proc. Natl. Acad. Sci. 78,* 2957-2961.

Watanabe, T., Kobayashi, M., Hongu, A., Nakazato, M., Hiyama, T. & Murata, N. (1985) *FEBS Lett. 191,* 252-?.

Williams-Smith, D. L., Heathcote, P., Sihra, C. K., & Evans, M. C. W. (1978) *Biochem. J. 170*, 365-371.

Williams, J. G. K., & Chisholm, D. A. (1987) in *Progress in Photosynthesis Research* (Biggins, J., Ed.), Martinus Nijhoff, Dordrecht, vol 4, 809-812.

Worland, S. T., Yamagishi, A., Isaacs, S., Sauer, K., & Hearst, J. E. (1987) *Proc. Natl. Acad. Sci. USA 84,* 1774-1778.

Yachandra, V. K., Guiles, R. D., McDermott, A. E., Britt, R. D., Dexheimer, S. L., Sauer, K., & Klein, M. P. (1986a) *Biochim. Biophys. Acta 850,* 324-332.

Yachandra, V. K., Guiles, R. D., Sauer, K. S., & Klein, M. P. (1986b) *Biochim. Biophys. Acta 850,* 333-342.

Yachandra, V. K., Guiles, R. D., McDermott, A. E., Cole, J. L., Britt, R. D., Dexheimer, S. L., Sauer, K., & Klein, M. P. (1987) *Biochem.* in press.

Yamagishi, A., & Katoh, S. (1983) *Arch. Biochem. Biophys. 225,* 836-846.

Youvan, D. C., Bylina, E. J., Alberti, M., Begusch, H. & Hearst, J. E. (1984) *Cell 37* 949-957.

Ziegler, K. Lockau, W., & Nitschke, W. (1987) *FEBS Lett 217,* 16-20.

Zimmermann, J.-L., & Rutherford, A. W. (1986) *Biochem. 25,* 4609-4615.

LAWRENCE BERKELEY LABORATORY
TECHNICAL INFORMATION DEPARTMENT
UNIVERSITY OF CALIFORNIA
BERKELEY, CALIFORNIA 94720